SBORNÍK XXI. VÝROČNÍ KONFERENCE ČESKÉ AEROSOLOVÉ SPOLEČNOSTI

3. 10. – 4. 10. 2022, Kutná Hora

PROCEEDINGS OF 21st ANNUAL CONFERENCE OF THE CZECH AEROSOL SOCIETY

3. 10. – 4. 10. 2022, Kutná Hora

czech aerosol society

Vydala Česká aerosolová společnost
Published by the Czech Aerosol Society
Editor: Radek Lhotka
ISBN: 978-80-908653-0-3

OBSAH – CONTENT

PROGRAM

PONDĚLÍ – MONDAY 3. 10. 2022 DOPOLEDNE – MORNING	
8:30 – 9:00 Registrace – Registration	
9:00 -9:15 Zahájení konference – Opening of the conference	
9:15	**VLIV VZDUCHOVÝCH HMOT NA KONCENTRACE AEROSOLOVÝCH ČÁSTIC MĚŘENÝCH V SÍTI ULTRAJEMNÝCH ČÁSTIC** Adéla HOLUBOVÁ ŠMEJKALOVÁ, Marcela HEJKRLÍKOVÁ, Helena PLACHÁ, Miroslav BITTER
9:30	**ČIŠTĚNÍ KNIHOVNÍCH DOKUMENTŮ POMOCÍ DVOUFÁZOVÉHO SPREJE** Ludmila MAŠKOVÁ, Jiří SMOLÍK, Petra VÁVROVÁ, Jitka NEORALOVÁ, Magda SOUČKOVÁ, Dana NOVOTNÁ, Věra JANDOVÁ, Jakub ONDRÁČEK, Lucie ONDRÁČKOVÁ, Tereza KŘÍŽOVÁ, Kateřina KOCOVÁ
9:45	**SEZÓNNÍ ZMĚNY STABILNÍHO IZOTOPOVÉHO SLOŽENÍ UHLÍKU (δ13C) V AEROSOLU A PLYNNÉ FÁZI NA PŘEDMĚSTSKÉ STANICI V PRAZE** Petr VODIČKA, Kimitaka KAWAMURA, Jaroslav SCHWARZ, Vladimír ŽDÍMAL
10:00	**A SEVEN-YEARS BASED CHARACTERISATION OF AEROSOL LIGHT SCATTERING PROPERTIES AT CENTRAL EUROPEAN RURAL SITE: VARIABILITY AND SOURCE APPORTIONMENT** Lenka SUCHÁNKOVÁ, Saliou MBENGUE, Nadežda ZÍKOVÁ, Jakub ONDRÁČEK, Adéla HOLUBOVÁ ŠMEJKALOVÁ, Roman PROKEŠ, Ivan HOLOUBEK, Vladimír ŽDÍMAL
10:15	**LIDAR VERTICAL PROFILE ANALYZES AT NATIONAL ATMOSPHERIC OBSERVATORY KOŠETICE DURING VOLCANO ERUPTION ON LA PALMA ISLAND** Juraj KOSTYK, Adéla HOLUBOVÁ ŠMEJKALOVÁ, Tomáš IŠTOK, Vladimír ŽDÍMAL
10:30– 11:00 Přestávka na kávu – Coffee Break	
11:00	**DYNAMIKA PROSTOROVÝCH A ČASOVÝCH ZMĚN PM2,5 A VLIV LOKÁLNÍCH TOPENIŠŤ V OVZDUŠÍ OBCE ZADNÍ TŘEBAŇ BĚHEM TOPNÉ SEZÓNY** Karolína WALLENFELSOVÁ, Jan HOVORKA
11:15	**THE IMPACT OF THE IMO-2020 SHIPPING REGULATION ON THE ATMOSPHERIC DEPOSITION OF SULFUR AROUND THE WESTERN ENGLISH CHANNEL AND THE USE OF THE V/NI RATIO AS A SHIPPING MARKER** L.C. WINDELL, T.G. BELL, C. WHITE, A. MILNE, J. SCHWARZ, S.J. USSHER
11:30	**CHEMICKÉ SLOŽENÍ A ZDROJE ATMOSFÉRICKÝCH AEROSOLŮ NA POZAĎOVÉ STANICI FRÝDLANT** Radek LHOTKA, Petra POKORNÁ, Petr VODIČKA, Naděžda ZÍKOVÁ, Jakub ONDRÁČEK, Shubhi ARORA, Laurent POULAIN, Hartmut HERMANN, Jaroslav SCHWARZ, Vladimír ŽDÍMAL
11:45	**DYNAMIKA PROSTOROVÝCH A ČASOVÝCH ZMĚN PM2.5 A VLIV LOKÁLNÍCH TOPENIŠŤ V OVZDUŠÍ OBCE DRUŽEC BĚHEM TOPNÉ SEZÓNY** Dominik ŠMOK, Jan HOVORKA
12:00	**THE STORY OF TEAMWORK AND THE BIRTH OF THE FFP3* (FILTER BACKPACK)** Max FRAENKL, Milos KRBAL, Jakub HOUDEK, Zuzana ZMRHALOVA, Borivoj PROKES, Petr HEJDA, Stanislav SLANG, Jan PRIKRYL, Jakub ONDRACEK, Otakar MAKES, Juraj KOSTYK, Petr NASADIL, Pavel MALCIK, Vladimir ZDIMAL, Miroslav VLCEK
12:15	**METHOD AND INSTRUMENTATION FOR DIRECT MEASUREMENT OF CORROSIVE SPECIES FROM COMBUSTION** Erkki LAMMINEN, Oskari VAINIO, Markus NIKKA
12:35 – 14:00 Přestávka na oběd – Lunch	

PONDĚLÍ – MONDAY 3. 10. 2022 ODPOLEDNE – AFTERNOON	
14:00	**10LETÉ MONITOROVÁNÍ OXIDAČNÍHO STRESU U OSOB PROFESIONÁLNĚ EXPONOVANÝCH NANOČÁSTICÍM POMOCÍ NEINVAZIVNÍCH METOD** **PLENÁRNÍ PŘEDNÁŠKA** Daniela PELCLOVÁ, Vladimír ŽDÍMAL
14:30	**TOTAL AND BIOACCESSIBLE FRACTION OF ELEMENTS IN URBAN AEROSOL** Pavel MIKUŠKA, Hana CIGÁNKOVÁ, Jitka HEGROVÁ
14:45	**OXIDATIVE POTENTIAL OF PM1 AND PM2.5 URBAN AEROSOL AND ASSOCIATED ELEMENTS IN THREE SIMULATED LUNG FLUIDS** Hana CIGÁNKOVÁ, Pavel MIKUŠKA, Jitka HEGROVÁ
15:00	**ORGANICKÉ SLOUČENINY A MARKERY ZE SPALOVÁNÍ DŘEVA V KOTLÍCH POUŽÍVANÝCH PRO VYTÁPĚNÍ DOMÁCNOSTÍ** Kamil KŘŮMAL, Pavel MIKUŠKA, Jiří HORÁK, Miroslav JAROCH, František HOPAN, Lenka KUBOŇOVÁ
15:15	**PARALLEL DETERMINATION OF PARTICULATE AMMONIUM BY USING A CONTINUOUS AEROSOL SAMPLER AND CASCADE IMPACTOR** LUKÁŠ ALEXA, HANA HLAVÁČKOVÁ, HANA CIGÁNKOVÁ, PAVEL MIKUŠKA
15:30	**PRAKTICKÉ LIMITY OVĚŘENÍ FUNKCE FILTRŮ ČÁSTIC DÁLKOVÝM MĚŘENÍM** Michal VOJTÍŠEK, Martin PECHOUT
15:45	**NMR AEROSOLOMICS STUDY OF WATER-SOLUBLE ORGANIC COMPOUNDS IN SIZE-RESOLVED PARTICULATE MATTER** Štěpán HORNÍK, Petr VODIČKA, Petra POKORNÁ, Jaroslav SCHWARZ, Vladimír ŽDÍMAL, Jan SÝKORA
16:00 – 16:30 Přestávka na kávu – Coffee Break	
16:30	**ZÁVISLOST AKTIVACE AEROSOLU NA METEOROLOGICKÝCH PODMÍNKÁCH** Naděžda ZÍKOVÁ, Petra POKORNÁ, Pavel SEDLÁK, Vladimír ŽDÍMAL
16:45	**STANOVENÍ KONCENTRACE A VELIKOSTNÍ DISTRIBUCE RADIOAKTIVNÍCH AEROSOLOVÝCH ČÁSTIC** Petr OTÁHAL, Michaela KOZLOVSKÁ, Eliška FIALOVÁ
17:00	**AN IMPROVED METHOD FOR CALCULATION OF THE WET PARTICLE DIAMETER AND THE KAPPA PARAMETER FROM THE CCN DATA** Zdeněk WAGNER, Gaurav MISHRA, Pavel MORAVEC, Naděžda ZÍKOVÁ
17:15	**PLANETARY BOUNDARY LAYER EFFECT ON VERTICAL TRANSPORT OF BLACK CARBON CONCENTRATION UNDER DIFFERENT METEOROLOGICAL CONDITIONS** Kajal JULAHA, Nadežda ZÍKOVÁ, Saliou MBENGUE, Vladimír ŽDÍMAL
17:30	**THE IMPACT OF COVID-19 RESTRICTIONS ON CARBONACEOUS AEROSOLS AT RURAL BACKGROUND SITE: IMPORTANCE OF VERTICAL DISTRIBUTION** Saliou MBENGUE, Petr VODIČKA, Katerina KOMÍNKOVÁ, Jaroslav SCHWARZ, Nadezda ZÍKOVÁ, Roman PROKES, Lenka SUCHÁNKOVÁ, Kajal JULAHA, Jakub ONDRÁČEK, Ivan HOLOUBEK, Vladimir ŽDÍMAL
17:45	**HARMONIZED UFP NUMBER AND SIZE DISTRIBUTION MEASUREMENTS ACCEPTED BY ACTRIS, EMEP AND NATIONAL MONITORING NETWORKS** Lucia BUSTIN, Torsten TRITSCHER, Sebastian H. SCHMITT, Andrea J. TIWARI, Jürgen SPIELVOGEL, Thomas KRINKE, and Oliver F. BISCHOF
18:00	**SMOKEMANOVO DESATERO SPRÁVNÉHO TOPIČE – AUDIOVIZUÁLNÍ VERZE** Jiří HORÁK, František HOPAN
18:15 – 18:20 Kráká přestávka – Short Break	
18:20 – 19:00 SCHŮZE VÝBORU ČAS	
19:00 Společenský večer – Conference dinner	
ÚTERÝ – TUESDAY 4. 10. 2022 DOPOLEDNE – MORNING	

8:30 – 9:10 ČLENSKÁ SCHŮZE ČAS	
9:10 – 9:15 Krátká přestávka Short break	
9:15	**ENDOSKOPICKÉ ZÁKROKY V DOBĚ COVID-19** **KEYNOTE** Martin WASSERBAUER, Štěpán HLAVA, Raden KEIL
9:35	**PHYSICOCHEMICAL PROPERTIES AND ORIGIN OF PM1 MEASURED AT A RURAL BACKGROUND SITE** Petra POKORNÁ, Naděžda ZÍKOVÁ, Petr VODIČKA, Radek LHOTKA, Saliou MBENGUE, Adéla HOLUBOVÁ ŠMEJKALOVÁ, Véronique RIFFAULT, Jakub ONDRÁČEK, Jaroslav SCHWARZ, Vladimír ŽDÍMAL
9:50	**THREE YEARS OF EXPERIENCE WITH MEASUREMENT OF CLOUD CONDENSATION NUCLEI CONCENTRATIONS USING CLOUD CONDENSATION NUCLEI COUNTER CCN-200** Pavel MORAVEC, Radek LHOTKA, Vladimír ŽDÍMAL
10:05	**ANALÝZY ATMOSFÉRICKÝCH AEROSOLŮ POMOCÍ SVAZKU URYCHLENÝCH IONTŮ** Vladimír HAVRÁNEK
10:20	**TRANSPORT OF PLASMA REACTIVE SPECIES INTO AEROSOLS VS. BULK WATER** Mostafa Elsayed HASSAN, Mário JANDA, Zdenko MACHALA
10:35	**CHANGE IN SIZE-RESOLVED FILTRATION EFFICIENCY OF RESPIRATORS AFTER DECONTAMINATION/DISINFECTION TREATMENTS** Jakub ONDRÁČEK, Lucie ONDRÁČKOVÁ, Michal DŘEVÍNEK, Petr OTÁHAL, Josef VOŠÁHLÍK
10:50	**THE FLOW OF INHALED FIBRES IN A MODEL OF THE FIRST BIFURCATION IN HUMAN AIRWAYS UNDER TRANSIENT CONDITIONS** František LÍZAL, Matouš CABALKA, Milan MALÝ, Miloslav BĚLKA, Ondrej MIŠÍK, Jan JEDELSKÝ
11:05 -11:30 Přestávka na kávu – Coffee break	
11:30	**ON PARTICLE COAGULATION IN ELECTROSTATIC PRECIPITATOR** Oleksandr MOLCHANOV, Kamil KRPEC, Jiří HORÁK, František HOPAN
11:45	**DEKATI® OXIDATION FLOW REACTOR DOFR™ FOR SECONDARY AEROSOL FORMATION STUDIES** Markus NIKKA, Elmeri LAAKKONEN, Anssi ARFFMAN, Oskari VAINIO
12:05	**ASSESSMENT OF THE SOURCES' IMPACT ON PM10** Tomasz OLSZOWSKI
12:20	**KONCENTRÁCIA A ANORGANICKÁ ELEMENTÁRNA ANALÝZA PEVNÝCH ČASTÍC V PROSTREDÍ CESTNÉHO TUNELA** Dušan JANDAČKA, Daniela ĎURČANSKÁ
12:35	**IMPACTS OF VARIOUS PARAMETERIZATIONS ON ORGANIC AEROSOL MODELLING IN CENTRAL EUROPE** Lukáš BARTÍK, Peter HUSZÁR, Ondřej VLČEK, Kryštof EBEN
12:50	**EXPERIMENTAL MEASURING OF HOMOGENEOUS NUCLEATION RATE OF WATER IN THE PRESENCE OF VARIOUS GASES IN PULSE EXPANSION CHAMBER** Tetiana LUKIANOVA, Mykola LUKIANOV, Jan HRUBÝ
13:05 – 13:10 Kráká přestávka – Short Break	
13:10 – 13:30 Výhlášení výsledků soutěže o nejlepší přednášku mladého vědce a zakončení konference– Dekati Aword Announcement and End of Conference	
13:30 – 15:00 Oběd – Lunch	

SPONZOŘI – SPONSORS

ECM ECO Monitoring

DEKATI BIOWELL

Excellence in Particle Measurements

www.dekati.com www.biowell.sk

ÚVOD – INTRODUCTION

Milé kolegyně, milí kolegové, takto členové České aerosolové společnosti.

Jak bývá mým zvykem, rád bych vás pozdravil jako předseda společnosti při příležitosti letošní výroční konference ČAS konané 3. a 4. října v Kutné hoře, v hotelu Mědínek. Kvůli pauze vynucené pandemií COVID-19 se letos setkáme po 3 letech od poslední konference. O to více se těším, že vás konečně všechny zase uvidím. Ještě na konci srpna mne pokladník společnosti Pavel Moravec upozorňoval, že konference pravděpodobně dopadne finančním fiaskem, protože je přihlášeno málo účastníků. Ve chvíli, kdy píši tento úvodník, to vypadá, že budeme mít největší počet konferenčních prezentací za celou historii VK ČAS. Dokonce jsme museli prodloužit program konference až do úterního odpoledne, protože se nám do poledne všechny vaše příspěvky nevešly.

A zároveň bych vás rád upozornil na jednu novinku. Po delší době máme opět dva pozvané přednášející. Paní profesorka Daniela Pelclová bude mít půlhodinovou plenární přednášku o vlivu aerosolových částic na zdraví v pracovním prostředí. Pan doktor Martin Wasserbauer nám zase ve své Keynote prozradí, jak se mohou vyšetřující lékaři chránit před patogeny uvolňovanými z trávicího traktu pacientů při vyšetření žaludku. Vřele vám doporučuji se na obě tyto přednášky přijít podívat.

Jako obvykle se nám letos přihlásili sponzoři, již tradičně jde o českou firmu ECM Ecomonitoring, a finskou firmu Dekati, reprezentovanou slovenským Biowellem. Děkuji našim sponzorům, že nám zachovali přízeň i po dvouletém odkladu. Díky nim si budete moci užít bohatou konferenční večeři a mladší kolegové se mohu těšit na ocenění v soutěži nejlepších prezentací.

V této souvislosti bych rád připomněl, že stále trvá možnost pro mladší vědecké pracovníky a doktorandy, aby získali podporu pro cestu na významnou zahraniční mezinárodní konferenci, pokud se jim podaří na takové konferenci prezentovat formou přednášky. V minulosti jsme touto formou podpořili celou řadu vašich zahraničních cest, ale obávám se, že během COVIDu jsme kvůli omezenému cestování na tuto možnost téměř zapomněli. Rád bych jí proto všem připomněl a povzbuzuji všechny mladší kolegy, kterých se to týká, aby se nebáli o tento typ podpory požádat.

Na závěr bych vám chtěl poděkovat za přízeň, kterou jste mi projevovali po celých téměř 9 let ve funkci předsedy České aerosolové společnosti. Jak již jsem avizoval v jarním emailu, rozhodl jsem se ze zdravotních důvodů odstoupit z pozice předsedy společnosti a nechat výbor vybrat předsedu nového. Proto vás prosím, abyste se v hojném počtu zúčastnili členské schůze, která se bude konat v úterý ráno před první přednáškou. Rozumím tomu, že někteří z vás budou po pondělní konferenční večeři unaveni, ale snad vás ranní káva probudí natolik, abyste se již probuzení mohli na schůzi dostavit. Přeji vám všem hodně zdraví a dobré mysli a těším se na vás v Kutné hoře.

Váš

Vláďa Ždímal

VLIV VZDUCHOVÝCH HMOT NA KONCENTRACE AEROSOLOVÝCH ČÁSTIC MĚŘENÝCH V SÍTI ULTRAJEMNÝCH ČÁSTIC

Adéla HOLUBOVÁ ŠMEJKALOVÁ[1], Marcela HEJKRLÍKOVÁ[1], Helena PLACHÁ[1], Miroslav BITTER[1]

[1] Český hydrometeorologický ústav, Praha, Česká republika, adela.holubova@chmi.cz

Klíčová slova: Vzduchové hmoty, Koncentrace aerosolových částic, Síť ultrajemných částic

SUMMARY

The influence of different air mass origins on particle number size distribution was studied at five stations within Ultrafine aerosol particle network. The significant differences between concentrations were observed in accumulation mode in different air masses - the long-range transport affected concentrations. Local sources probably more contribute to aerosol concentrations in Aitken and nucleation mode at urban traffic stations.

ÚVOD

Koncentrace aerosolových částic měřených na dané lokalitě jsou výsledkem působení několika faktorů. Jedná se jak o lokální zdroje znečištění, meteorologické podmínky, tak i o vliv vzdálenějších zdrojů. Právě vliv dálkového transportu na receptorovou lokalitu lze sledovat díky pohybu vzduchových hmot (VH) různého původu (Colbeck a Lazaridis 2010; López a kol. 2019; Wonaschütz a kol. 2015). Od roku 2019 jsou kontinuálně měřeny koncentrace aerosolových částic na pěti stanicích v rámci sítě Ultrajemných částic (UJČ) Českého hydrometeorologického ústavu. Na výsledcích měřených na těchto stanicích bylo sledováno, zda převažuje vliv na početní rozdělení velikosti aerosolových částic (particle number size distribution – PNSD) z lokálních zdrojů znečištění či z dálkového transportu. Stanice se nacházejí v různých typech prostředí a jsou ovlivňovány různými typy zdrojů (intenzita a vzdálenost dopravy, lokální vytápění, průmysl, těžební činnost).

METODY MĚŘENÍ

PNSD byla sledována na stanicích **Mladá Boleslav** (50° 25′ 43.126"S, 14° 54′ 49.894"V, 224 m n.m.), **Hradec Králové-Brněnská** (50° 11′ 43.304"S, 15° 50′ 46.955"V, 232 m n.m.), **Plzeň-Slovany** (49° 43′ 56.815"S, 13° 24′ 8.211"V, 340 m n.m.), **Ústí nad Labem** (50° 39′ 39.941"S, 14° 2′ 35.027"V, 147 m n.m.), **Lom** (50° 35′ 8.757"S, 13° 40′ 24.305"V, 26 m n.m.). Detailní popis přístrojového vybavení pro měření PNSD je uveden v Tabulce 1. Původ VH byl analyzován z klastrovaných zpětných tratektorií vypočtených programem HYbrid Single-Particle Lagrangian Integrated Trajectory HYSPLIT_4 model (HYSPLIT) (Draxler, Roland R. a Rolph 2013). Každých 6 hodin byly generovány 96 hodinové zpětné trajektorie s časem začátku v 00:00 UTC a výškou receptoru 500 m n.m. K výpočtům byly použity meteorologická data Global Data Assimilation System (GDAS) s rozlišením 1° × 1°. PNSD data byla rozdělena na nukleační, Aitkenův a akumulační mód. Změny koncentrací v jednotlivých VH byly hodnoceny jak pro jednotlivé módy, tak i pro

koncentrace znečišťujících látek PM_{10}, $PM_{2,5}$, NO_X. Data byla hodnocena v období od 1. června 2019 do 31. června 2021.

Tab. 1: Přístrojové vybavení a měřicí rozsahy PNSD na jednotlivých stanicích UJČ.

Stanice	Spektrometr	Čítač částic	Velikostní rozsah měření
Hradec Králové-Brněnská	SMPS 3938 (TSI)	CPC 3750 (TSI)	7–500 nm
Lom	SMPS – zakázková výroba (IfT Tropos)	CPC 3772 (TSI)	10–800 nm
Mladá Boleslav	SMPS 3938 (TSI)	CPC 3750 (TSI)	7–500 nm
Plzeň-Slovany	SMPS 3938 (TSI)	CPC 3750 (TSI)	7–500 nm
Ústí n/L-město	SMPS – zakázková výroba (IfT Tropos)	CPC 3772 (TSI)	10–800 nm

VÝSLEDKY, DISKUSE, ZÁVĚRY

Vliv původu VH na koncentrace částic akumulačního módu byl potvrzen u stanic Mladá Boleslav, Hradec Králové-Brněnská a Plzeň-Slovany. Koncentrace částic Aitkenova módu zpravidla nebyly ovlivněny typem VH na stanicích Mladá Boleslav a Hradec Králové-Brněnská. Výsledek v těchto lokalitách pravděpodobně ukazuje na převládající vliv lokálních zdrojů znečištění na koncentrace částic Aitkenova módu. Obdobné výsledky byly zaznamenány i u částic nukleačního módu na stanici Hradec Králové-Brněnská. Na všech stanicích byly měřeny nejvyšší koncentrace PM_{10} (>20 $\mu g \cdot m^{-3}$) ve VH č. 3 (kontinentální VH). Koncentrace NO_X byly v jednotlivých VH velmi podobné, což naznačuje menší ovlivnění dálkovým transportem.

Cílem této práce je zjistit, zda na PNSD, které je měřeno na 5 stanicích v České republice, ovlivných různými zdroji, má vliv více lokální či dálkovým transportem přemísťované znečištění. Dosavadní výsledky ukazují zejména na vliv dálkového transportu na koncentrace částic akumulačního módu. Vliv lokálního znečištění na koncentrace částic Aitkenova a nuklečního módu byl zaznamenán na městské dopravní stanici Hradec Králové-Brněnská.

PODĚKOVÁNÍ

Tato práce vznikla za podpory projektu ARAMIS SS02030031.

LITERATURA

Colbeck, I. a Lazaridis, M. *Naturwissenschaften* 97(2), 117–131, (2010).

Draxler, R. R. a Rolph, G. D.,HYSPLIT (HYbrid Single-Particle Lagrangian Integrated Trajectory), (2013).

LÓPEZ, V. a kol.. *Environmental Science and Pollution Research*. 26(29), 30426–30443, (2019).

WONASCHÜTZ, A. a kol.., 2015. *Atmospheric Environment*. 118, 118–126, (2015).

ČIŠTĚNÍ KNIHOVNÍCH DOKUMENTŮ POMOCÍ DVOUFÁZOVÉHO SPREJE

Ludmila MAŠKOVÁ[1], Jiří SMOLÍK[1], Petra VÁVROVÁ[2], Jitka NEORALOVÁ[2], Magda SOUČKOVÁ[2], Dana NOVOTNÁ[2], Věra JANDOVÁ[1], Jakub ONDRÁČEK[1], Lucie ONDRÁČKOVÁ[1], Tereza KŘÍŽOVÁ[2], Kateřina KOCOVÁ[2]

[1] Ústav chemických procesů AV ČR, Praha, Česká republika, maskova@icpf.cas.cz
[2] Národní knihovna ČR, Praha, Česká republika

Klíčová slova: Dvoufázový sprej, Suché čištění, Oxid uhličitý

SUMMARY

The cleaning of particles from library materials (paper, textile, and collagen materials) using a high-speed CO_2 snow jet was investigated. The measurements included determination of the cleaning efficiency, and evaluation of possible adverse effects. The method was compared with nitrogen jet cleaning. The results showed that the CO_2 snow jet is able to effectively remove particles from the surfaces. Any adverse effects were not observed at paper and textile. However, application on collagen materials caused degradation of the surface.

ÚVOD

Čištění povrchu archiválií a knih patří mezi základní konzervátorské zásahy. Důvodem je zejména přiblížení se původnímu vzhledu a zastavení degradačních procesů vlivem přítomných nečistot. Jemné částice (< 1 μm) ve vnitřním prostředí knihoven a archivů obsahují zejména saze, organické látky, síran a dusičnan amonný a sloučeniny kovů. Hrubé částice (>1 μm) jsou pak převážně tvořeny minerálními a organickými látkami (Mašková a kol., 2015). Saze a organické látky přispívají zejména k znečištění povrchů, dusičnan a síran amonný, sole a některé organické látky jsou hygroskopické a mají tak tendenci podporovat růst plísní, kyselé složky přispívají k degradaci materiálu, minerální částice jsou abrazivní a napomáhají tak k mechanickému poškození (Hatchfield, 2005).

Tradiční metody suchého čištění většinou zahrnují štětec, gumu, vysavač, stlačený vzduch atd. Jejich pomocí se však odstraňují převážně pouze hrubé částice. Cílem této práce bylo otestovat alternativní metodu čištění knihovních materiálů pomocí dvoufázového spreje sněhových částic oxidu uhičitého v nosném plynu.

METODIKA

K čištění byl použit přístroj SnoPen 2000 (CleanLogix), generující dvoufázový sprej sněhových mikročástic oxidu uhličitého v proudu dusíku jako nosného plynu. Pro srovnání byl k čištění použit i pouze samotný proud dusíku. K ověření vhodnosti metody byly připraveny vzorky papíru Whatman no. 1, papíru Holmen 2.0, textilu Coloret Natural a třísločiněné usně teletiny jako zástupce kolagenních materiálů o rozměru 4 x 4 cm. Vybrané vzorky byly následně znečištěny třemi druhy prachových částic, a to prachem Ashrae (Test Dust #1, Particle Technology Ltd), slonovinovou černí pravou 12000 (Kremer Pigmente GmbH & Co.) a knihovním prachem z depozitářů Národní knihovny ČR,

odebraným při čistění knih pomocí vysavače. Prach byl nanášen pomocí pryžového válečku vždy ve dvou vrstvách, aby bylo dosaženo rovnoměrného pokrytí povrchu vzorků.

Účinnost odstranění prachu byla sledována před a po aplikaci prachu a následně po mechanickém čištění pomocí analytických vah s přesností ±0.01 mg (XS105, Mettler Toledo). Estetická účinnost čištění byla hodnocena pomocí změny baravnosti v barevném prostoru CIELab. Měření bylo provedeno pomocí spektrofotometru Minolta CM-508d s měřící clonou o velikosti 3 mm v režimu SAV. Bezpečnost dané metody čištění byla posuzována pomocí Elektornové skenovací mikroskopie (SEM, Tescan Indus s detektorem sekundárních elektronů) a 3D optická mikroskopie (Hirox).

VÝSLEDKY, DISKUSE, ZÁVĚRY

Výsledky ukázaly, že nejsnáze byl odstraňován knihovní prach, čištění vzorků se slonovinovou černí bylo obtížnější a prach Ashrae byl nejodolnější. Výsledky také ukázaly, že čištění dvoufázovým sprejem ani proudem dusíku nezpůsobilo poškození u papíru a textilu. Naopak v případě kolagenních materiálů bylo pozorováno narušení povrchu jak v případě použití dvoufázového spreje, tak i samotného proudu dusíku bez částic oxidu uhličitého. Příklady čištění papíru Whatman kontaminovaného prachem Ashrae jsou uvedeny na Obr. 1.

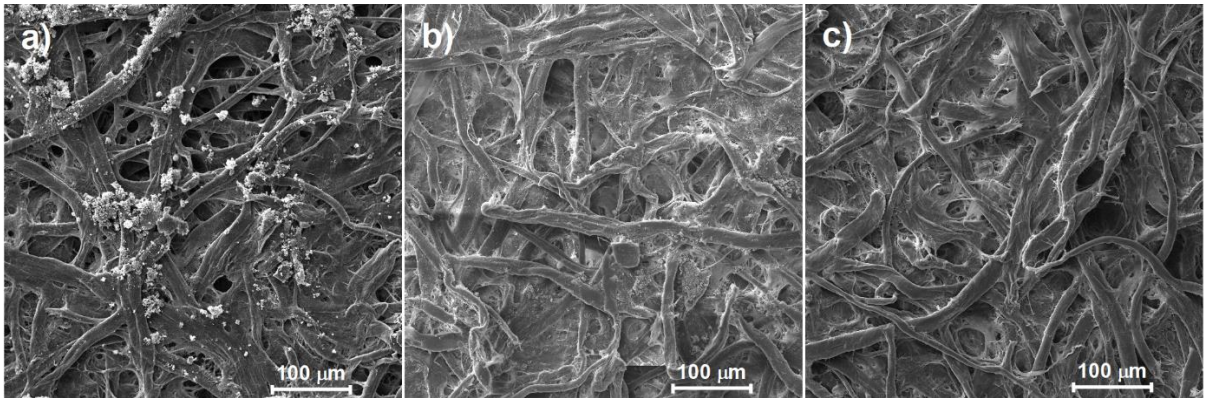

Obr. 1: Příklad papírů Whatman kontaminovaných prachem Ashrae a) před čištěním, b) po čištění proudem dusíku a c) po čištění dvoufázovým sprejem

PODĚKOVÁNÍ

Tato práce byla podpořena grantem Ministerstva kultury NAKI II DG18P02OVV048.

LITERATURA

Mašková, L., Smolík, J., Vodička, P. Characterisation of particulate matter in different types of archives. *Atmos Environ*, 107, 217 – 224, (2015).

Hatchfield, P.B. Pollutants in the Museum Environment, London: Archetype Publications, (2005).

SEZÓNNÍ ZMĚNY STABILNÍHO IZOTOPOVÉHO SLOŽENÍ UHLÍKU ($\Delta^{13}C$) V AEROSOLU A PLYNNÉ FÁZI NA PŘEDMĚSTSKÉ STANICI V PRAZE

Petr VODIČKA[1,2], Kimitaka KAWAMURA[2], Jaroslav SCHWARZ[1], Vladimír ŽDÍMAL[1]

[1] Ústav chemických procesů, AV ČR, Praha, Česká republika, vodicka@icpf.cas.cz
[2] Chubu Institut for Advanced Studies, Chubu University, Kasugai, Japonsko

Klíčová slova: Atmosférický aerosol, Plynná fáze, $\delta^{13}C$, Sezónní variace

SUMMARY

In this work, seasonal variations in the stable carbon isotope ratio ($\delta^{13}C$) of total carbon (TC; $\delta^{13}C_{TC}$) and water-soluble organic carbon (WSOC; $\delta^{13}C_{WSOC}$) in fine aerosol particles ($PM_{2.5}$) as well as in the total carbon of the gas phase (TCgas; $\delta^{13}C_{TCgas}$) were studied. Despite the different seasonal compositions of carbonaceous aerosols, the isotope differences ($\Delta\delta^{13}C$) between the analyzed bulk aerosol parts and gas phases were similar during the seasons. This shows that the fractionation of stable carbon isotopes is a predominantly physical process in which the chemical composition of individual compounds in bulk aerosols does not play a major role. Details in Vodička et. al (2022).

ÚVOD

Izotopová frakcionace mezi plynnou a aerosolovou fází je důležitým jevem při studiu atmosférických procesů. V této práci jsme zkoumali sezónní změny poměru stabilních izotopů uhlíku ($\delta^{13}C$) celkového uhlíku (TC; $\delta^{13}C_{TC}$) a organického uhlíku rozpustného ve vodě (WSOC; $\delta^{13}C_{WSOC}$) v jemných aerosolových částicích ($PM_{2,5)}$ a celkového uhlíku plynné fáze (TCgas; $\delta^{13}C_{TCgas}$) na příměstské lokalitě v Praze.

METODY MĚŘENÍ

Odběr vzorků byl proveden na příměstské stanici Praha-Suchdol (50°7′39.79″ N, 14°23′ 4.30″ E, 277 m n. m.). Vzorkování probíhalo každý 6. den po dobu 48 hodin od 14. 4. 2016 do 1. 5. 2017 na dva křemenné filtry v sérii. Na přední filtr byla vzorkována frakce aerosolu $PM_{2,5}$ + plynné frakce, zatímco na zadní filtr byla odebrána pouze plynná frakce. Vzorky byly následně zváženy a analyzovány na obsah TC, organického a elementárního uhlíku (OC a EC) a WSOC. Hmota TC a WSOC byla dále analyzována na poměr $\delta^{13}C$. V této studii nově, byl na $\delta^{13}C$ analyzován i zadní filtr obsahující plynou frakci. Získaná data byla následně vyhodnocena v závislosti na sezónních a meteorologických změnách. Detaily jsou uvedeny v práci Vodička a kol. (2022).

VÝSLEDKY

Obrázek 1 ukazuje průměrné sezónní hodnoty $\delta^{13}C_{WSOC}$, $\delta^{13}C_{TC}$ a celkového uhlíku v plynné fázi ($\delta^{13}C_{TCgas}$). Největší obohacení ^{13}C bylo zjištěno u WSOC, následovaného částicemi TC, zatímco největší úbytek ^{13}C byl zjištěn v plynné frakci TC. Jasný sezónní vzorec pro všechny hodnoty $\delta^{13}C$ (s nejvyššími hodnotami v zimě a nejnižšími v létě) poskytuje důkaz o přítomnosti různých zdrojů aerosolů na lokalitě během roku. Navzdory

rozdílnému sezónnímu složení uhlíkatých aerosolů byly izotopové rozdíly ($\Delta\delta^{13}C$) mezi analyzovanými objemovými částmi aerosolů a jejich fázemi během ročních období podobné. To ukazuje, že frakcionace stabilních izotopů uhlíku je převážně fyzikální proces, ve kterém chemické složení jednotlivých uhlíkatých sloučenin v celkovém aerosolu/plynné fázi nehraje hlavní roli.

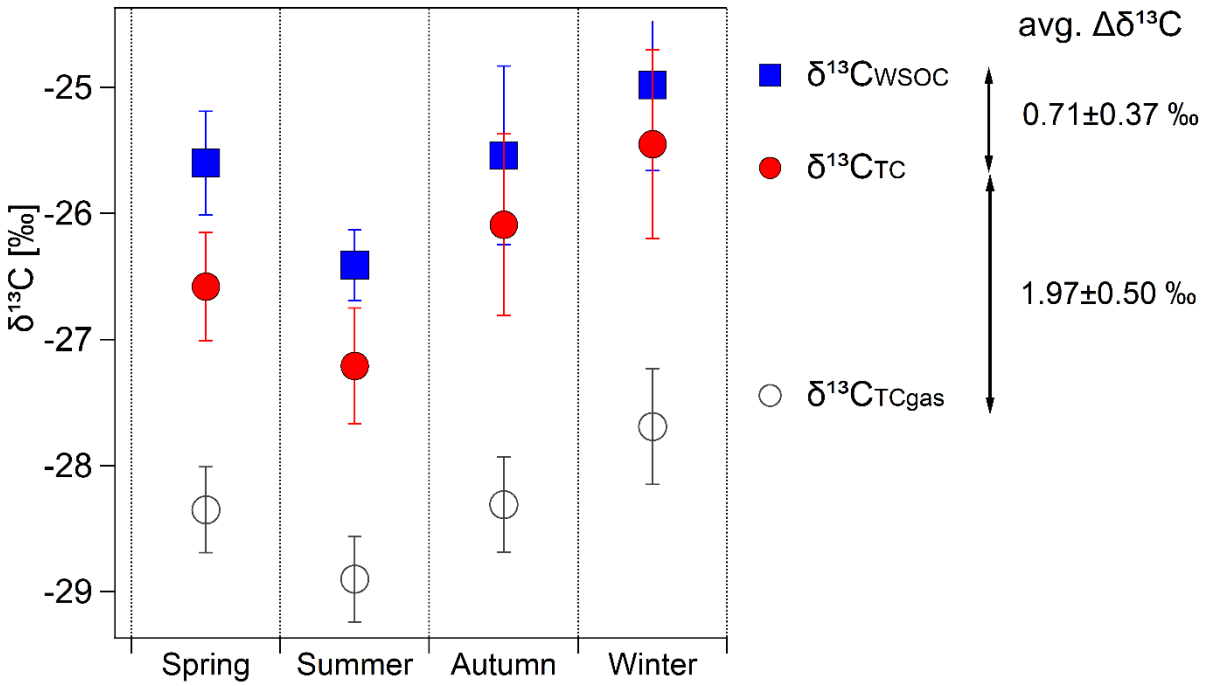

Obr. 1: Průměrné sezónní hodnoty $\delta^{13}C$ ve vodě rozpustného organického uhlíku v $PM_{2,5}$ ($\delta^{13}C_{WSOC}$), celkového uhlíku v $PM_{2,5}$ ($\delta^{13}C_{TC}$) a celkového uhlíku v plynné fázi ($\delta^{13}C_{TCgas}$).

PODĚKOVÁNÍ

Tato práce byla podpořena grantem č. 24221001 japonské společnosti JSPS (Japan Society for the Promotion of Science) a projektem MŠMT ČR v rámci grantů ACTRIS-CZ LM2018122 a ACTRIS-CZ RI (CZ.02.1 .01/0.0/0.0/16_013/0001315). Dále děkujeme ČHMÚ na poskytnutí meteorologických dat.

LITERATURA

Vodička, P., Kawamura, K., Schwarz, J., Ždímal, V. Seasonal changes in stable carbon isotopic composition in the bulk aerosol and gas phases at a suburban site in Prague. *Science of the Total Environment*, 803, 149767, (2022), https://doi.org/10.1016/j.scitotenv.2021.149767

A SEVEN-YEARS BASED CHARACTERISATION OF AEROSOL LIGHT SCATTERING PROPERTIES AT CENTRAL EUROPEAN RURAL SITE: VARIABILITY AND SOURCE APPORTIONMENT

Lenka SUCHÁNKOVÁ[1,2,3], Saliou MBENGUE[2], Nadežda ZÍKOVÁ[3], Jakub ONDRÁČEK[3], Adéla HOLUBOVÁ ŠMEJKALOVÁ[4], Roman PROKEŠ[1,2], Ivan HOLOUBEK[1,2], Vladimír ŽDÍMAL[3]

[1] RECETOX, Faculty of Science Masaryk University, Brno, Czech Republic, suchankova.l@czechglobe.cz
[2] Global Change Research Institute of the Czech Academy of Science, Brno, Czech Republic.
[3] Institute of Chemical Process Fundamentals of the CAS, Prague, Czech Republic.
[4] Czech Hydrometeorological Institute, Košetice Observatory, Košetice, Czech Republic.

Keywords: Aerosol optical properties, Scattering and backscattering coefficient, Climate change, Nephelometer, Long-term measurement, Source apportionment

INTRODUCTION

Atmospheric aerosols have a significant impact on the radiative forcing of Earth's climate, either directly through aerosol radiative interactions (ARIs), i.e., scattering or absorption of incoming solar and outgoing infrared radiation, or indirectly through aerosol-cloud interactions (ACIs) (Boucher, 2015; IPCC, 2013; Luoma et al., 2019; Ramanathan et al., 2001). The aerosol radiative forcing of the direct effect consists of a warming effect and a cooling effect (Boucher et al., 2013; Charlson et al., 1992). The predominant cooling effect results from the scattering of radiation by certain species of atmospheric aerosols (including sea salts, nitrates, sulfates, mineral and organic matter, etc.) that reduce the amount of solar radiation reaching the Earth's surface. This phenomenon offsets the greenhouse effect and alters the radiation balance (Pandolfi et al., 2018).

According to a number of studies, radiative forcing by aerosols remains one of the main sources of uncertainty in climate models estimations due to the strong spatial and temporal variations in chemical and physical properties of aerosols, their short lifetime compared to greenhouse gases, and diversity of aerosol sources (Boucher, 2015; Charlson et al., 1992; Lee et al., 2016; Luoma et al., 2019). These studies are important for a better understanding of local and long-range transport of both anthropogenic pollutants and natural aerosols and for unbiased long-term trends.

The aim of this study is to focus on the temporal variations of light-scattering properties of aerosols at a rural background site in Central Europe. The total light scattering (σ_{sp}) and backscattering (σ_{bsp}) coefficients and associated calculated optical properties such as the Ångström exponent (SAE), the backscattering ratio (b), and the asymmetry factor (g), are characterized considering different time scales (annual, seasonal, monthly, or diurnal) based on long-term measurement. The optical properties were compared with meteorological conditions (fog, cloudiness); the concentrations of gaseous pollutants such as NO_x and SO_2 were inspected as well as potential sources of atmospheric aerosols. In addition, radiative forcing, and the influence of other meteorological conditions (e.g., height of planetary boundary layer), chemical

composition and particle size distribution at the National Atmospheric Observatory Košetice (NAOK) are being further investigated to better understand the direct effects of aerosols on the local climate.

METHODS

We measured σ_{sp} and σ_{bsp} at three wavelengths (450, 550, and 700 nm) using the Integrating Nephelometer TSI 3563, equipped with a PM10 inlet and a Nafion drier. Measurements were performed at the rural background site National Atmospheric Observatory Košetice (NAOK; 49°34'20.787 "N, 15°4'48.155 "E') located in the central part of Czech Republic. Sampling was conducted at five-minute intervals from August 2012 to February 2013, and then at one-minute intervals till December 2019. All data were processed according to the standard monitoring procedure of the European Monitoring and Evaluation Program (EBAS-EMEP). Periodic control calibrations were performed with CO_2 gas and filtered air to ensure credible results. Moreover, the instrument took part in regular intercomparison exercises organized by ECAC at TROPOS.

Data processing and statistical analysis were performed using R software version 4.1.0. Data were referenced to standard conditions, *SAE* was calculated and used for correction of nonideal light source illumination and cutoff error in the near forward (0 ° -10 °) and near backward (170 ° -180 °) directions using correction factor *C* (Anderson and Ogren, 1998; Massoli et al., 2009; Müller et al., 2009). Later, *b* and *g* were calculated with all temporal variability. Potential source contribution function (PSCF) for estimation of potential aerosol sources was calculated using R software version 4.1.0.

RESULTS

The preliminary results show that the general trend for both σ_{sp} and σ_{bsp} is downward from 2012 to 2019 (Mann-Kendall test; α=0.05, $p < 0.05$; except σ_{bsp} at 700 nm). The median slopes of all aerosol light scattering properties are shown in Tab. 1.

SO_2 and NO_x concentrations were correlated with σ_{sp} and σ_{bsp} throughout the period, confirming their contribution to light scattering enhancement (Spearman correlation test; SO_2 and σ_{sp} – p=1.69e^{-08}, rho=0.557; NO_x and σ_{sp} – p=3.91e^{-13}, rho=0.678; SO_2 and σ_{bsp} – p=2.29e^{-09}, rho=0.584; NO_x and σ_{bsp} – p=5.18e^{-06}, rho=0.464).

Although σ_{sp} and σ_{bsp} decreased over time, *b* showed a positive slope of the median trend line, indicating a more efficient light backscattering with time. The possible explanation is that the chemical composition of the aerosol changed in favor of cooling (relative decrease in organic/elemental carbon concentration ratio and more scattering chemical species); therefore, aerosol particles become more effective in backscattering at lower aerosol concentrations.

Relative shift from higher to lower *SAE* values (shift to bigger particles) could be an indication of effective policies against industrial/residential emissions. The smallest particles are mainly produced directly at the source (e.g., combustion, heating) or as a product of secondary aerosol (SOA) formation. The trend leading to smaller *SAE* values signals a shift toward larger particles that may be produced by reactions of pre-existing particles in the atmosphere (so-called aerosol aging). Furthermore, long-range transport of aerosol particles might have become a more significant source of aerosol particles in NAOK.

As can be seen in Fig. 1 that σ_{sp} (and σ_{bsp}) reached higher values in the cold season than in the summer. Both σ_{sp} and σ_{bsp} dominated in February, March, and November; 63.2,

58.7, 58.0 Mm^{-1} and 8.0, 7.2 and 7.0 Mm^{-1}, respectively. This phenomenon is probably related to the higher aerosol load in winter due to higher energy consumption, poorer dispersion of pollutants, and lower altitude of the planetary mixing layer.

Tab. 1: Slopes of the annual median trends found for aerosol light scattering properties throughout 2012-2019 period.

	450 nm	**550 nm**	**700 nm**
σ_{sp} [Mm^{-1} /year]	-3.22	-2.50	- 1.03
σ_{bsp} [Mm^{-1} /year]	-0.18	-0.18	-0.09
SAE [/ year]	-0.002	-0.010	-0.018
b [/ year]	0.015	0.012	0.013
g [/ year]	-0.027	-0.021	-0.022

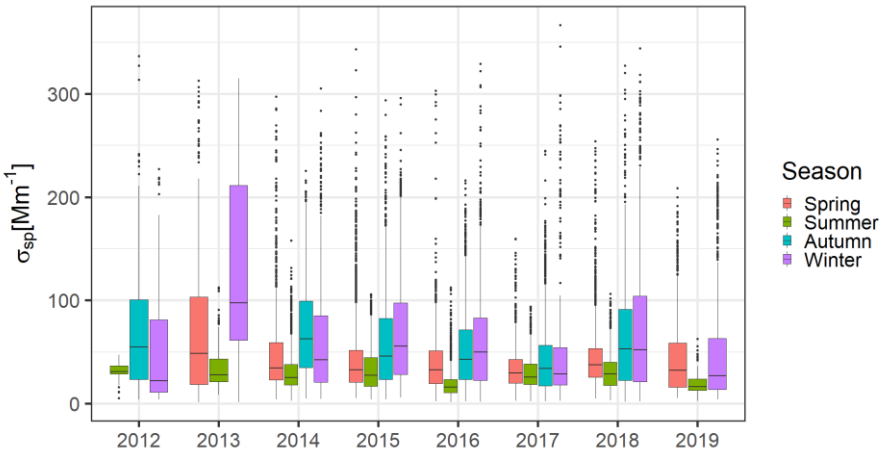

Fig. 1: The annual and seasonal variation of σ_{sp} at 550 nm. Black line represents median, solid black circles represent outliers.

The elevated levels of *SAE* in summer might indicate enhanced formation of SOA during the photochemically active season. SAE levels reached the highest monthly value 2.09 in July. This is supported by the correlation of the increase in isoprene concentration at NAOK in summer as well as by the results published in Mbengue et al. (2021, 2020). In contrast, particles remain longer in the atmosphere during the winter season and can overcome several chemical reactions during aerosol aging and thus grow, reaching the lowest monthly value of SAE in February; 1.62.

The overall annual trend of *b* is upward from 2012 to 2019 (Tab. 1) what could be explained by possible partial change in particle size and chemical composition of aerosols toward more backscattering species, e.g., secondary organic aerosols or transport of oxidized/sea-salt aerosol particles during summer, which is mainly pronounced in summer period. The maximum was observed in May, June, and July; 0.16 in all cases, and the minimum in November; 0.12.

As the *g* ranges from -1 to 1 (total backscattering to total forward scattering), the overall lowering of the *g* value shows a shift to stronger backscattering. Maximum values of *g* were observed in November, February, and March; 0.6 in all cases. Since higher values

of *g* represent a dominance of forward scattering, this suggests less backward scattering species in winter, e.g., aerosol mixtures containing carbonaceous substances. However, median values of *g* remain in the positive values for the whole inspected period indicating prevalence of forward scattering of light, which is in agreement with theoretical predictions.

The diurnal variations of σ_{sp} and σ_{bsp} were downward from midnight and reached their minimum around noon (29.6 Mm^{-1} and 4.3 Mm^{-1}, respectively) and started to increase to reach their maximum at 9 p.m. (39.58 Mm^{-1} and 5.6 Mm^{-1}, respectively). The main reason for this is the higher stability of the atmosphere and the lower planetary boundary layer during nighttime.

The daily variation of *SAE* included two maximum peaks (the smallest size), one in the early morning at 3-5 a.m.; 1.86 and the second at 1 p.m.; 1.85. The lowest SAE values were observed daily between 6 am and 8 a.m., indicating the occurrence of largest particles during this part of the day. No visible variations were observed for *b* during the week, and the median remained stable at 0.14.

The PSCF visualization of aerosol potential source identification is shown in Fig. 2. PSCF showed a higher probability of source location identification of the observed values

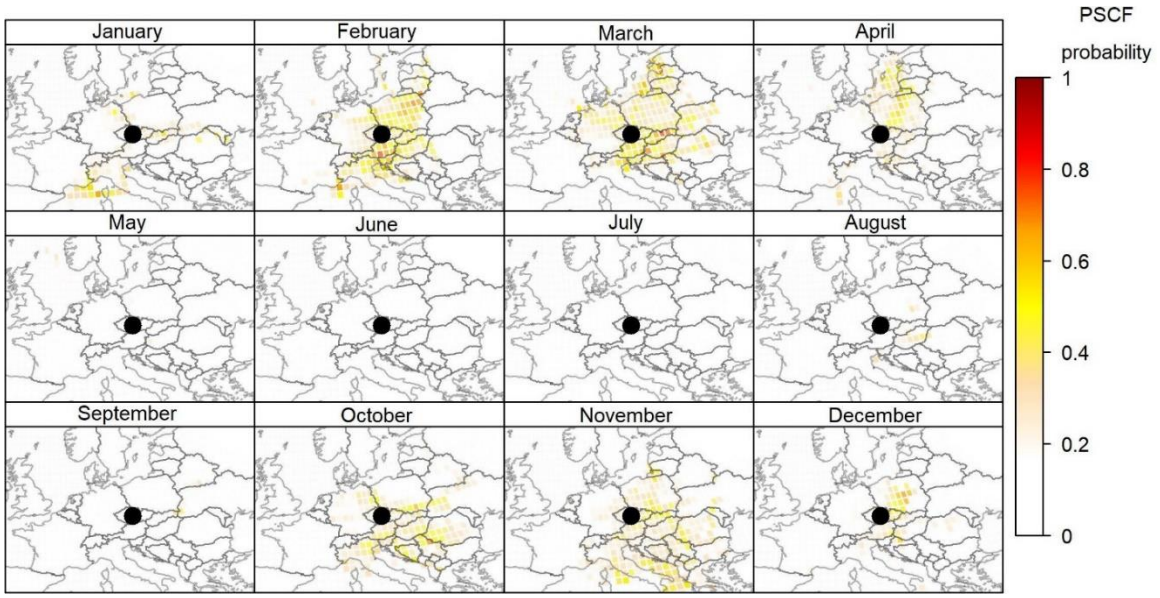

Fig. 2: PSCF of σ_{sp} at 550 nm calculated separately for different months with monthly 75th percentile as the limit value. The location of NAOK is marked with black circle.

over 75th percentile of σ_{sp} during late autumn, winter, and early spring. This probability correlates with higher σ_{sp} and σ_{bsp} levels during cold season. As the probability is not dense in any region, the results may be more by synoptic situation than potential sources of aerosols.

To compare AOP with cloudiness, we defined four categories according to WMO definition – fine F (no clouds), partly cloudy PC, cloudy C and overcast O days (completely covered sky without breaks).

Higher values of σ_{sp} and σ_{bsp} observed during O days could be caused by compressed boundary layer. However, we expect more precipitation during O days, thus removing aerosol particles from the atmosphere, which was not proven in this study. For F days, the hypothesis suggests higher solar activity and photooxidative processes in the

atmosphere causing higher production of secondary organic aerosols. At 550 nm, the σ_{sp} medians were 36.46 Mm^{-1}, 28.81 Mm^{-1}, 28.12 Mm^{-1} and 41.42 Mm^{-1} and the σ_{bsp} medians 5.47 Mm-1, 4.61 Mm-1, 4.41 Mm^{-1} and 5.52 Mm^{-1} for days F, PC, C, and O, respectively.

A study of fog influence on AOP showed increased scattering potential of aerosols during days without the fog, because the multiple-scattering of light on particles might occur during the foggy days causing decreased intensity of measured light coming to the instrumental cell.

CONCLUSIONS

In this study, we focused on temporal variations of long-term measurement of AOP at a rural site in Central Europe, as well as on the comparison with different meteorological conditions, concentration of gaseous pollutants, and source apportionment.

The overall trend of σ_{sp} and σ_{bsp} was decreasing from 2012 to 2019. Similar decreasing trend was observed for *SAE*, indicating shift to relatively bigger particles, increased *b* and decreased *g* suggests increased efficiency of backscattering at lower concentration, bigger particle size and possible change in chemical composition. Elevated *SAE* in the summer implies SOA formation, decreased *SAE* in winter denotes aerosol aging, and higher atmospheric stability. Decreased *b* in winter suggests the occurrence of atmospheric particles with lower backscattering potential, e.g., carbonaceous aerosols originating from different types of combustion. The backscattering potential was decreased during fog events (multiple scattering of light). The source identification did not show a high probability of occurrence in any of the regions, suggesting the prevalent influence of the synoptic situation over Europe more than the potential sources of aerosols.

ACKNOWLEDGEMENTS

This work was supported by the Ministry of Education, Youth and Sports of CR within the CzeCOS program, grant number LM2018123,within ACTRIS-CZ project, grant number LM201818122, within the National Sustainability Program I (NPU I), grant number LO1415, ACTRIS IMP (www.actris.eu) which is supported by the European Commission under the Horizon 2020 – Research and Innovation Framework Programme, H2020-INFRADEV-2019-2, Grant Agreement number: 871115.

REFERENCES

Anderson, T.L., Ogren, J.A., Determining Aerosol Radiative Properties Using the TSI 3563 Integrating Nephelometer, *Aerosol Sci. Technol.,* 29, 57–69, (1998).

Boucher, O., Atmospheric Aerosols, in: Atmospheric Aerosols, *Springer Netherlands, Dordrecht*, pp. 9–24, (2015).

Boucher, O., Randall, D., Artaxo, P., Bretherton, C., Feingold, G., Forster, P., Kerminen, V.-M., Kondo, Y., Liao, H., Lohmann, U., Rasch, P., Satheesh, S.K., Sherwood, S., Stevens, B., Zhang, X.Y., 2013. Clouds and Aerosols. In: Climate Change 2013: The Physical Science Basis. Contribution of Working Group I to the Fifth Assessment Report of the Intergovernmental Panel on Climate Change, *Cambridge, United Kingdom and New York, USA,* (2013).

Charlson, R.J., Schwartz, S.E., Hales, J.M., Cess, R.D., Coakley, J.A., Hansen, J.E., Hofmann, D.J., Climate forcing by anthropogenic aerosols, *Science*, 255, 423–430, (1992).

IPCC, 2013. Summary for Policymakers. In: Climate Change 2013: The Physical Science Basis. Contribution of Working Group I to the Fifth Assessment Report of the Intergovernmental Panel on Climate Change, (2013).

Lee, L.A., Reddington, C.L., Carslaw, K.S., On the relationship between aerosol model uncertainty and radiative forcing uncertainty, *Proceedings of the National Academy of Sciences*, 113, 5820–5827, (2016).

Luoma, K., Virkkula, A., Aalto, P., Petäjä, T., Kulmala, M., Over a 10-year record of aerosol optical properties at SMEAR II, *Atmos. Chem. Phys.*, 19, 11363–11382, (2019).

Massoli, P., Murphy, D.M., Lack, D.A., Baynard, T., Brock, C.A., Lovejoy, E.R., Uncertainty in Light Scattering Measurements by TSI Nephelometer: Results from Laboratory Studies and Implications for Ambient Measurements, *Aerosol Sci. Technol.*, 43, 1064–1074, (2009).

Mbengue, S., Serfozo, N., Schwarz, J., Zíková, N., Šmejkalová, A.H., Holoubek, I., Characterization of Equivalent Black Carbon at a regional background site in Central Europe: Variability and source apportionment, Environ. Pollut., 260, 1–11, (2020).

Mbengue, S., Zíková, N., Schwarz, J., Vodička, P., Šmejkalová, A.H., Holoubek, I., Mass absorption cross-section and absorption enhancement from long term black and elemental carbon measurements: A rural background station in Central Europe, Sci. Total Environ., 794, 1–14, (2021).

Müller, T., Nowak, A., Wiedensohler, A., Sheridan, P., Laborde, M., Covert, D.S., Marinoni, A., Imre, K., Henzing, B., Roger, J.C., Dos Santos, S.M., Wilhelm, R., Wang, Y.Q., De Leeuw, G., Angular illumination and truncation of three different integrating nephelometers: Implications for empirical, size-based corrections, Aerosol Sci. Technol., 43, 581–586, (2009).

Pandolfi, M., et al., A European aerosol phenomenology - 6: Scattering properties of atmospheric aerosol particles from 28 ACTRIS sites, Atmos. Chem. Phys., 18, 7877–7911, (2018).

Ramanathan, V., Crutzen, P.J., Kiehl, J.T., Rosenfeld, D., Atmosphere: Aerosols, climate, and the hydrological cycle, Science., 294, 2119–2124, (2001).

LIDAR VERTICAL PROFILE ANALYZES AT NATIONAL ATMOSPHERIC OBSERVATORY KOŠETICE DURING VOLCANO ERUPTION ON LA PALMA ISLAND

Juraj KOSTYK[1,2], Adéla HOLUBOVÁ ŠMEJKALOVÁ[1], Tomáš IŠTOK[1], Vladimír ŽDÍMAL[2]

[1] Czech Hydrometeorological Institute, Prague, Czech Republic, adela.holubova@chmi.cz
[2] Institute of Chem. Process Fundamentals, AS CR, Prague, Czech Rep., kostyk@icpf.cas.cz

Keywords: Volcano eruption, LIDAR, Scattering, Backscatter coefficient

INTRODUCTION

Volcanic eruptions are one of the most important sources of natural aerosol (Ravindra Babu et al., 2022; Tomasi et al., 2017). Their negative impacts on air quality (the effects of volcanic exhaust) can be observed via long-range transport to locations far from the eruption (Kvietkus et al., 2013; Ravindra Babu et al., 2022; Revuelta et al., 2012). One of the most recent events of volcanic activity was a volcanic eruption on La Palma in the fall of 2021 (Cumbre Vieja Volcano, La Palma Island, Canary Islands, 28°36'54 "N 17°52'07 "W, 1,949 m a.s.l.). The impact of the volcanic eruption on air quality, which occurred 3600 km from the National Atmospheric Observatory Košetice, was studied using a combination of ground-based measurements and vertical profile analyzes. Since a new instrument (LIDAR) has extended the equipment of our station, vertical profile analyzes were performed.

EXPERIMENTAL SETUP

Air quality was analyzed at the National Atmospheric Observatory Košetice (NAOK - 49°34'24 "N, 15°4'49 "E, 534 m a.s.l.) from September 1 to October 31, 2021. NAOK is a rural background station located in the Czech-Moravian Highlands, in the central part of the Czech Republic. Vertical profile characteristics were measured using LIDAR (LR211-D300, Raymetrics). The measurement principle of LIDAR is to emit a laser beam into the atmosphere, which is scattered by particles. Part of the emitted light is scattered back to the LIDAR's telescope. Based on the time it takes for the light to return, the distance of the aerosol layers can be determined. The received power due to elastic scattering can be described by the lidar equation (1) (Raymetrics SA, 2020). The meaning of the variables can be found in Baars (2007) and Baars (2011).

$$P(z) = P_o \frac{c\tau}{2} \beta(z) A_{tel} O(z) \frac{1}{z^2} \exp\left[-2 \int_0^z a(z^*) dz^* \right] \quad (1)$$

Air quality measurements were performed with automatic analyzers: SO_2 (T100U, Teledyne Advanced Pollution Instrumentation); PM_{10}, $PM_{2.5}$ (MP101M Environnement SA), Hg_0 - (2537B, Tekran), SO_4, NO_3 - custom-made sampler (according to EMEP).

RESULTS AND CONCLUSIONS

During the period studied, there were two dates when the volcano's SO_2 plume passed over central Europe – September 26 and October 20. From about 8:00 p.m. on September 26 to 3:00 a.m. on September 27, several layers at altitudes of 10-12 km were recorded by LIDAR (Fig. 1). A huge increase in the backscatter coefficient (up to $1.6 \cdot 10^{-5}$ m^{-1} sr^{-1}) was observed at altitudes of 10-12 km during 24 hours (from 25 September to 26 September) (Fig. 2).

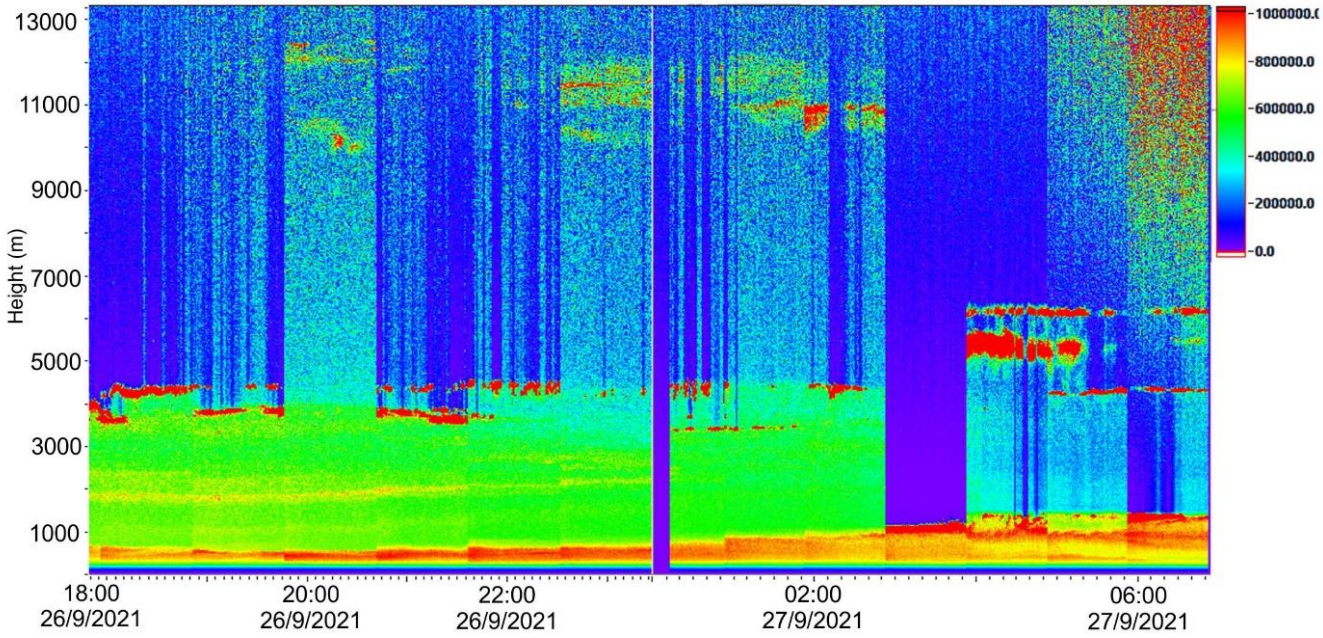

Fig. 1: Lidar measurements from 09/26/2021 to 09/27/2021. Time series of the range-corrected signal for the 355 nm channel.

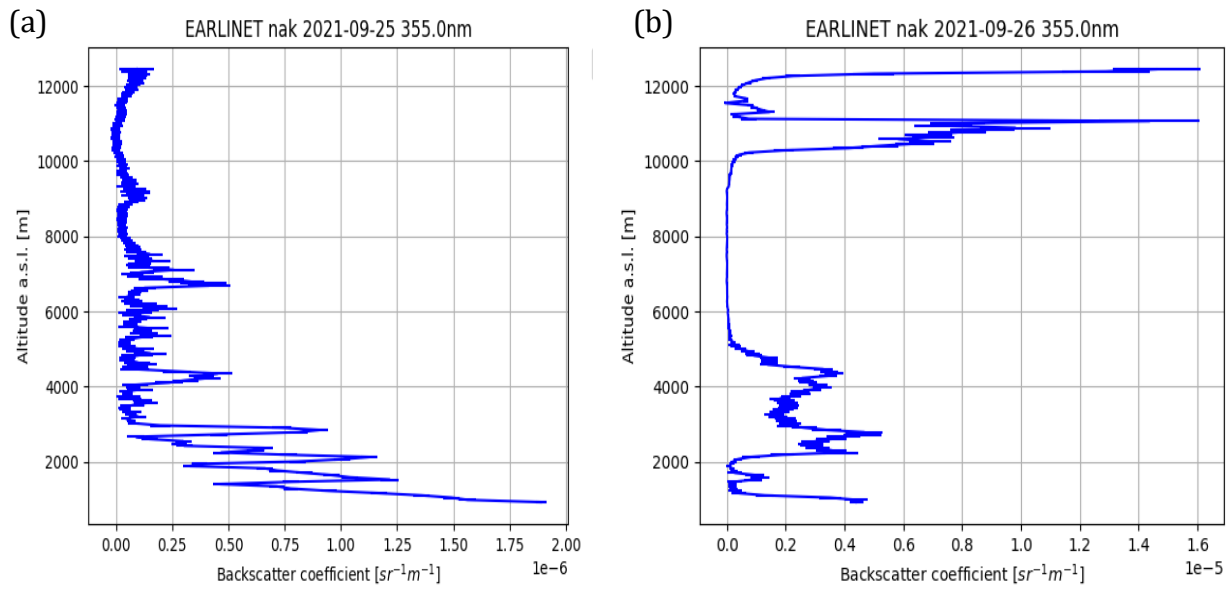

Fig. 2: 355 nm particle backscatter coefficient observed on 25 September 2021, 18:02 – 18:21 UTC (a), on 26 September 2021, 20:02 – 20:21 (b) processed in SCC platform (19 min signal average).

ACKNOWLEDGEMENT

This work was supported by the project ACTRIS-CZ LM2018122 and ACTRIS-CZ RI (CZ.02.1.01/0.0/0.0/16_013/0001315). The authors would like to thank the MARS group for their professional help and support (https://www.inoe.ro; http://environment.inoe.ro/article/261/magurele-center-for-atmosphere-and-radiation-studies-mars).

In addition, this work is part of a project supported by the European Commission under the Horizon 2020 - Research and Innovation Framework Program, H2020-INFRADEV-2019-2, Grant Agreement number: 871115; and is part of a project supported by the European Commission under the Horizon 2020 - Research and Innovation Framework Program, H2020-INFRAIA-2020-1, Grant Agreement number: 101008004.

REFERENCES

Babu, S. R., Nguyen, L. S. P., Sheu, G. R., Griffith, S. M., Pani, S. K., Huang, H. Y., & Lin, N. H., Long-range transport of La Soufrière volcanic plume to the western North Pacific: Influence on atmospheric mercury and aerosol properties. *Atmospheric Environment*, *268*, 118806 (2022).

Tomasi, C., Fuzzi, S., & Kokhanovsky, A. (Eds.). *Atmospheric aerosols: life cycles and effects on air quality and climate*. John Wiley & Sons. (2017).

Santoso, M., Lestiani, D. D., Kurniawati, S., Damastuti, E., Kusmartini, I., Atmodjo, D. P. D., Suprayadi, L. S. Assessment of urban air quality in Indonesia. *Aerosol and Air Quality Research*, 20, 2142-2158., (2020).

Kvietkus, K., Šakalys, J., Didžbalis, J., Garbarienė, I., Špirkauskaitė, N., & Remeikis, V. Atmospheric aerosol episodes over Lithuania after the May 2011 volcano eruption at Grimsvötn, Iceland. *Atmospheric research*, 122, 93-101. (2013).

Revuelta, M. A., Sastre, M., Fernández, A. J., Martín, L., García, R., Gómez-Moreno, F. J., Molero, F. Characterization of the Eyjafjallajökull volcanic plume over the Iberian Peninsula by lidar remote sensing and ground-level data collection. Atmospheric Environment, 48, 46-55. (2012).

LR211-D300 Depolarization Raman LIDAR, Raymetrics SA, (2020).

Baars, H. Continuous monitoring of the planetary-boundary-layer depth with lidar. Master's thesis, Universität Leipzig, Germany, (2007).

Baars H., Dissertation thesis, University of Leipzig. Dissertation thesis, Aerosol profiling with lidar in the Amazon Basin during wet and dry season (2011).

DYNAMIKA PROSTOROVÝCH A ČASOVÝCH ZMĚN $PM_{2,5}$ A VLIV LOKÁLNÍCH TOPENIŠŤ V OVZDUŠÍ OBCE ZADNÍ TŘEBAŇ BĚHEM TOPNÉ SEZÓNY

Karolína WALLENFELSOVÁ[1], Jan HOVORKA[1]

[1] Ústav pro životní prostředí, PřF UK, Praha, Česká republika

Klíčová slova: Aerosol, PM2.5, Malé sídlo, Topeniště na pevná paliva, Stacionární versus mobilní měření PMx, Koncentrace submikronových částic – PNC

SUMMARY

The impact of local heating on $PM_{2.5}$ concentrations monitored in a village Zadní Třebaň in Central Bohemia between 21. 12. 2021 and 3. 2. 2022 was evaluated and the effect of wind speed and temperature on $PM_{2.5}$ concentrations was examined. The $PM_{2.5}$ concentrations were measured using both stationary and mobile monitoring.

For the stationary monitoring, 7 DustTrak 8520 monitors (integration time 1 min) were used. A network of these monitors was built to cover different settlement (village edge, village center) as well as geological types of locations (valley, hill). The mobile monitoring took place 31. 1. 2022 over the course of 7 walks during which $PM_{2.5}$ and PNC concentration were measured using portable monitors (DustTrak DRX and P-Trak). The integration time for both monitors was 1 s. The aim of the mobile monitoring was to supplement knowledge gained from the stationary monitoring.

It was confirmed that at wind speeds higher than approximately 1 $m \cdot s^{-1}$) the PM concentrations started to drop significantly (to values between 4 and 12 $\mu g \cdot m^{-3}$). The PM concentrations in the village were also indirectly affected by temperature. In general, on days when the temperature was higher, PM concentrations were lower and vice versa. In case of both of these factors combining a higher PM concentrations is to be expected.

The concentration field of $PM_{2.5}$ in Zadní Třebaň was generally low, the US EPA limit was exceeded on less than 1 % of all measuring days. No sites with repeatedly high PNC values have been identified. Continually highest PNC values were measured during walk No. 7, which took place from 7 to 8 p.m.

ÚVOD

V malých obcích do 3 000 obyvatel žije přibližně třetina všech obyvatel České republiky, zároveň však data o kvalitě ovzduší v nich buď nejsou dostupná vůbec a nebo jsou nepřesná. Často může být kvalita ovzduší v malých obcích horší, než v okolních velkých městech (Braniš a Domasová, 2003). Tomuto trendu, především v zimní sezóně, přispívají lokální topeniště.

Při nepříznivých meteorologických podmínkách, jakými je nízká teplota a nízká rychlost vzduchu, může zejména v obcích v kotlinách docházet k akumulaci znečištění ze zdrojů s nízkou emisní výškou, mezi které lokální topeniště patří (Tecer a kol., 2008).

METODY MĚŘENÍ

Pro charakterizaci koncentračního pole $PM_{2,5}$ byla využita kombinace stacionárního a mobilního měření. Stacionární měření bylo realizováno pomocí sedmi nefelometrů Dust-Trak (model 8520, TSI) s impaktory pro $PM_{2,5}$, které byly rozmístěny po obci Zadní Třebaň tak, aby vytvořily rovnoměrnou měřicí síť. Stacionární měření probíhalo od 21. 12. 2021 do 3. 2. 2022. Integrační doba měření pro stacionární měření byla 1 min. Při mobilních měření byly měřeny PM1, PM2.5, PM10 a početní koncentrace submikronových částic aerosolu přístroji DustTrak (model DRX, TSI) a P-Trak (TSI). Mobilní měření proběhlo 31. 1. 2021 v rámci sedmi přibližně 3km procházek po stanovené trase v Zadní Třebani. Integrační doba měření pro mobilní měření byla nastavena na 1 s. Pro záznam polohy při mobilním měření byla použita GPS (Garmin).

Současně probíhalo také měření meteorologických podmínek, které bylo uskutečněno pomocí meteorologické stanice (model WMR300, Oregon Scientific).

VÝSLEDKY, DISKUSE, ZÁVĚRY

Celková průměrná koncentrace $PM_{2,5}$ na všech stanicích za celé období měřicí kampaně byla 14 $\mu g \cdot m^{-3}$. To je nižší hodnota než dříve naměřené průměrné koncentrace $PM_{2,5}$ v roce 2003 ve Žloukovicích, kde byla průměrná koncentrace 26 $\mu g \cdot m^{-3}$ (Braniš a kol, 2007) $PM_{2,5}$ a v letech 2009 až 2010 v Košeticích, kde byla průměrná koncentrace 22,5 $\mu g \cdot m^{-3}$ (Schwarz a kol, 2016).

Koncentrace $PM_{2,5}$ v obci byly vysoce heterogenní, a to jak časově, tak prostorově. K nejvyšším nárůstům koncentrací $PM_{2,5}$ dochází v ranních a především nočních hodinách a zároveň je možné pozorovat vyšší koncentrace $PM_{2,5}$ v centrálních částech obce. K překročení limitu US EPA pro 24h průměrné koncentrace $PM_{2,5}$ došlo za dobu měření pouze 3x z celkových 43 dní. K prvnímu překročení došlo ve dnech 22. a 23. 12. 2021 (Průběh koncentrací v noci z 22. na 23. 12. viz Obr. 1), kdy byla naměřena jedna z nejnižších teplot (-6 °C) a zároveň se jednalo o předvánoční období, můžeme tedy předpokládat, že bylo doma více lidí než v běžné pracovní dny.

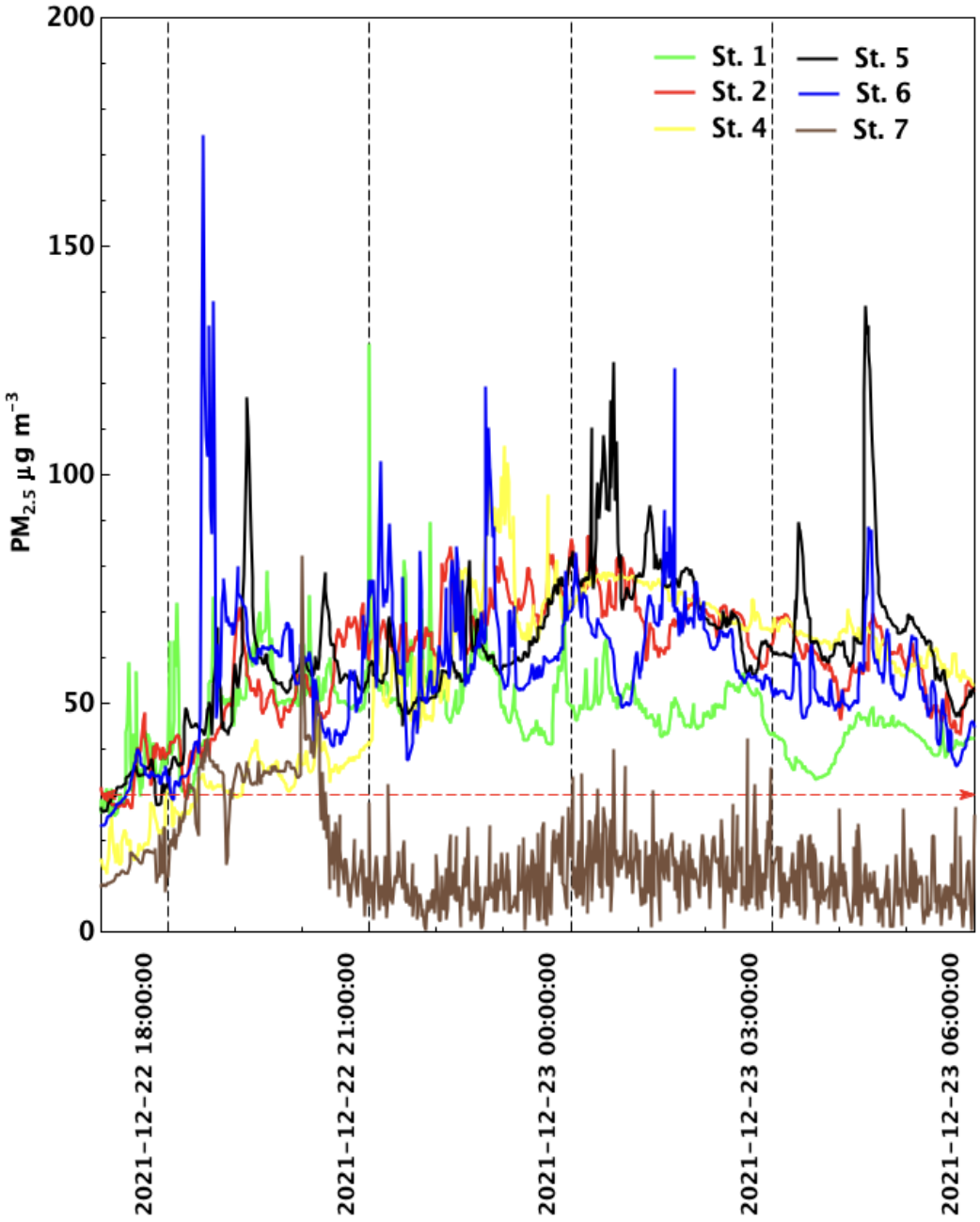

Obr. 1: Graf průběhu minutových koncentrací PM2,5 v µg m^{-3} na Stanicích 1, 2, 4, 5, 6 a 7 od 18:00 22. 12. 2021 do 6:00 23. 12. 2021.

Zároveň bylo celé období měřicí kampaně charakterizováno nízkými rychlostmi větru, které v kombinaci s nízkou teplotou vytvořily zhoršené rozptylové podmínky, a došlo tak k akumulaci $PM_{2,5}$ na území obce. Nejednalo se ale o situaci, která by byla ojedinělá v Zadní Třebani, k poklesu teploty a nárůstu koncentrací $PM_{2,5}$ došlo celorepublikově. Rychlost větru byla hlavním činitelem ovlivňujícím koncentrace $PM_{2,5}$ v obci, při rychlostech větru přibližně nad 1 $m \cdot s^{-1}$ došlo k rozmývání znečištění, a tím rychlému poklesu koncentrací $PM_{2,5}$ (Obr. 2), což bylo v souladu s výsledky studií provedených mezi lety 2013 a 2016 ve Wuhanu (Zhang a kol., 2017) a v roce 2001 v Los Angeles (Zhu a kol., 2002).

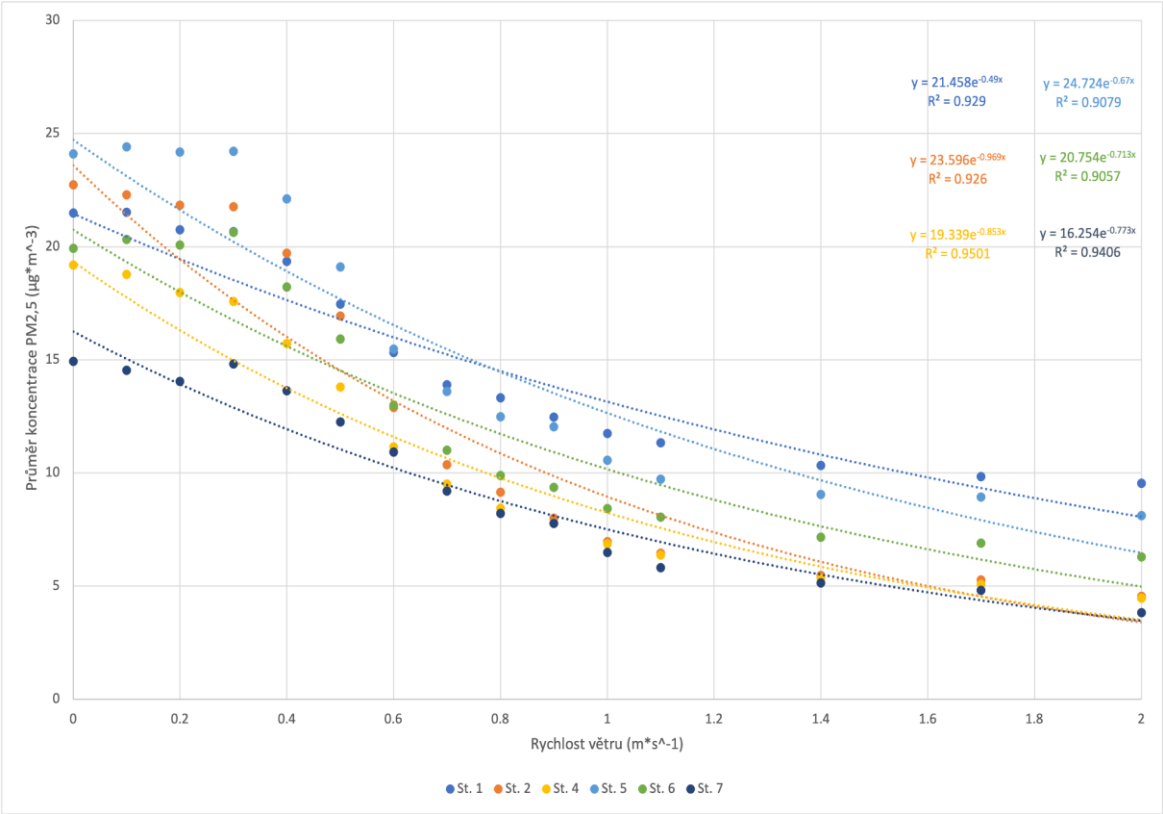

Obr. 2: Graf vlivu rychlosti větru od 0 do 2 m·s^{-1} na průměr koncentrace PM2,5 proložen křivkami lineární regrese pro každou ze Stanic 1, 2, 4, 5, 6 a 7.

Průměrná rychlost větru za celé období měřicí kampaně byla 0,7 m·s^{-1}. Nejnižší teplota v obci nastala mezi 26. a 27. 12, v tyto dny ale nedošlo k překročení limitu US EPA. Ačkoliv byla splněna podmínka nízké teploty, rychlosti větru byly v tento den vyšší než 22. a 23. 12 a jeho směr se také častěji měnil, došlo proto k rychlejšímu rozptylu $PM_{2,5}$.

Pro určení míry příspěvku lokálních topenišť na 24h průměrné hodnoty koncentračního pole $PM_{2,5}$ v obci bylo nejprve nutné stanovit pozaďové koncentrace $PM_{2,5}$ na každé z lokalit pro každý den, jelikož nebylo provedeno měření na pozaďové lokalitě (lokalita 5 – 20 km od obce, u které předpokládáme minimální ovlivnění antropogenními zdroji). Z minutových hodnot koncentrací byly pro každý den (od půlnoci do půlnoci) a každou lokalitu vypočteny 1. decily (10 % nejnižších naměřených hodnot), které byly určeny jako koncentrace pozadí (Brantley a kol., 2014).

Lokální topeniště se ukázaly být hlavním zdrojem $PM_{2,5}$ na většině měřicích stanic, průměrné příspěvky za celé měření na každé stanic viz Tab. 1.

Tab. 1: Příspěvky lokálních topenišť v $\mu g \cdot m^{-3}$ ke 24h koncentracích $PM_{2,5}$ naměřených v obci Zadní Třebaň zprůměrované pro období celé měřicí kampaně.

	St. 1	**St. 2**	**St. 3**	**St. 4**	**St. 5**
Prům. za celé měření	9	10	7	8	8

Průměrný relativní příspěvek topenišť k $PM_{2.5}$ za celé období měření na všech stanicích byl 61 %. Mobilní měření neodhalilo žádné hot spoty $PM_{2,5}$ ani PNC, byly však identifikována místa, které byly opakovaně ovlivňované různými zdroji $PM_{2,5}$. Na těchto místech se nacházely měřící přístroje stacionárního měření, které opakovaně zaznamenávaly vyšší koncentrace $PM_{2,5}$ než přístroje mimo tyto lokality.

Nutné je zmínit, že výsledky mobilního měření nemohou být vztaženy na celé období měřicí kampaně, jelikož se jedná o relativně krátký úsek měření. Stejně tak stacionární měření poskytuje údaje pouze o daném období (zima 2021).

ZÁVĚRY

Z dat získaných ze stacionárního měření koncentrací $PM_{2,5}$ na území obce Zadní Třebaň bylo zjištěno, že lokální topeniště jsou majoritním zdrojem $PM_{2,5}$ v obci v zimnímobdobí. Jejich příspěvky na celkové koncentrace $PM_{2,5}$ se pohybovaly od 48 do 72 % (průměrně 7 až 10 $\mu g \cdot m^{-3}$).

Koncentrace $PM_{2,5}$ jsou závislé na meteorologických podmínkách. S rostoucí rychlostí větru naměřené koncentrace $PM_{2,5}$ klesají, naopak s klesající teplotou rostou. Je proto možné očekávat, že stabilním charakteru počasí, kdy jsou nízké rychlosti větru a zároveň nízká teplota, budou koncentrace $PM_{2,5}$ v obci narůstat.

Mobilní měření potvrdilo časovou heterogenitu koncentrací v obci a doplnilo poznatky o prostorové heterogenitě. Ačkoliv nebyly identifikovány žádné hotspoty, byly stanoveny oblasti se zhoršenou kvalitou ovzduší. Na těchto lokalitách bylo také identifikováno nejvíce možných zdrojů $PM_{2,5}$ v podobě lokálních topenišť.

LITERATURA

Braniš, M. a Domasová, M., PM10 and black smoke in a small settlement: case study from the czech republic, *Atmospheric Environment*, 37(1), 83–92. doi: 10.1016/s1352-2310(02)00700-8, (2003).

Tecer, L. H., Süren, P., Alagha, O., Karaca, F. a Tuncel, G., Effect of meteorological parameters on fine and coarse particulate matter mass concentration in a coal-mining area in zonguldak, turkey, *Journal of the Air & Waste Management Association*, 58(4), 543–552. doi: 10.3155/1047-3289.58.4.543, (2008).

Braniš, M., Domasová, M. a Řezáčová, P., Particulate air pollution in a small settlement: The effect of local heating, *Applied Geochemistry*, 22(6), 1255–1264. ISSN 0883-2927. doi: 10.1016/j.apgeochem.2007.03.016, (2007).

Schwarz, J., Cusack, M., Karban, J., Chalupníčková, E., Havránek, V., Smolík, J. a Ždímal, V., PM2.5 chemical composition at a rural background site in central europe, including correlation and air mass back trajectory analysis, *Atmospheric Research*, 176-177, 108–120. ISSN 0169-8095. doi: 10.1016/j.atmosres. 2016.02.017, (2016).

Zhang, B., Jiao, L., Xu, G., Zhao, S., Tang, X., Zhou, Y. a Gong, C., Influences of wind and precipitation on different-sized particulate matter concentrations (PM2.5, PM10, PM2.5–10), *Meteorology and Atmospheric Physics*, 130(3), 383–392. doi: 10.1007/s00703-017-0526-9, (2017).

Zhu, Y., Hinds, W. C., Kim, S. a Sioutas, C., Concentration and size distribution of ultrafine particles near a major highway, *Journal of the Air & Waste Management Association*, 52(9), 1032–1042. doi: 10.1080/10473289.2002.10470842, (2002).

Brantley, H. L., Hagler, G. S. W., Kimbrough, E. S., Williams, R. W., Mukerjee, S. a Neas, L. M., Mobile air monitoring data-processing strategies and effects on spatial air pollution trends, *Atmospheric Measurement Techniques*, 7 (7), 2169–2183. doi: 10.5194/amt-7-2169-2014, (2014).

THE IMPACT OF THE IMO-2020 SHIPPING REGULATION ON THE ATMOSPHERIC DEPOSITION OF SULFUR AROUND THE WESTERN ENGLISH CHANNEL AND THE USE OF THE V/NI RATIO AS A SHIPPING MARKER

Laurence WINDELL[1,3], Thomas BELL[1,2], Caroline WHITE[1], Angela MILNE[1], Jaroslav SCHWARZ[3], Simon USSHER[1]

[1] Biogeochemistry Research Centre, University of Plymouth, Plymouth, UK, windell@icpf.cas.cz
[2] Plymouth Marine Laboratory, Plymouth, UK
[3] Institute of Chemical Process Fundamentals of the CAS, Prague, Czech Republic

Keywords: IMO-2020 Global sulfur cap, Shipping emissions, Sulfur, V/Ni ratio

INTRODUCTION

Anthropogenic aerosols are shown to have a great impact on marine ecosystems and human health, with the shipping industry contributing as a significant source of these emissions, and annual growth on the rise. In the marine environment, shipping emissions often dominate atmospheric deposition of sulfur. With around 70% of shipping activity being carried out within 400 km of the coast, its contribution to atmospheric sulfur is of great interest. The International Maritime Organisation (IMO) introduced a regulation on 01/01/2020 restricting global marine fuel sulfur content from 3.5% to 0.5% w/w.

The vanadium/nickel (V/Ni) ratio has been widely used as a marker of shipping emissions, with the range of 2.5 to 4 indicating shipping activity. The regulation has called into question the viability of the earlier use of the V/Ni ratio.

EXPERIMENTAL SETUP

The present study investigated the changes in marine aerosol chemical character around Penlee Point Atmospheric Observatory (PPAO; 50◦19′ N, 4◦11′ W) to gain insight into the efficacy of the IMO-2020 regulation. The observatory in Southwest England is ideally located next to a shipping lane with high marine traffic. Aerosol filter samples were collected from 2020-2021 (n=53). Filter samples were water-leached and subsequent leachates analysed for major ions using Ion Chromatography (IC), and trace elements using Inductively Coupled Plasma – Mass Spectrometry (ICP-MS). Concentrations of V/Ni and calculated non-sea-salt sulfate (nss-SO_4^{2-}) were compared to PPAO datasets from 2015-16 (n=56) and 2017-18 (n=51) respectively. Where possible, HYSPLIT air mass back trajectories were run (Stein et al., 2015).

RESULTS AND CONCLUSIONS

Trace element analysis showed a drop in median V from 2.91 pmol/m^3 to 1.44 pmol/m^3, and Ni increase from 0.95 pmol/m^3 to 4.8 pmol/m^3 with the decrease of V being in line with a similar post-IMO-2020 study in China (Guangyuan et al., 2021). Median V/Ni ratio post-IMO decreased from 3.3 to 0.28.

Post-IMO-2020 nss-SO_4^{2-} concentrations were significantly lower than pre-IMO-2020 values (n=109, $p<0.05$), which was observed throughout all classified air masses,

with total median nss-SO_4^{2-} concentration dropping from 1.35 μg/m^3 to 0.33 μg/m^3 (Fig 1.).

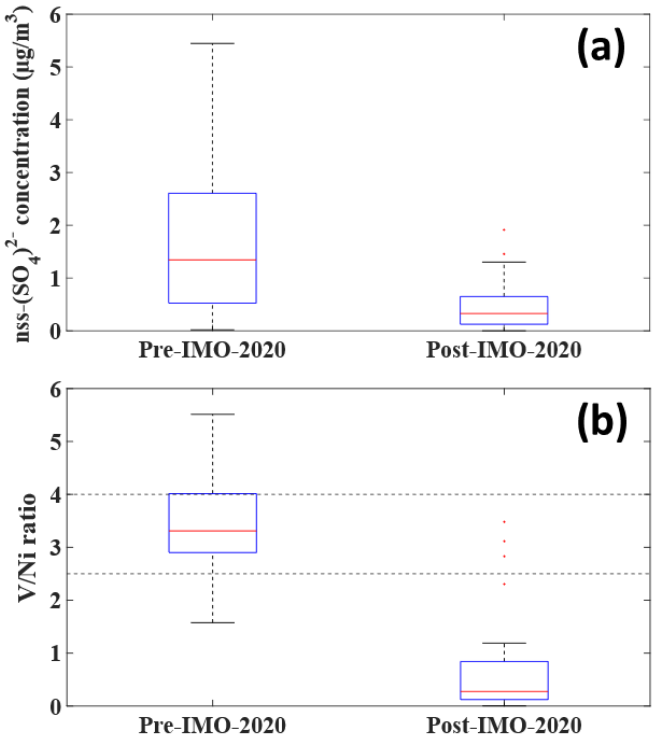

Figure 1. (a) Pre- and post-regulation nss-SO_4^{2-}, (b) Pre- and post-regulation V/Ni ratios. Horizontal lines represent previous ratio range for shipping emissions.

Results from the major ion analysis suggest great differences in marine atmospheric nss-SO_4^{2-} post-regulation, pointing towards a noticeable decrease in nss-SO_4^{2-} around PPAO, potentially influenced by the S regulation. Trace element results indicate a drastic change in V/Ni ratios, far different from the generally agreed-upon range of 2.5 to 4. The results have presented a need to further investigate the viability of the V/Ni ratio as a marker of shipping emissions, where the previous ratio must be re-evaluated.

AKNOWLEDGEMENT

The work was partially supported by MEYS of the Czech Republic under grant ACTRIS-CZ LM2018122.

REFERENCES

Yu, G., Zhang, Y., Yang, F., He, B., Zhang, C., Zou, Z., ... & Chen, J., Dynamic Ni/V Ratio in the Ship-Emitted Particles Driven by Multiphase Fuel Oil Regulations in Coastal China. *Environ. Sci. Tech.*, *55*(22), 15031-15039 (2021).

Stein, A. F., Draxler, R. R., Rolph, G. D., Stunder, B. J., Cohen, M. D., & Ngan, F., NOAA's HYSPLIT atmospheric transport and dispersion modeling system. *Bulletin of the American Meteorological Society*, *96*(12), 2059-2077(2015).

CHEMICKÉ SLOŽENÍ A ZDROJE ATMOSFÉRICKÝCH AEROSOLŮ NA POZAĎOVÉ STANICI FRÝDLANT

Radek LHOTKA[1,2], Petra POKORNÁ[1], Petr VODIČKA[1], Naděžda ZÍKOVÁ[1], Jakub ONDRÁČEK[1], Shubhi ARORA[3], Laurent POULAIN[3], Hartmut HERMANN[3], Jaroslav SCHWARZ[1], Vladimír ŽDÍMAL[1]

[1] Ústav chemických procesů, AV ČR, Praha, Česká republika, lhotka@icpf.cas.cz
[2] Ústav pro životní prostředí, PřF UK, Praha, Česká republika
[3] Leibniz-Institut für Troposphärenforschung e.V., Lipsko, Německo

Klíčová slova: Organické aerosoly, Positive matrix factorization with multi-linear engine, Nerefraktorní aerosol, Korekce na účinnost odběru

SUMMARY

This study assesses the variability of organic aerosol (OA) sources monitored at the rural background site Frýdlant. Non-refractory PM_1 was evaluated in two seasons of 2021. The positive matrix factorization with the multi-linear engine was used to determine the sources of OA at Frýdlant site, with four factors resolved both in winter and summer.

ÚVOD

Zdroje jemných atmosférických aerosolů (PM_1), resp. organických aerosolů (OA) v ovzduší Střední Evropy jsou určeny jen velmi hrubě. Cílem této práce proto bylo zhodnotit vývoj koncentrací PM_1 a OA spolu s variabilitou jejich zdrojů sledovaných na venkovské pozaďové stanici, Frýdlant (50°56´26"N, 15°4´11"E, 366 m n. m.) ve dvou obdobích roku 2021. Zimní kampaň proběhla od 17.1. do 12.3. a letní od 29.6. do 24.8.

METODY MĚŘENÍ

Měření přístrojem compact-Time of Flight-Aerosol Mass Spectrometer (c-ToF-AMS, který stanovuje v 5minutovém kroku nerefraktorní část frakce PM_1 – NR-PM_1, Drewnick a kol., 2005), byla doplněna o minutová měření ekvivalentního černého uhlíku (eBC) pomocí aethalometru (Model AE33, Magee Scientific, Berkeley, CA). Ve vodě rozpustné ionty (SO_4^{2-}) v PM_1 byly vzorkovány s 24hodinovým časovým rozlišením pomocí nízkoobjemového vzorkovače Leckel (LVS-3, IC).

Metoda positive matrix factorization (PMF) with multi-linear engine (ME-2) byla aplikována na 30minutová hmotnostní spektra organických látek měřená AMS (po aplikované korekci na účinnost odběru tzv. collection efficiency – CE pomocí SO_4^{2-} stanoveného iontovou chromatografií ve vzorku PM_1) za účelem rozdělení OA na různé faktory z hlediska jejich hmotnostních spekter a časových řad. Ke spuštění PMF i ME-2 byl využit program Source Finder (SoFi), konkrétně SoFi Pro (Canonaco a kol., 2013).

VÝSLEDKY

Celkové koncentrace PM_1 byly v létě více než 2x vyšší než v zimě. V obou sezónách tvořil OA největší podíl PM_1, v zimě byl doplněn zejména o dusičnany a v létě o sírany.

Celkové koncentrace Cl^- a eBC byly výrazně vyšší v zimě, a to zejména kvůli výraznému vlivu lokálních topenišť na kvalitu ovzduší na hodnocené stanici (Tab. 1).

Tab. 1: Použité CE, medián koncentrací sledovaných veličin ($\mu g \cdot m^{-3}$), a jejich podíl na celkové hmotě PM_1 ve srovnávaných sezónách.

	Zima (CE = 0,29)		**Léto (CE = 0,68)**	
Složka	**$\mu g \cdot m^{-3}$**	**podíl (%)**	**$\mu g \cdot m^{-3}$**	**podíl (%)**
PM_1	5,5		11,7	
OA	1,7	31	7,0	60
SO_4^{2-}	0,7	13	2,6	22
NO_3^-	1,4	26	0,6	5
NH_4^+	0,7	12	1,1	9
Cl^-	0,1	3	0,02	0,2
eBC	0,9	15	0,4	3

V programu SoFi byly pro zimní sezónu identifikovány čtyři zdroje OA. Tři z těchto zdrojů, uhlovodíkové aerosoly (hydrocarbon-like organic aerosol, HOA) spalování biomasy (biomass burning organic aerosol, BBOA) a spalování uhlí (coal combustion organic aerosol, CCOA) patří do skupiny zdrojů primárních. Poslední faktor, označený jako oxidovaný organický aerosol (oxidized organic aerosol, OOA), patří do skupiny zdrojů sekundárních. Pro letní sezónu byly identifikovány rovněž čtyři zdroje OA. Dva z těchto zdrojů byly označeny jako primární (HOA a BBOA). Sekundární zdroje byly rovněž dva, více oxidovaný organický aerosol (more oxidized organic aerosol MO-OOA) a částečně oxidovaný organický aerosol (less oxidized organic aerosol LO-OOA).

PODĚKOVÁNÍ

Tato práce byla podpořena německo-českou spoluprací v projektu TRACE, založenou na GAČR grantu 20-08304 J a DFG grantu 431895563, rovněž projektem MŠMT ČR v rámci grantů ACTRIS-CZ LM2018122 a ACTRIS-CZ RI (CZ.02.1 .01 / 0.0 / 0.0 / 16_013 / 0001315), projektem Horizont 2020 Evropské unie a výzkumným a inovačním programem ACTRIS IMP (871115). Dále děkuji zaměstnancům ČHMÚ za poskytnutí dat a všem milým kolegům z našeho oddělení Ústavu chemických procesů AV ČR za všechny poskytnuté rady, a to nejen při tvorbě tohoto příspěvku.

LITERATURA

Canonaco, F., Crippa, M., Slowik, J. G., Baltensperger, U., Prévôt, A. S. SoFi, an IGOR-based interface for the efficient use of the generalized multilinear engine (ME-2) for the source apportionment: ME-2 application to aerosol mass spectrometer data. *Atmosph. Measur. Tech.*, 6(12), 3649-3661, (2013).

Drewnick, F., Hings, S. S., DeCarlo, P., Jayne, J. T., Gonin, M., Fuhrer, K., Worsnop, D., R., A new time-of-flight aerosol mass spectrometer (TOF-AMS) —Instrument description and first field deployment. *Aeros. Science and Tech.*, 39(7), 637-658, (2005).

DYNAMIKA PROSTOROVÝCH A ČASOVÝCH ZMĚN $PM_{2.5}$ A VLIV LOKÁLNÍCH TOPENIŠŤ V OVZDUŠÍ OBCE DRUŽEC BĚHEM TOPNÉ SEZÓNY

Dominik ŠMOK[1], Jan HOVORKA[1]

[1] Ústav pro životní prostředí, PřF UK, Praha, Česká republika, smokd@natur.cuni.cz

Klíčová slova: Prostorová a časová variabilita $PM_{2.5}$, Lokální topeniště, Malé sídlo, Topná sezóna

SUMMARY

Residential heating by solid fuel combustion in small settlements has great potential to degrade air quality, especially $PM_{2.5}$ emissions, during the winter heating season, to such an extent, that WHO and US-EPA limits for $PM_{2.5}$ are frequently exceeded.

During the 14-day measuring campaign in the village Družec, Kladno district, using a stationary network of 6 monitors measuring minute concentration of $PM_{2.5}$ and a mobile measurement of PNC and $PM_{2.5}$ at 1Hz acquisition rate, there were found significant temporal variability and spatial heterogeneity of the $PM_{2.5}$ concentration field. Campaign average exceeded the 24h limit for $PM_{2.5}$ (US-EPA, 35 $\mu g \cdot m^{-3}$) at the primary school garden. In the other sites, the limit was usually exceeded occasionally except one day, when the limit exceedance was recorded in all the sites as well at the whole area of the Czech Republic. The analysis of time course of minute values of $PM_{2.5}$ shows that the residential heating increased $PM_{2.5}$ concentrations on average by 40-49% (6-10 $\mu g \cdot m^{-3}$) or 61-72% (16-25 $\mu g \cdot m^{-3}$) at background or exposed sites, respectively. $PM_{2.5}$ values decreased exponentially with wind speed up to 2 $m \cdot s^{-1}$, when they stabilized at 8-16 $\mu g \cdot m^{-3}$. At the microscale of the village, there were also found spatial and temporal heterogeneity of $PM_{2.5}$ and aerosol particle concentrations PNC. That was found by mobile measurement, during seven identical walks during one day. There were identified hot-spots for $PM_{2.5}$ with max values over 1000 $\mu g \cdot m^{-3}$. Concurrent photos of the smoking chimneys of the residential heating boilers confirmed the residential fuel combusting being the main cause of PNC and $PM_{2.5}$ variability and dominant source of $PM_{2.5}$ in ambient air in the village.

ÚVOD

Zatímco ve větších sídlech jako jsou města a velkoměsta, kde je vytápění velkého množství domovů více centralizované do tepláren, s komíny s vysokou emisní výškou, nebo je zde více alternativ k tuhým palivům či dostupnější jiné způsoby vytápění, tak naopak na venkově je stále spalování tuhých látek v lokálních topeništích hlavním zdrojem energie, a tedy i znečišťujících látek v ovzduší (Szidat a kol., 2007). V období největšího spalování tuhých látek, tedy během topné sezóny, tak dochází k vytvoření velké emisní mohutnosti znečišťujících látek z lokálních topenišť s nízkou emisní výškou, kdy se tyto emise mohou hromadit, obzvlášť během stabilního rázu počasí, v přízemní vrstvě vzduchu v obci (Wallace a kol., 2010). Může tak docházet k častému překračování zdravotně nezávadných imisních limitů určené organizacemi US-EPA nebo WHO.

Cílem této studie bylo proměřit koncentrační pole $PM_{2.5}$ během topné sezóny v obci Družec, okres Kladno, pomocí 14denní měřící kampaně (od 4. 2. 2021 do 19. 2.

2021) skládající se ze stacionárního měření minutových koncentrací $PM_{2.5}$ probíhající po celou dobu kampaně a jednodenního mobilního měření vteřinových koncentrací $PM_{2.5}$ a PNC. Ze získaných dat poté stanovit a vyhodnotit dynamiku koncentračního pole $PM_{2.5}$ v obci porovnáním s 24hod. limitem pro $PM_{2.5}$ US-EPA (35 $\mu g \cdot m^{-3}$) a určit vliv, především lokálních topenišť a meteorologických podmínek (teploty a větru), na koncentrační hladinu $PM_{2.5}$. To doplnit o zjištění z mobilního měření vteřinových koncentrací $PM_{2.5}$ a PNC, v podobě lokalizování úseků s opakovanými výraznými maximy $PM_{2.5}$, tzv. hot-spot $PM_{2.5}$, a pomocí fotografií a souběžného měření PNC určit zdroj $PM_{2.5}$.

METODY MĚŘENÍ

Stacionární měření bylo provedeno s využitím 6 nefelometrů DustTrak™ (TSI, DustTrak™ Aerosol monitor, model 8520) měřící $PM_{2.5}$ s mezí detekce 1 $\mu g \cdot m^{-3}$, rozmístěných v intravilánu obce Družec na zpřístupněných pozemcích občanů (Obr. 1). Měření meteorologických podmínek, jako je teplota vzduchu (Comet 200-80/E), rychlost a směr větru (Wind-Sonic M, Gill), relativní vlhkost, tlak a příkon radiace, bylo měřeno meteorologickou stanicí simultánně. Integrační doba měření byla 1 minuta. Stacionární síť byla koncipována tak, aby se 2 aerosolové monitory DustTrak™ nacházely ve vyšších polohách na okraji intravilánu (stanoviště 1 a 6), kde byl očekáván nejmenší vliv antropogenních zdrojů $PM_{2.5}$, tato stanoviště se měla stát pozaďovými (skutečnými pozaďovými stanovišti byla stanoviště 5 a 6).

Mobilní měření bylo provedeno s využitím nefelometru DustTrak™ DRX (TSI, DustTrak™ DRX Aerosol monitor, model 8533) měřící $PM_{2.5}$ s mezí detekce 1 $\mu g \cdot m^{-3}$, kondenzačním čítačem částic P-Trak® (TSI, P-Trak® Ultrafine Particle Counter, model 8525) měřící počet submikronových částic o velikosti 0.02 <d <1 μm (dále jen ‚PNC'') s mezí detekce 0 cm^{-3} a GPS trackerem GPSMAP® 64s (GARMIN, GPSMAP® 64s). Tyto přístroje byly umístěny v upravené krosně na zádech chodce s ústím odběrových hlavic v celkové výšce cca 2 m. Mobilní měření proběhlo formou 7 procházek po jedné trase vedoucí intravilánem a z menší části také extravilánem obce (Obr. 1). Integrační doba měření byla 1 sekunda.

Vliv lokálních topenišť na koncentrační hladinu $PM_{2.5}$ byl určen s využitím potenciálního podílu lokálních topenišť k průměrné denní koncentraci $PM_{2.5}$. Potenciální podíl lokálních topenišť k průměrné denní koncentraci $PM_{2.5}$ na stanovišti je definován jako

$$\text{Potenciální podíl} = \frac{\int_{t_1}^{t_2} c_{st.}(t)\,dt - \int_{t_1}^{t_2} c_{Q0.1\ poz.\ st.}(t)\,dt}{\int_{t_1}^{t_2} c_{st.}(t)\,dt} \qquad (1)$$

kde t_1 je čas počátku dne a t_2 čas konce dne. $c_{st.}$ (t) je koncentrace $PM_{2.5}$ na stanovišti v čase t a $c_{Q0.1\ poz.\ st.}$ (t) je decil koncentrace $PM_{2.5}$ za 24h interval na pozaďovém stanovišti s nejnižší průměrnou denní koncentrací $PM_{2.5}$ v čase t, představující, „přirozené'' pozadí ovzduší v obci (Brantley a kol., 2014). Potenciální příspěvek lokálních topenišť [$\mu g \cdot m^{-3}$] k průměrné denní koncentraci $PM_{2.5}$ na jednotlivých stanovištích byl spočten vynásobením potenciálního podílu lokálních topenišť k průměrné denní koncentraci $PM_{2.5}$ a průměrné denní koncentrace $PM_{2.5}$ na jednotlivých stanovištích. Využití této metodiky bylo provedeno za podmínek, kdy se v oblasti měření vyskytoval pouze jeden dominantní typ zdroje $PM_{2.5}$ (lokální topeniště) se zanedbatelným zasahováním jiného typu zdroje $PM_{2.5}$ (doprava). Početnost a frekvence průjezdů automobilů obcí byla v době prováděné měřící kampaně snížena i z důvodu epidemiologických opatřeních proti šíření koronaviru.

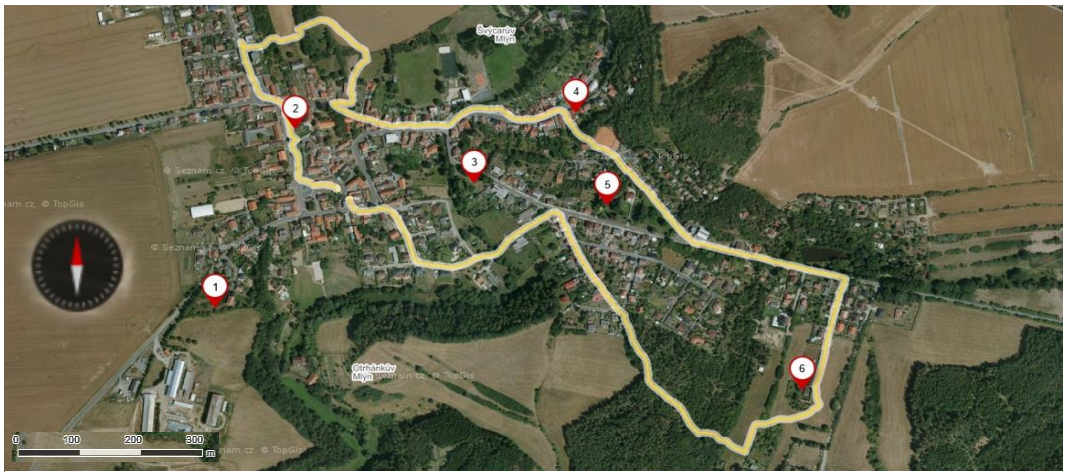

Obr. 1: Letecký snímek obce Družec s lokalizací šesti stanovišť měření $PM_{2.5}$ a trasou mobilního měření.

VÝSLEDKY A DISKUSE

Nadlimitní průměrné denní koncentrace $PM_{2.5}$ ve sledovaném období se především vyskytovaly za nízkých teplot (Obr. 2), nízké rychlosti větru (Obr. 3) a rostoucího tlaku vzduchu. V takové situaci se emise škodlivin ze zdrojů s nízkou emisní výškou hromadí v přízemní vrstvě vzduchu (Hovorka a kol., 2016). Vzniklá meteorologická situace stabilního rázu počasí potlačuje vliv dálkového transportu škodlivin (Wallace a kol., 2010; Bendl a kol., 2017).

Zároveň ale dne 15. 2. k tomuto zhoršení rozptylu škodlivin došlo i v regionálním měřítku na celém území ČR v důsledku stabilního rázu počasí, charakterizovaný nízkou oblačností a slabým větrem z důvodu výskytu tlakové výše nad střední Evropou (ČHMI, 2021).

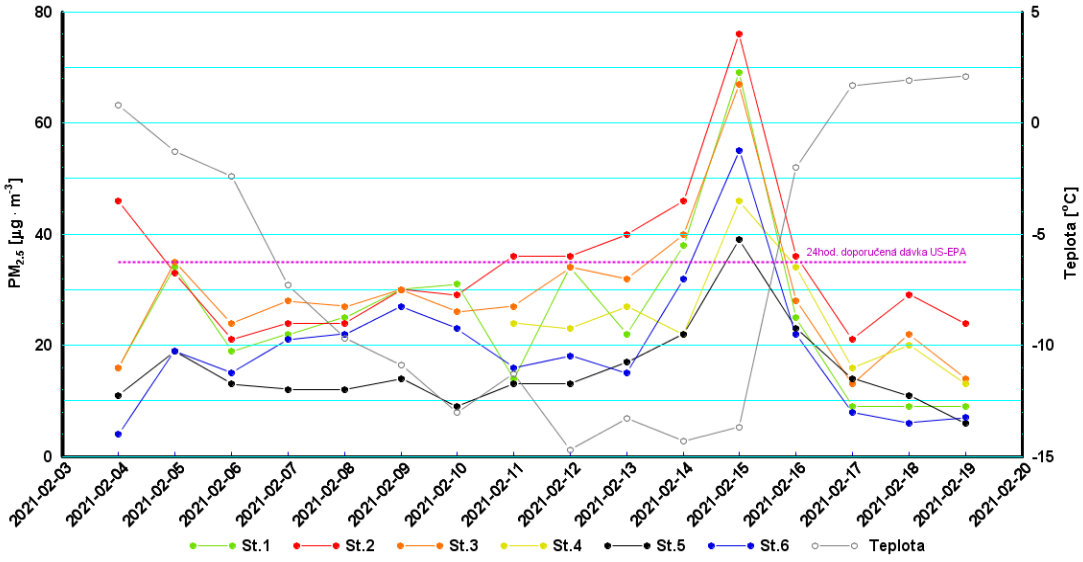

Obr. 2: Průběh průměrných denních koncentrací $PM_{2.5}$ na stanovišti 1 (zelená), 2 (červená), 3 (oranžová), 4 (žlutá), 5 (černá), 6 (modrá) a průměrné denní teploty (šedá), Družec 4. - 19. 2. 2021.

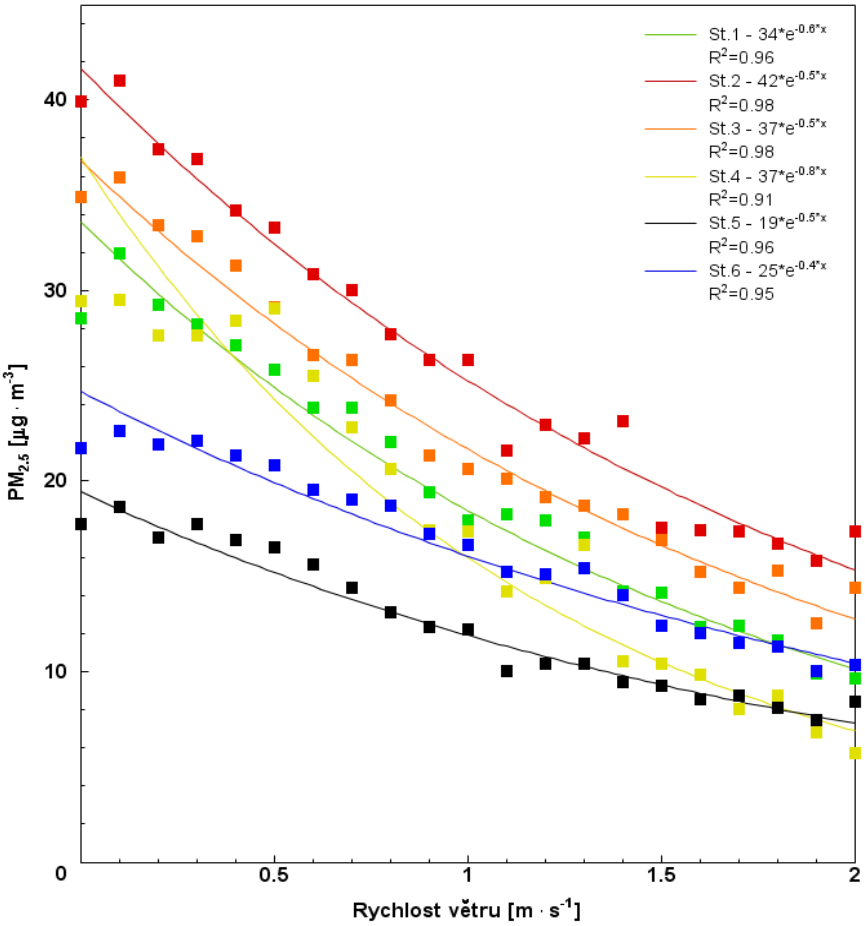

Obr. 3: Exponenciální regrese průměrné koncentrace $PM_{2.5}$ v intervalu rychlosti větru na stanovišti 1 (zelená), 2 (červená), 3 (oranžová), 4 (žlutá), 5 (černá) a 6 (modrá). Družec, 4. - 19. 2. 2021.

Průměrné denní koncentrace $PM_{2.5}$ na některých stanovištích v Družci byly v období měřící kampaně vyšší než republikové průměry $PM_{2.5}$. Důvodem tohoto zvýšení koncentrace $PM_{2.5}$ byly emise lokálních topenišť na pevná paliva, jejichž komíny ústí několik metrů nad zemí. To bylo zjištěno z časového průběhu koncentrace $PM_{2.5}$, kdy se kouřová vlečka ze zdroje $PM_{2.5}$ v krátké vzdálenosti od monitoru projevovala rychlým vzrůstem a poklesem krátkodobých vysokých koncentrací $PM_{2.5}$ (Brantley a kol., 2014). Emise z lokálních topenišť v průměru zvyšovaly koncentrace $PM_{2.5}$ ze 40-49 % na pozaďových stanovištích a ze 61-72 % na ostatních stanovištích. Tomu odpovídá zvýšení denní koncentrace $PM_{2.5}$ o 6-10 $\mu g \cdot m^{-3}$ na pozaďových stanovištích oproti 16-25 $\mu g \cdot m^{-3}$ na ostatních stanovištích (Tab. 1).

Mobilní měření bylo provedeno ke konci epizody chladného počasí, dne 15.2.2021, kdy ranní teplota klesla až na -24 °C. Během 1. a 2. procházky byly naměřeny jak nejvyšší maximální, tak i průměrné koncentrace $PM_{2.5}$ a největší místní rozdíly (Tab. 2). Během dne pak docházelo k poklesu a postupnému vyrovnání hladin koncentrací $PM_{2.5}$, započatému v čase mezi 2. a 3. procházkou, respektive mezi 10 a 11 hodinou. Vyšší hodnoty koncentrace $PM_{2.5}$ jako v ranních časech bylo opět možné naměřit v průběhu 6. a 7. procházky. Z opakování procházek vyplývá, zda k vysokému navýšení koncentrace $PM_{2.5}$ dochází opakovaně na některých úsecích, tzv. hot-spot $PM_{2.5}$. Takovýchto úseků bylo objeveno 5 a nejvyšší naměřené koncentrace $PM_{2.5}$ v těchto hot-spotech byly 10krát až 40krát vyšší, nežli je 24hod. limit US-EPA pro $PM_{2.5}$.

Tab. 1: Potenciální příspěvek [µg·m^{-3}] a podíl [%] lokálních topenišť k průměrné denní koncentraci $PM_{2.5}$ na 6 stanovištích, Družec 4. - 19. 2. 2021. NA znamená výpadek dat.

Datum	Stanoviště 1		Stanoviště 2		Stanoviště 3		Stanoviště 4		Stanoviště 5		Stanoviště 6	
	$PM_{2.5}$ [µg·m^{-3}]	[%]	$PM_{2.5}$ [µg·m^{-3}]	[%]	$PM_{2.5}$ [µg·m^{-3}]	[%]	$PM_{2.5}$ [µg·m^{-3}]	[%]	$PM_{2.5}$ [µg·m^{-3}]	[%]	$PM_{2.5}$ [µg·m^{-3}]	[%]
4.2.2021	13	81	43	94	13	81	NA	NA	8	73	1	25
5.2.2021	19	56	18	55	20	57	NA	NA	4	21	4	21
6.2.2021	7	37	9	43	12	50	NA	NA	1	8	3	20
7.2.2021	12	55	14	58	18	64	NA	NA	2	17	11	52
8.2.2021	15	60	14	58	17	63	NA	NA	2	17	12	55
9.2.2021	18	60	18	60	18	60	NA	NA	2	14	15	56
10.2.2021	23	74	21	72	18	69	NA	NA	1	11	15	65
11.2.2021	5	36	27	75	18	67	15	63	4	31	7	44
12.2.2021	31	91	33	92	31	91	20	87	10	77	15	83
13.2.2021	16	73	34	85	26	81	21	78	11	65	9	60
14.2.2021	28	74	36	78	30	75	12	55	12	55	22	69
15.2.2021	44	64	51	67	42	63	21	46	14	36	30	55
16.2.2021	13	52	24	67	16	57	22	65	11	48	10	45
17.2.2021	3	33	15	71	7	54	10	63	8	57	2	25
18.2.2021	7	78	26	90	19	86	18	90	9	82	4	67
19.2.2021	5	56	20	83	10	71	9	69	2	33	3	43
Průměr	16	61	25	72	20	68	16	68	6	40	10	49

Tab. 2: Začátek, konec, maximální, minimální, průměrná a medián koncentrace $PM_{2.5}$ během jednotlivých procházek, Družec 15. 2. 2021.

Procházka	Začátek	Konec	Max. $PM_{2.5}$ [$\mu g \cdot m^{-3}$]	Min. $PM_{2.5}$ [$\mu g \cdot m^{-3}$]	Průměr $PM_{2.5}$ [$\mu g \cdot m^{-3}$]	Medián $PM_{2.5}$ [$\mu g \cdot m^{-3}$]
1	6:52	7:40	1334	73	136	118
2	8:54	9:40	881	131	226	211
3	11:01	11:47	282	60	102	88
4	12:40	13:30	257	69	84	81
5	14:48	15:40	380	94	123	117
6	17:03	18:00	487	88	133	117
7	19:04	20:02	697	107	150	195

ZÁVĚR

Stacionární měření v obci Družec odhalilo výraznou heterogenitu koncentračního pole $PM_{2.5}$ v prostoru a čase, zapříčiněnou zejména provozem lokálních topenišť na tuhá paliva. Během špatným rozptylových podmínek, charakterizovaných nízkou rychlostí větru a nízkou teplotou vzduchu, docházelo ke zvýraznění heterogenity koncentračního pole $PM_{2.5}$, a k běžnému překračování 24hod. limitu US-EPA pro $PM_{2.5}$ v obci. Zároveň bylo odhaleno, že i hluboko v intravilánu obce lze mít ovzduší s nízkými koncentracemi $PM_{2.5}$.

Měření minutových koncentrací $PM_{2.5}$ ze stacionárního měření neodhalí variabilitu koncentračního pole $PM_{2.5}$ v mikroměřítku obce v okamžiku měření, k tomu bylo využito mobilní měření vteřinových koncentrací $PM_{2.5}$, které rozšířilo náhled do zmíněného mikroměřítka obce a výsledky měřící kampaně obohatilo o úseky opakovaných vysokých koncentrací $PM_{2.5}$, hot-spoty $PM_{2.5}$. Společně s dokumentováním mobilního měření byla lokální topeniště potvrzena jako dominantní zdroj $PM_{2.5}$ v obci.

LITERATURA

Bendl, J., & Hovorka, J. Temperature and Relative Humidity Vertical Profiles within Planetary. IOP Conference Series: *Earth and Environmental Science*, 95, p. 052003. doi:10.1088/1755-1315/95/5/052003, (2017).

Brantley, H., Hagler, G., Kimbrough, E., Williams, R., Mukerjee, S., & Neal, L. Mobile air monitoring data-processing strategies and effects on spatial air pollution trends. *Atmospheric Measurement Techniques*, 7(7), pp. 2169-2183. doi:10.5194/amt-7-2169-2014, (2014).

ČHMI. Český Hydrometeorologický institut. Retrieved April 17, 2022, from Kvalita ovzduší na území České republiky, únor 2021: https://www.chmi.cz/files/portal/docs/uoco/mes_zpravy/UNOR_2021.pdf, (2021).

Hovorka, J., Cecilia, L., Dočekalová, V., Ondráček, J., & Zíková, N. Aerosol Distribution in The Planetary Boundary Layer Aloft a Residential Area. IOP Conference Series: *Earth and Environmental Science*, 44, p. 052017. doi:10.1088/1755-1315/44/5/052017, (2016).

Szidat, S., Prévôt, A., Sandradewi, J., Alfarra, M., Synal, H.-A., Wacker, L., & Baltensperger, U. Dominant impact of residential wood burning on particulate matter in Alpine valleys during winter. Geophysical Research Letters, 34(5). doi:https://doi.org/10.1029/2006GL028325, (2007).

THE STORY OF TEAMWORK AND THE BIRTH OF THE FFP3* (FILTER BACKPACK)

Max FRAENKL[1], Milos KRBAL[1], Jakub HOUDEK[1], Zuzana ZMRHALOVA[1], Borivoj PROKES[1], Petr HEJDA[1], Stanislav SLANG[1], Jan PRIKRYL[1], Jakub ONDRACEK[2], Otakar MAKES[2], Juraj KOSTYK[2], Petr NASADIL[3], Pavel MALCIK[3], Vladimir ZDIMAL[2], Miroslav VLCEK[1]

[1] Center of Materials and Nanotechnologies, Faculty of Chemical Technology, University of Pardubice, Nam. Cs. Legii 565, Pardubice, 53002, Czech Republic, Max.Fraenkl@upce.cz
[2] Institute of Chemical Process Fundamentals, v.v.i., Academy of Sciences of the Czech Republic, Rozvojova 135, 16502, Prague, Czech Republic
[3] Textile Testing Institute, Cejl 480/12, 60200, Brno, Czech Republic

Keywords: COVID-19, Filtration efficiency, Regeneration, Reusable, Low-cost, PPE

INTRODUCTION

Soon after the outbreak of the coronavirus crisis in the Czech Republic and the first lockdown (2020), we enthusiastically decided to fight the coronavirus with scientific means. Originally materials engineers, we decided to develop an effective protective respiratory device, which was in short supply at the time. We soon found out; (1) that every textile material (handkerchief 10%) has a certain ability to catch an aerosol particle carrying the corona virus, (2) the slower the aerosol particle (d<300 nm) passes through the filter, the greater the chance it has of being caught, (3) with the thickness of the filter, the amount of passed particles decreases exponentially and breathing resistance increases linearly. On this basis, we decided to experiment with a large-area filter placed on the user's back (it wouldn't fit anywhere else) and commercially available textile filter material.

EXPERIMENTAL SETUP

We chose the filter material from commonly available textile materials. The two candidates included cotton (T-shirt) and polyester knit with a fleece finish (blanket). A filter cartridge with an area of 1200 cm^2 was assembled from both filter materials, which is eight times the area of the respirator. Filter efficiency and pressure drop at an air flow of 95 lpm (hard physical work) were tested for the cartridge set up in this way.

Subsequently, we optimized the size and useful properties of the filter cartridge. We assembled 25 filter cartridges with an area corresponding to (1, 2, 4, 6 and 8 times the size of the mask) with 1, 2, 4, 6 and 8 layers of knit polyester fleece. The selected filter cartridge, which resembled the book "2nd edition Aerosol Technology-W.C.Hinds" in size, was placed in a backpack and connected to a rubber half-mask with hoses. The resulting filter set (Fig. 1) was subjected to a pressure drop test and a 1000 m run.

Fig. 1: A) cartridge frame before wrapping with fleece polyester knit, B) filter set, C) diagram of the filter cartridge in the backpack

RESULTS AND CONCLUSIONS

Already the first assembled filter in April 2020 showed a high filtration efficiency (95%) when using a knit polyester fleece as the filter material. Knit polyester fleece has been shown to have a similar Q factor (ratio of aerosol passed to pressure drop) as nonwovens used for filtration (Zhao et al. 2020, Fraenkl et al. 2022). The results of the filtration efficiency measurements for the 25 cartridges we set up are shown in Fig. 2 (Fraenkl et al. 2022). The optimum for use in the filtration set was a cartridge with an area of 900 cm^2 whose size resolved filtration efficiency can be found in Figure 3 (Fraenkl et al. 2022).

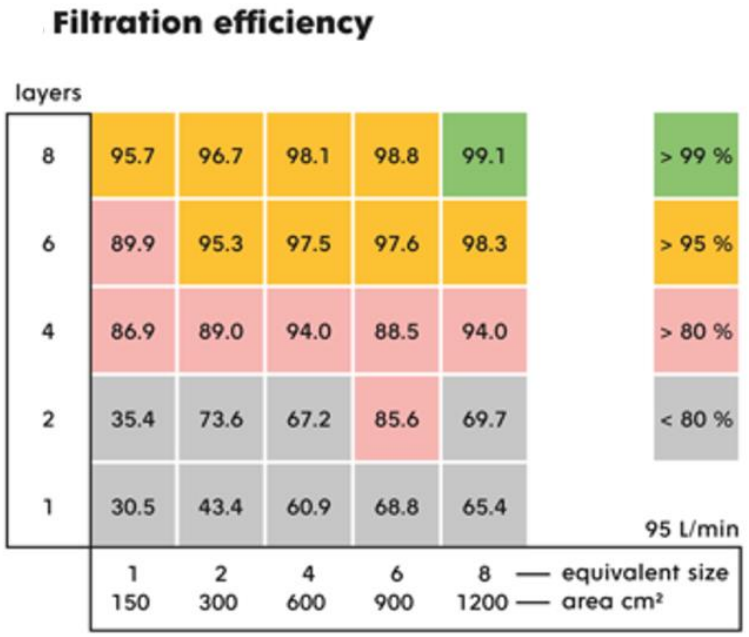

Fig. 2 shows the filtration ability of the PES fabric depending on the filter area, which was varied as multiples of the area of 150 cm^2 (the size of the mask) and the number of layers of filter material (adapted from Fraenkl et al. 2022).

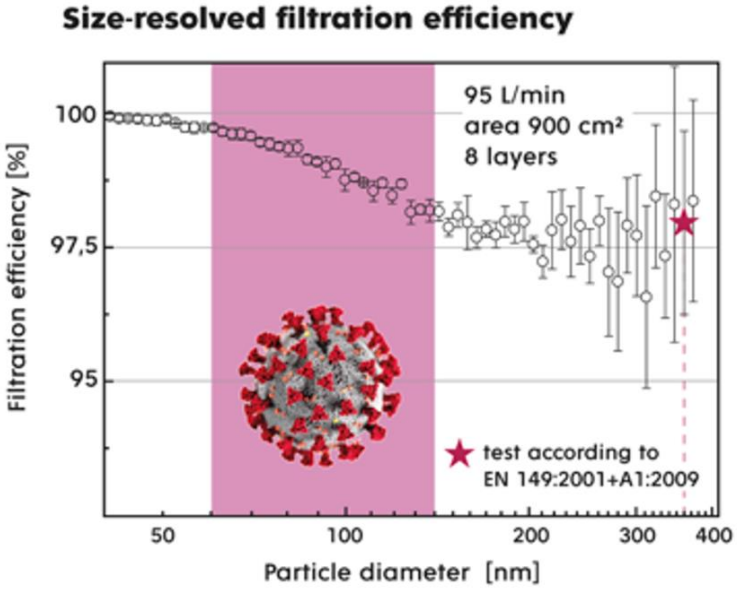

Fig. 3 shows the experimental curve of the filtration efficiency as a function of the particle diameter for the filter cartridge six times the size of a standard mask (900 cm^2) with eight layers of PES fabric. A red star represents a measurement of accredited laboratory VÚBP.

The assembled filter kit shows a low pressure loss of 84 Pa at a flow rate of 95 lpm, while only a quarter of about 19 Pa falls on the filter cartridge, the rest on the hose and half mask (Fig. 4). Low pressure loss means easier breathing and less bypass air.

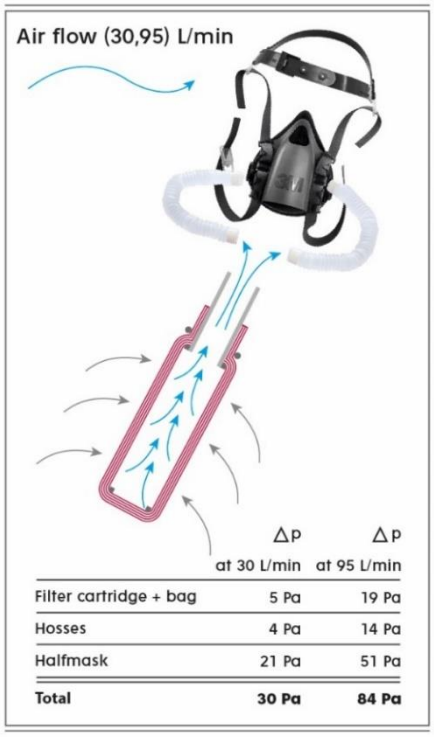

	ΔP at 30 L/min	ΔP at 95 L/min
Filter cartridge + bag	5 Pa	19 Pa
Hosses	4 Pa	14 Pa
Halfmask	21 Pa	51 Pa
Total	**30 Pa**	**84 Pa**

Fig. 4 shows the pressure drop of the filter kit and its components at volumetric flow rates of 30 and 95 L/min, which correspond to air inhalation during light and heavy physical exercise, respectively. The cross-section of the filter cartridge is shown.

According to a Canadian study, the filtering kit we designed shows better results in terms of pressure loss and filtration efficiency than 41 out of 43 commercially available respirators according to a Canadian study from 2020 (Brochot and Bahloul 2022).

A big advantage of the filtering kit is the "unlimited" lifetime. Fleece knit is a mechanically resistant material. As we have shown, compared to filters made of non-woven fabrics, polyester fleece knit can be regenerated very simply by boiling or washing (at least 10 times) without loss of filtration efficiency (Fraenkl et al. 2022).

Because it can be easily regenerated, our proposed solution has the potential to reduce the environmental impact and simplify access to high-quality respiratory protective devices for health care workers, especially in low-and middle-income countries or in crisis situations.

ACKNOWLEDGEMENT

This work was supported by the Ministry of Youth, Education and Sports of the Czech Republic (projects no. LM2018103 and LM201822) and Ministry of Interior of the Czech Republic, project No. VI04000048.

REFERENCES

Zhao M, Liao L, Xiao W, Yu X, Wang H, Wang Q, et al. Household Materials Selection for Homemade Cloth Face Coverings and Their Filtration Efficiency Enhancement with Triboelectric Charging. *Nano Lett.*;20: 5544–5552. doi:10.1021/acs.nanolett.0c02211, (2020).

Fraenkl M, Krbal M, Houdek J, Zmrhalova Z, Prokes B, et al. High-quality and easy-to-regenerate personal filter. *PLOS ONE*, (2022).

Brochot C, Bahloul A. Qualitative Knowledge of Filtering Facepiece. J *Int Soc Respir Prot.*;37, No. 2: 94–107, (2020).

METHOD AND INSTRUMENTATION FOR DIRECT MEASUREMENT OF CORROSIVE SPECIES FROM COMBUSTION

Erkki LAMMINEN[1], Oskari VAINIO[1], Markus NIKKA[1]

[1] Dekati Ltd., Kangasala, Finland, oskari.vainio@dekati.fi

Keywords: Sample conditioning, Aerosol measurement, Instrumentation, Combustion

INTRODUCTION

Climate change and reduction of CO_2 emissions drives the need to replace fossil fuels, especially coal from use in power generation. This change presents known challenges for power plant operators. Power plants that fire biofuel or waste have been shown to suffer from boiler and heat exchanger surface degradation due to corrosion. This problem can be mitigated using additives, co-firing of biomass and coal or lowering combustion temperature. These methods aim to eliminate the formation or adsorb the corrosive species. Evaluating the effectiveness has been mainly carried out by inspecting the boiler and heat exchanger surfaces after some time of operation, which makes optimization of the process slow and expensive. In this work, we present instrumentation and a method how to measure the corrosive species directly from combustion zone. In addition, we will present measurement results from using this method in a modern biomass power plant.

EXPERIMENTAL SETUP

The used instrumentation can be divided into two parts, the sample conditioning system and the measurement instrumentation. The key component of the sample conditioning system is a patented high temperature probe, which allows sampling from up to 1200 °C. The high temperature probe (Fig. 1) operates as follows: A high temperature sample is drawn from combustion zone into the probe where it is immediately diluted, and the temperature is dropped to ~200-400 °C in a controlled fashion.

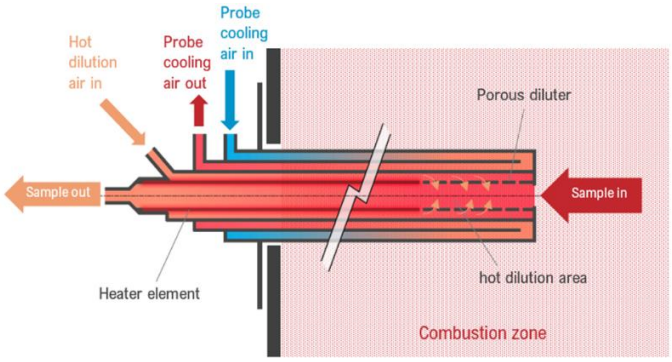

Fig. 1: Dekati High Temperature Probe operating principle

This temperature drop is similar to what happens on boiler and heat exchanger surfaces. In the high temperature probe however, the corrosive species are captured in particulate form instead of depositing on surfaces. The high temperature probe is

followed by the Dekati eDiluter Pro, which acts as the pump of the sample conditioning system and further dilutes the sample while dropping the sample temperature to ambient level. The diluted sample is then measured with the Dekati Electrical Low-Pressure Impactor (ELPI+) which measures the particulate concentration and size distribution from 6nm to 10µm in real time (Järvinen et al., 2014). It has been found in previous studies that if corrosive species are present, they form a distinctive nucleation mode which can be measured with the ELPI+ instrument. Subsequent chemical analysis is typically used to understand the source and nature of the corrosive species. Chemical analysis can be carried out from samples collected on the ELPI+ collection substrates or from a parallel gravimetric collection instrument.

RESULTS AND CONCLUSIONS

The High Resolution ELPI+ particle size distribution results from a modern biomass power plant (Fig. 2) showed significant differences between different load points, especially for the relative size of the nucleation mode.

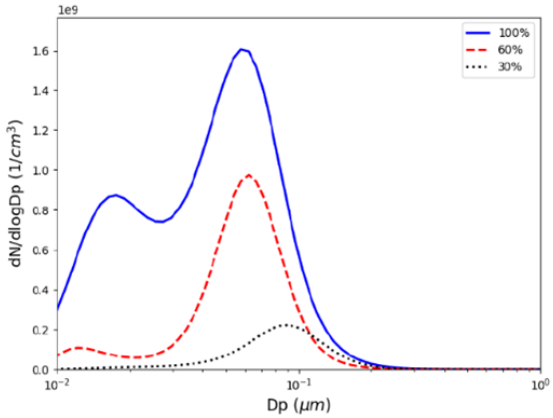

Fig. 2: High Resolution ELPI+ distributions of three load points

The proposed method and instrumentation allow fast tuning of process parameters with the aim to reduce the use of additives and coal in co-combustion, while increasing the combustion temperature. Therefore, the overall efficiency of the plant can be increased while reducing the harmful effects of corrosion. Using this method in the modern biomass power plant showed the effect of combustion zone sampling location and power plant load on concentration and size of produced particulates.

ACKNOWLEDGEMENT

The measurement campaign at the modern biomass power plant in Helsinki was done in co-operation with Tampere University, Finnish Meteorological Institute and Valmet.

REFERENCES

Järvinen, A., Aitomaa, M., Rostedt, A., Keskinen, J. Yli-Ojanperä, J., Calibration of the new electrical low-pressure impactor (ELPI+). *J. Aerosol Sci.*, 69, 150-159, (2014).

10LETÉ MONITOROVÁNÍ OXIDAČNÍHO STRESU U OSOB PROFESIONÁLNĚ EXPONOVANÝCH NANOČÁSTICÍM POMOCÍ NEINVAZIVNÍCH METOD

Daniela PELCLOVÁ[1], Vladimír ŽDÍMAL[2]

[1] Klinika pracovního lékařství 1. LF UK a VFN Praha, Česká republika, daniela@pelclova.cz
[2] Ústav chemických procesů, AV ČR, Praha, Česká republika,

Klíčová slova: Monitorování, Nanočástice, Oxidační stres, Pracovníci

SUMMARY

The long-term effects of exposure to nanoparticles in humans are not known, and experimental data suggest oxidative stress and cellular damage. In practice, there is a lack of guidelines for biomonitoring the effects of worker exposure to nanoparticles. Over the past 10 years, our group has studied oxidative stress markers in several exposed groups of workers. Aerosol exposure has been monitored during the following work activities: nanoTiO_2 production (2012 and 2013), Fe oxide pigment production (2013), and nanocomposites research (2016-2020). Both online and offline instruments were used for the studies, including the Berner Low Pressure Cascade Impactor (BLPI), gravimetric analysis, Scanning Mobility Particle Sizer (SMPS), Aerodynamic Particle Sizer (APS), Condensation Particle Counter (CPC), and other instruments as described in our publications.

Elemental contents were analyzed by scanning electron microscopy/energy dispersive X-ray spectroscopy (SEM /EDS). The total particle number concentration ranged from $1.98x10^4$ to $5.4x10^5$/cm3 and the nanoparticle fraction was 40-95%. Panels of oxidative stress biomarkers in the form of lipids, nucleic acids and protein damage were analyzed in exhaled breath condensate (EBC), plasma and urine pre-shift and post-shift using liquid chromatography-electrospray ionization tandem mass spectrometry (LC-ESI-MS /MS). Markers for oxidation of lipids, nucleic acids, and proteins in EBC and plasma were already elevated in pre-shift samples ($p < 0.05$) of workers compared to controls and showed additional post-shift elevation. The best time to collect all samples is post-shift at the end of the work week. Then, markers of oxidative stress in all three biological fluids, including urine, reflect both acute (cross-shift) and chronic effects of exposure.

ÚVOD

Zdravotní účinky expozice nanočásticím na člověka nejsou dosud známy, experimentální údaje dokumentují oxidační stres a poškození buněk v souladu s nálezem zvýšených markerů oxidačního u pacientů se silikózou plic a nemocemi z azbestu, tedy s expozicí prokázaným karcinogenům pro člověka (Pelclova et al. 2007, 2008). Přes rychle rostoucí počet osob exponovaných nanočásticím je počet publikací velmi nízký a zcela chybí doporučené postupy pro biomonitoring vlivu expozice nanočásticím na pracovníky (Liou et al. 2017).

METODY

Během posledních 10 let studovala naše skupina markery oxidačního stresu v biologickém materiálu u několika skupin exponovaných pracovníků. Expozice aerosolu byly měřeny u těchto pracovních operací: výroba pigmentů nanoTiO_2 (2012 a 2013),

výroba pigmentů Fe-oxidů (2013) a výzkum a příprava nanokompozitních materiálů (2016-2020). Souběžně byli v roce 2013 vyšetřeni zaměstnanci z kanceláří, kontrolující provoz v dílnách s TiO2 po 15 min pracovní doby denně, a ve všech letech také srovnatelně velké kontrolní skupiny ze stejné lokality bez expozice nanomateriálům.

V kondenzátu vydechovaného vzduchu, plazmě a moči byly analyzovány biomarkery oxidativního stresu z poškození lipidů malondialdehyd (MDA) a 8-isoProstaglandinF2α (8-isoprostan); markery oxidace nukleových kyselin 8-hydroxy-2-deoxyguanosin (8-OHdG), 8-hydroxyguanosin (8-OHG), a 5-hydroxymethyl uracil (5-OHMeU); a markery poškození proteinů o-tyrosin (o-Tyr), 3-chlorotyrosin (3-CLTyr) a 3-nitrotyrosin (3-NOTyr).

Tab. 1 Charakteristika vyšetřovaných osob a základní parametry expozice.

	Počet osob	Věk	Podíl nano částic	Doba expozice /den	Hmotnostní koncentrace (medián) mg/m³	Početní koncentrace (medián) No/cm³
TiO_2 2012 dělníci	20	34±8	80 %	7,5 hod	0,65	19 800
TiO_2 2013 dělníci	14	34±5	80 %	7,5 hod	0,40	23 200
TiO_2 2013 úředníci	22	44±4	80 %	15 min	0,40	23 200
Fe-oxidy 2013 dělníci	14	43±8	80 %	7,5 hod	0,083	66 800
Nanokompozity výzkumníci 2016-2018	61	40±12	40-95 %	3,0 hod	0,12-1,84	48 000-540 000
Kontroly 2012-2018	Srovnatelný počet osob, věk, pohlaví			Bez expozice nanočásticím		

VÝSLEDKY A DISKUSE

Údaje o expozici jsou uvedeny v Tab. 1. Markery oxidace lipidů, nukleových kyselin a proteinů byly zvýšeny v biologických vzorcích od pracovníků již před směnou ($p<0,05$) ve srovnání s kontrolními osobami. Efekt byl ještě výraznější po směně, kde byly zvýšeny markery u všech skupin osob proti kontrolní skupině (Pelclova et al., 2020). Jedinou výjimkou byl 8-isoprostan u pracovníků z kanceláří provozu TiO_2, i zde však marker vykazoval obdobný trend, viz Obr. 1.

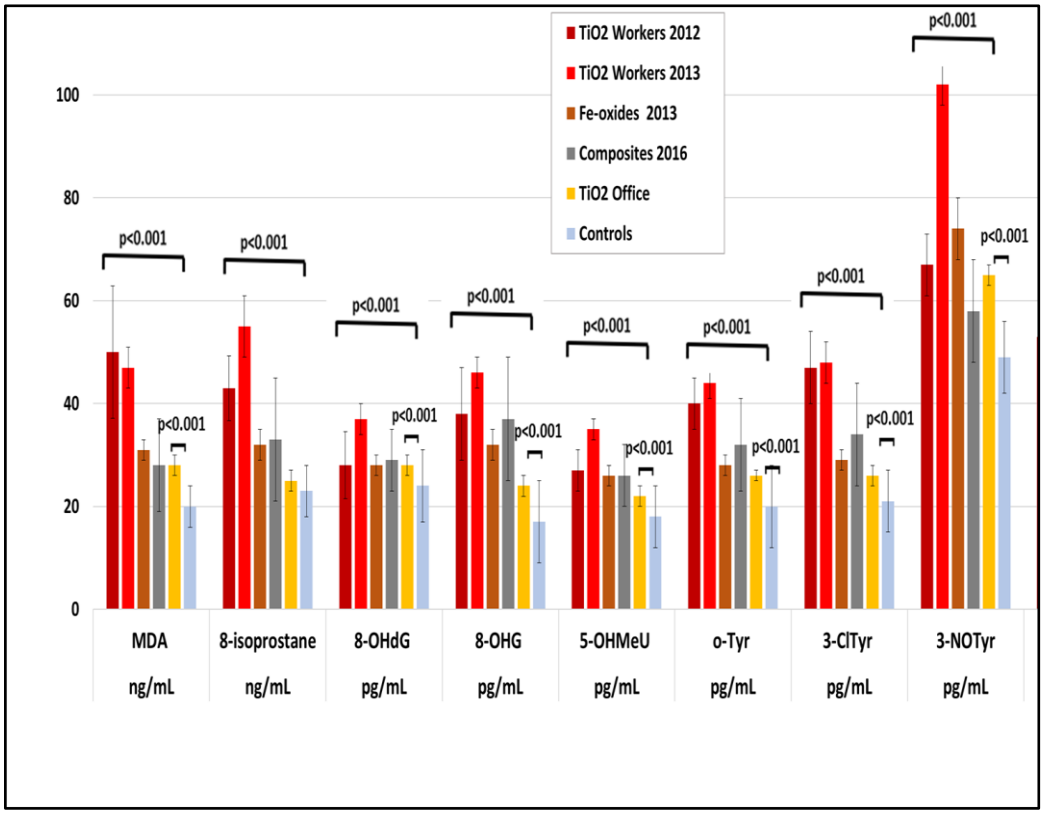

Obr 1: Markery oxidačního stresu v kondenzátu vydechovaného vzduchu u profesionálně exponovaných skupin pracovníků na konci pracovní směny a v kontrolní skupině. MDA = malondialdehyd, 8-isoprostane = 8-isoProstaglandinF2α, 8-OHdG = 8-hydroxy-2-deoxyguanosin, 8-OHG = 8-hydroxyguanosin, 5-OHMeU = 5-hydroxymethyl uracil, o-Tyr = o-tyrosin, 3-ClTyr = 3-chlorotyrosin, 3-NOTyr = 3-nitrotyrosin.
Vzorky moči vykazovaly stejný trend, avšak bez statistické významnosti a bez zvýšení po směně. Naše data byla porovnána se studiemi jiných výzkumníků a EBC a plazmatické markery oxidačního stresu měřené vysoce citlivými metodami LC-ESI-MS/MS souhlasily s našimi daty a vykázaly nárůst ihned po směně (Wu et al. 2021), na rozdíl od markerů v moči, které se zvyšují až o 24-více hodin později (Zhang et al. 2022).

ZÁVĚRY

Markery oxidačního stresu mohou být dostupnou metodou k monitorování efektu při inhalaci nanočásticím v pracovním prostředí, lze přitom využít neinvazivního odběru tekutin. Vzhledem k experimentálním studiím i výsledkům studií u pacientů s inhalační expozicí karcinogennímu SiO_2 a azbestu je potřebné monitorovat expozici kromě měření aerosolů v ovzduší také tímto expozičním testem z biologického materiálu. Minimální velikost skupiny je 20 pracovníků a 20 kontrolních osob ze stejné lokality. Doporučujeme vyšetřit alespoň jeden marker oxidace lipidů, nukleových kyselin a proteinů. Vhodné načasování je po směně na konci týdne, kdy markery oxidačního stresu ve všech třech biologických tekutinách odrážejí jak akutní, tak chronický efekt expozice.

PODĚKOVÁNÍ

Autoři děkují grantům GAČR 22-08358S, NANOEX2 a Cooperatio 207041-3 Univerzity Karlovy v Praze

LITERATURA

Liou, S. H., Wu, W. T., Liao, H. Y., Chen, C. Y., Tsai, C. Y., Jung, W. T., Lee, H. L., Global DNA methylation and oxidative stress biomarkers in workers exposed to metal oxide nanoparticles. J. Hazard Mater., 331, 329–335, (2017).

Pelclova, D., Fenclova, Z., Kacer, P., Navrátil, T., Kuzma, M., Lebedova, J., Klusackova, P., 8-isoprostane and leukotrienes in exhaled breath condensate in Czech subjects with silicosis. Ind. Health., 5, 766-74, (2007).

Pelclova, D., Fenclova, Z., Kacer, P., Kuzma, M., Navratil, T., Lebedova, J., Increased 8-isoprostane, marker of oxidative stress in EBC in asbestos exposure. Ind. Health, 46, 484–489, (2008).

Pelclova, D., Zdimal, V., Komarc, M., Schwarz, J., Ondracek, J., Ondrackova, L., ¨ Kostejn, M., Vlckova, S., Fenclova, Z., Dvorackova, S., Lischkova, L., Klusackova, P., Kolesnikova, V., Rossnerova, A., Navratil, T. , Three-Year Study of Markers of Oxidative Stress in Exhaled Breath Condensate in Workers Producing Nanocomposites, Extended by Plasma and Urine Analysis in Last Two Years. Nanomaterials (Basel), 10, 2440, (2020).

Wu, W. T., Jung, W. T., Lee, H. L., Lipid peroxidation metabolites associated with biomarkers of inflammation and oxidation stress in workers handling carbon nanotubes and metal oxide nanoparticles. Nanotoxicology, 15, 577–587, (2021).

Zhang, Y., Bello, A., Ryan, D. K., Demokritou, P., Bello, D. , Elevated Urinary Biomarkers of Oxidative Damage in Photocopier Operators following Acute and Chronic Exposures. Nanomaterials (Basel), 12, 715, (2022).

TOTAL AND BIOACCESSIBLE FRACTION OF ELEMENTS IN URBAN AEROSOL

Pavel MIKUŠKA[1], Hana CIGÁNKOVÁ[1], Jitka HEGROVÁ[2]

[1] Institute of Analytical Chemistry of the CAS, v. v. i., Brno, Czech Republic,
mikuska@iach.cz
[2] Transport Research Center (CDV), Brno, Czech Republic

Keywords: Aerosol, Elements, Bioaccessible fraction, PM_1, $PM_{2.5}$

INTRODUCTION

Atmospheric aerosols (Particulate Matter, PM) have significant impact on health and environment. Elements constitute an important particulate component which have received the attention to understand their environmental and health impacts (Witt M. L. I., 2010; Li, 2013). Elements enter the human body through inhalation of aerosols causing several health issue (asthma, cardiovascular and respiratory diseases, lung cancer).

The potential health effects of elements in PM depend on their toxicity, concentration, and bioaccessibility. It is assumed that the bioaccessible fraction of elements is more relevant for evaluating human health risks than the total concentration of elements (Cigánková et al., 2021a).

The aim of this study was to determine the total and bioaccessible concentration of elements in urban PM_1 and $PM_{2.5}$ aerosol during four seasons.

EXPERIMENTAL SETUP

PM_1 and $PM_{2.5}$ aerosols were sampled in parallel using two high-volume samplers (DHA-80 and DHA-77, Digitel, air flow 30 m^3/h) for 48 hours on nitrocellulose membrane filters (diameter 150 mm, porosity 3 μm, Sartorius). Sampling took place during four 2-week campaigns within each season of 2018.

Aerosol mass concentration was determined gravimetrically based on the difference in weight of the filters before and after sampling of aerosol.

The sampled aerosol filters were cut into 4 portions. The first part of the filter was decomposed in nitric acid using microwave decomposition (UltraWAVE, Milestone) and digests were analyzed for the total content of 22 elements (Cu, Pb, Cd, Mn, Fe, Cr, V, Co, Na, K, Al, Ca, Ni, Ti, Sr, As, Se, Mo, Sn, Sb, Ba, Zn) by triple quadrupole ICP-MS (ICP-MS 8800, Agilent). The other three quarters of each filter were extracted for 24 hours in three simulated lung fluids, i.e. deionized water (DW), Gamble solution (GS) and Simulated alveoli fluid (SAF) to determine the bioaccessible fraction of analysed elements using atomic absorption spectroscopy (AAnalyst 600, Perkin Elmer) or ICP-MS.

RESULTS AND CONCLUSIONS

The highest mass concentrations of both PM_1 and PM2.5 aerosol were observed in winter (Cigánková et al., 2021a).

The highest total concentration of most elements in PM_1 and $PM_{2.5}$ aerosol was found

in winter campaign (Cigánková et al., 2021b). PM_1 and $PM_{2.5}$ aerosols were also analysed for the bioaccessible content of elements in DW, GS and SAF (Fig. 1).

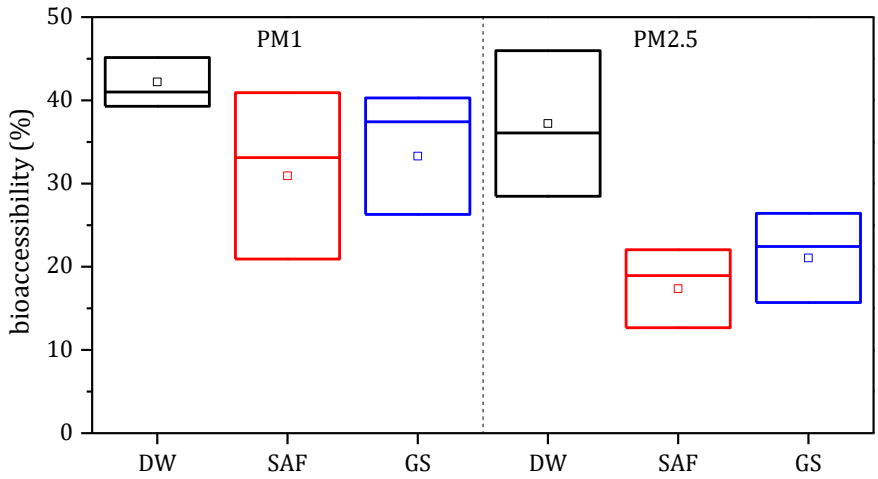

Fig. 1: Annual mean (square) and median (line) bioacessibility of sums of studied elements in DW, GS and SAF

ACKNOWLEDGEMENT

The authors thank the grant of the Czech Science Foundation P503/20/02203S. This work was also eleborated with financial support of the Ministry of Education, Youth and Sports within the National Sustainability Programme I, project of Transport R&D Centre (LO1610) and on the research infrastructure acquired from the Operation Programme Research and Development for Innovations (CZ.1.05/2.1.00/03.0064).

REFERENCES

Cigánková H., Mikuška P., Hegrová J., Krajčovič J., Comparison of oxidative potential of PM1 and PM2.5 urban aerosol and bioaccessibility of associated elements in three simulated lung fluids. *Sci. Total Environ.*, 800, 149502 (2021a).

Cigánková H., Mikuška P., Hegrová J., Pokorná P., Schwarz J., Krajčovič J., Seasonal variation and sources of elements in urban submicron and fine aerosol in Brno, Czech Republic. *Aerosol Air Qual. Res.*, 21, 200556 (2021b).

Li H., Qian X., Wang Q., Heavy metals in atmospheric particulate matter: A comprehensive understanding is needed for monitoring and risk mitigation, *Environ. Sci. Technol.*, 47, 13210-13211, (2013).

Witt M. L. I., Meheran N., Mather T. A., de Hoog J. M. C., Pyle D. M., Aerosol trace metals, particle morphology and total gaseous mercury in the atmosphere of Oxford, UK, *Atmos. Environ.*, 44, 1524-1538, (2010).

OXIDATIVE POTENTIAL OF PM1 AND PM2.5 URBAN AEROSOL AND ASSOCIATED ELEMENTS IN THREE SIMULATED LUNG FLUIDS

Hana CIGÁNKOVÁ[1], Pavel MIKUŠKA[1], Jitka HEGROVÁ[2]

[1] Institute of Analytical Chemistry of the CAS, v. v i., Brno, Czech Republic, cigankova@iach.cz
[2] Transport Research Center (CDV), Brno, Czech Republic

Keywords: Aerosol, Oxidative potential, Elements

INTRODUCTION

Mass concentration of particulate matter (PM) has been used in several epidemiologic studies as an indicatior conenecting PM concentrations with human health effects (Ostro, 1993). However, mass concentration of PM doesn´t consider the different compositions and toxicological effects of its components. Majority of PM mass constitutes low-toxicity components, while minority of trace components may have high toxicological activity (Tonne, 2012).

Oxidative potential (OP), defined as the ability of PM to induce oxidative stress, is in recent years recognized as one of the main biological mechanisms considered to be contributing to negative impacts from air pollution exposure. Oxidative stress is caused through the capability of PM to generate reactive oxygen species (ROS) within the lung, which leads to pro-inflammatory responses that can ultimately results in cell apoptosis (Borlaza, 2021).

EXPERIMENTAL SETUP

Aerosol (PM1, PM2.5) samples were collected in parallel using two high-volume samplers (DHA-80 and DHA-77, Digitel, air flow rate 30 m^3/h) for 48 hours on nitrocellulose membrane filters (diameter 150 mm, porosity 3 μm, Sartorius). Sampling took place during four 2-week campaigns in 2018 in Brno.

The sampled aerosol filters were cut into 4 portions. The first portion was analyzed for total metal content. The other three portions of the filter were extracted in three simulated lung fluis (SLFs; deionized water, Gamble solution, Simulated alveoli fluid) for 24 hours to determine the bioaccessibility of elements bound to PM and the OP of PM.

The OP was determined by a dithiothreitol (DTT) assay. An aliquot of each extract was incubated at 37 °C with DTT (100 μM; 1 mL total volume) for different times (7, 15, 30, 45, 60 and 90 min). 10% trichloroacetic acid (1 mL) was added to the mixture at the designated times to stop the DTT reaction. After incubation, 1 mL of 0.4 M Tris-HCl, containing 20 mM EDTA and 25 μL of 10 mM 5,5′-dithiobis-2-nitrobenzoic acid (DTNB) was added to 0.5 mL of the reaction mixture to react with the remaining DTT. The concentration of the formed 2-nitro-5-mercapto-benzoic acid was measured using a UV-VIS spectrometer (DU 250, Beckman) at wavelength 412 nm.

The OP of standard solutions of Cu^{2+}, Cu^{+}, Mn^{2+}, V^{5+}, Co^{2+}, Ni^{2+}, Cr^{3+}, Fe^{2+}, Fe^{3+}, As^{5+}, As^{3+}, Pb^{2+}, Zn^{2+}, Cd^{2+}, Al^{3+}, Ba^{2+}, Ca^{2+}, K^{+}, Mg^{2+}, Na^{+}, Sn^{2+}, Se^{2+}, Se^{4+}, Sr^{2+} and Hg^{2+} was also determined by DTT assay.

RESULTS AND CONCLUSIONS

The oxidative potential of the PM1 fraction was higher than that of the PM2.5 fraction (Fig. 1). Of the measured standard solutions, Cu^{2+}, Mn^{2+}, Fe^{3+} and, Zn^{2+} contributed the most to the OP of PM. Other elements contributed less (Cd^{2+}, Fe^{2+} V^{5+}, Co^{2+}, Ni^{2+}, Cr^{3+}, As^{5+}, Pb^{2+}) or not at all (Al^{3+}, Ba^{2+}, Ca^{2+}, K^{+}, Mg^{2+}, Na^{+}, Sn^{2+}, Se^{2+}, Se^{4+}, Sr^{2+}, Hg^{2+}, Cu^{+} and As^{3+}).

The OP of both PM size fractions, and standard solutions depended on the used SLF. The OP was the highest for filters extracted into deionized water (Fig. 1), which is the simplest SLF. The lower oxidative potential of PM and standard solutions in GS and SAF was probably caused by the interactions between some components of the fluids and redox-active components of the PM.

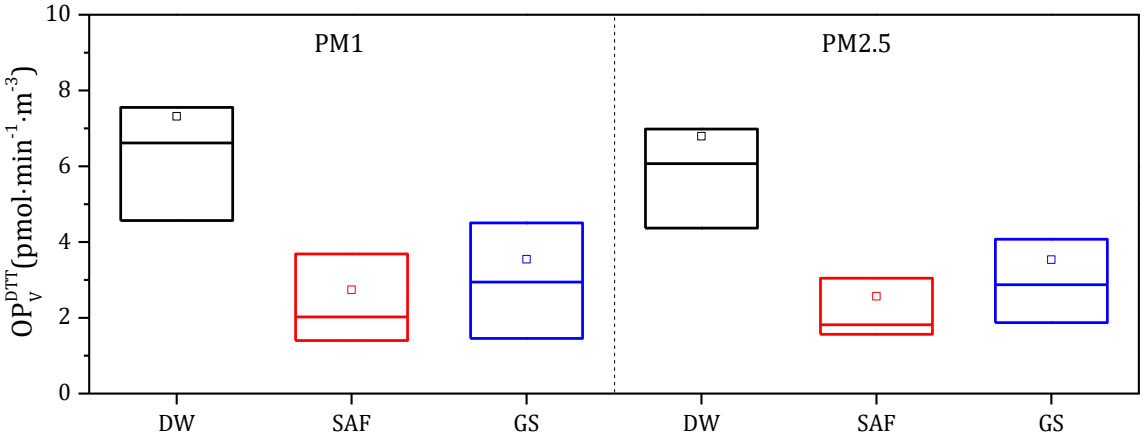

Fig. 2: Annual mean (square) and median (line) oxidative potetial of PM1 and PM2.5 aerosol in DW, SAF and GS.

ACKNOWLEDGEMENT

The authors thank the grant of the Czech Science Foundation P503/20/02203S. This work was also eleborated with financial support of the Ministry of Education, Youth and Sports within the National Sustainability Programme I, project of Transport R&D Centre (LO1610) and on the research infrastructure acquired from the Operation Programme Research and Development for Innovations (CZ.1.05/2.1.00/03.0064).

REFERENCES

Ostro B., The association of air pollution and mortality: exhamin the case for inference, *Arch. Environ. Health.,* 48, 5, 336-342, (1993).

Tonne, C., Yanosky, J. D., Beevers, S., Wilkinson, P., Kelly F. J., PM mass concentration and ¨ PM oxidative potential in relation to carotid intima-media thickness, *Epidemiology*, 23, 3, 486-494. (2012).

Borlaza, L. J. S., Weber, S., Jaffrezo, J.-L., Houdier, S., Slama, R., Rieux, C., Albinet, A., Micallef, S., Trébluchon, C., Uzu, G., Disparities in particulate matter (PM10) origins and oxidative potential at a city scale (Grenoble, France) – Part 2: Sources of PM10 oxidative potential using multiple linear regression analysis and the predictive applicability of multilayer perceptron neural network analysis, *Atmos. Chem. Phys.,* 21, 12, 9719-9732, (2021).

ORGANICKÉ SLOUČENINY A MARKERY ZE SPALOVÁNÍ DŘEVA V KOTLÍCH POUŽÍVANÝCH PRO VYTÁPĚNÍ DOMÁCNOSTÍ

Kamil KŘŮMAL[1], Pavel MIKUŠKA[1], Jiří HORÁK[2], Miroslav JAROCH[2], František HOPAN[2], Lenka KUBOŇOVÁ[2]

[1] Ústav analytické chemie AV ČR, v. v. i., Veveří 97, 602 00 Brno, krumal@iach.cz
[2] VŠB – Technická univerzita Ostrava, Výzkumné energetické centrum, 17. listopadu 15/2172, Ostrava-Poruba

Klíčová slova: domovní vytápění, spalování dřeva, levoglukosan

SUMMARY

Organic compounds (polycyclic aromatic hydrocarbons) and organic markers (monosaccharide anhydrides, diterpenoids) used for the identification of aerosol emission sources were measured in the emissions from the combustion of hard and soft wood. Wood was combusted in different boilers used for the residential heating in the Czech Republic, i.e., overfire boiler, boiler with down-draft combustion, gasification boiler and automatic boiler. Emission factors of particles and all measured organic compounds were the highest from the combustion of fuels in the oldest (overfire) boiler.

ÚVOD

Jedním z hlavních zdrojů aerosolových částic v ovzduší jsou spalovací procesy. Významnými zástupci těchto zdrojů jsou malá spalovací zařízení (MSZ) používaná k vytápění domácností během zimního období. Problémem MSZ je nízká výška komínů, která způsobuje hromadění aerosolových částic v dýchací zóně obyvatel měst a obcí. Tato zařízení také nemají žádné čištění spalin (filtry) a neplatí pro ně obdobné kontrolní a regulační mechanismy jako pro velké zdroje znečišťování ovzduší. Vysoká koncentrace aerosolových částic v ovzduší ovlivňuje lidské zdraví. Škodlivost aerosolových částic souvisí s jejich depozicí v dýchacím traktu. Hlavní cestou vstupu aerosolu do organismu jsou dýchací cesty. Hrubé částice jsou zadržovány v horních cestách dýchacích, zatímco jemné částice (PM2,5) pronikají hlouběji do plic, průdušek a plicních sklípků (Křůmal a kol., 2012). Bylo potvrzeno, že dlouhodobá expozice částicím snižuje obranyschopnost člověka (Brunekreef a Holgate, 2002). Aerosolové částice na sebe vážou toxické a karcinogenní sloučeniny, jako jsou například polycyklické aromatické uhlovodíky, polychlorované bifenyly a ostatní organochlorové sloučeniny, těžké kovy a další polutanty (Křůmal a kol., 2012), které se po depozici v plicích mohou z částic uvolňovat a pronikat do organismu.

Převážná část znečišťujících látek z MSZ je do ovzduší emitována během topné sezóny v zimním období. Samotná topná sezóna trvá cca 5 měsíců, takže reálný podíl MSZ na aktuálním lokálním znečištění během topné sezóny je podstatně vyšší, než jsou uváděné průměrné roční hodnoty. Staré technologie spalování (prohořívací a odhořívací kotle) jsou velmi rozšířené hlavně ve střední a východní části Evropy, což způsobuje značné znečištění ovzduší aerosolovými částicemi během topných sezón. Moderní spalovací zařízení (automatické kotle) produkují významně méně emisí znečišťujících látek, a proto se zvyšuje tlak na výměnu starých zařízení za nová.

METODY MĚŘENÍ

Spalovací zkoušky byly provedeny se zástupci tvrdého (buk) a měkkého (smrk) dřeva, v odlišných typech spalovacích zařízení a za odlišných podmínek spalování (jmenovitý a snížený výkon). Použitá spalovací zařízení představovaly jak zástupce starých konstrukčních řešení (prohořívací a odhořívací kotel), tak také moderní spalovací zařízení (zplyňovací a automatický kotel). Spalovací zkoušky byly provedeny za použití standardizovaných postupů (EN 303-5). Spaliny byly z kotlů odvedeny izolovaným komínem (dle standardních požadavků) k ředicímu tunelu. Ředicí poměr byl stanoven dle očekávaného množství spalin. Odběr vzorků spalin pro následné analýzy byl realizován v ředicím tunelu. Spaliny (TSP frakce) byly odebírány izokineticky na křemenné filtry, které byly podrobeny analýzám organických sloučenin, včetně toxických a karcinogenních polycyklických aromatických uhlovodíků (PAU), a vybraných organických markerů (anhydridy monosacharidů, diterpenoidy), pomocí kterých lze identifikovat emisní zdroje v městském aerosolu.

Filtry s navzorkovanými aerosoly byly rozstříhány na 2 části. První část byla použita pro společnou extrakci anhydridů monosacharidů a diterpenoidů (pryskyřičné kyseliny) pomocí směsi dichlormethan/methanol (1:1 v/v) v ultrazvukové vodní lázni. Extrakty byly po derivatizaci analyzovány pomocí GC-MS (Křůmal a kol., 2017). Ve druhé části filtrů byly analyzovány polycyklické aromatické uhlovodíky (PAU). Extrakce probíhaly směsí hexan/dichlormethan (1:1 v/v). Extrakty byly po frakcionaci analyzovány pomocí GC-MS (Křůmal a kol., 2013; Mikuška a kol., 2015).

VÝSLEDKY A DISKUSE

Emisní faktory částic (TSP) a organických sloučenin byly mnohem vyšší (Obr. 1) při spalování ve starých typech kotlů než v moderních typech pro obě spalovaná paliva, tj. měkké (smrkové) a tvrdé (bukové) dřevo. Nejvyšší emise částic byly ze spalování smrkového (až 3 727 mg/kg) a bukového dřeva (až 3 253 mg/kg) ve starších kotlích při sníženém výkonu (35–45 %). Naopak emisní faktory částic z automatického kotle pro spalování smrkových pelet byly nejnižší (69–118 mg/kg) a koncentrace mnoha organických sloučenin byly pod limitem detekce analytické metody. Důvodem tohoto rozdílu je jiný způsob přikládání paliva, odlišná konstrukce kotle a odlišný způsob spalování paliva. U automatického kotle je spalování plynulé, protože palivo je v menších dávkách přidáváno automaticky pomocí dopravníku paliva několikrát za minutu. Suma emisních faktorů pro PAU se pohybovala mezi 0,002 a 11,3 mg/kg v závislosti na použitém kotli a palivu. Sumy emisních faktorů anhydridů monosacharidů (organických markerů pro spalování biomasy) byly nejnižší v automatickém kotli (až 0,397 mg/kg). U ostatních kotlů dosahovaly až 405 mg/kg. Sumy emisních faktorů diterpenoidů (organických markerů pro spalování jehličnatého dřeva), tj. dehydroabitové kyseliny, abietové kyseliny a retenu, byly také nejnižší u automatického kotle (až 0,005 mg/kg), zatímco u ostatních kotlů dosahovaly až 22,2 mg/kg.

Naše pozornost byla zaměřena především na analýzu organických markerů a následné stanovení charakteristických poměrů, které slouží jako pomocné identifikátory emisních zdrojů částic v ovzduší. Charakteristické poměry pro levoglukosan/mannosan, tj. 13,4–18,6 pro spalování bukového a 2,11–4,16 pro spalování smrkového dřeva, byly přibližně shodné s hodnotami uvedenými v literatuře. Diagnostické poměry pro PAU byly naopak hodně odlišné od údajů v literatuře. PAU vznikají především při nedokonalém

spalování organického materiálu. Všechny poměry uváděné v literatuře jsou výsledkem spalování paliv v kamnech a krbech s dostatkem vzduchu (dokonalé hoření). Cílem našich experimentů bylo přiblížit se reálným emisím z domácností, proto bylo palivo spalováno v kotlích se jmenovitým a se dvěma sníženými výkony (cca 35–45 % a 60–70 %).

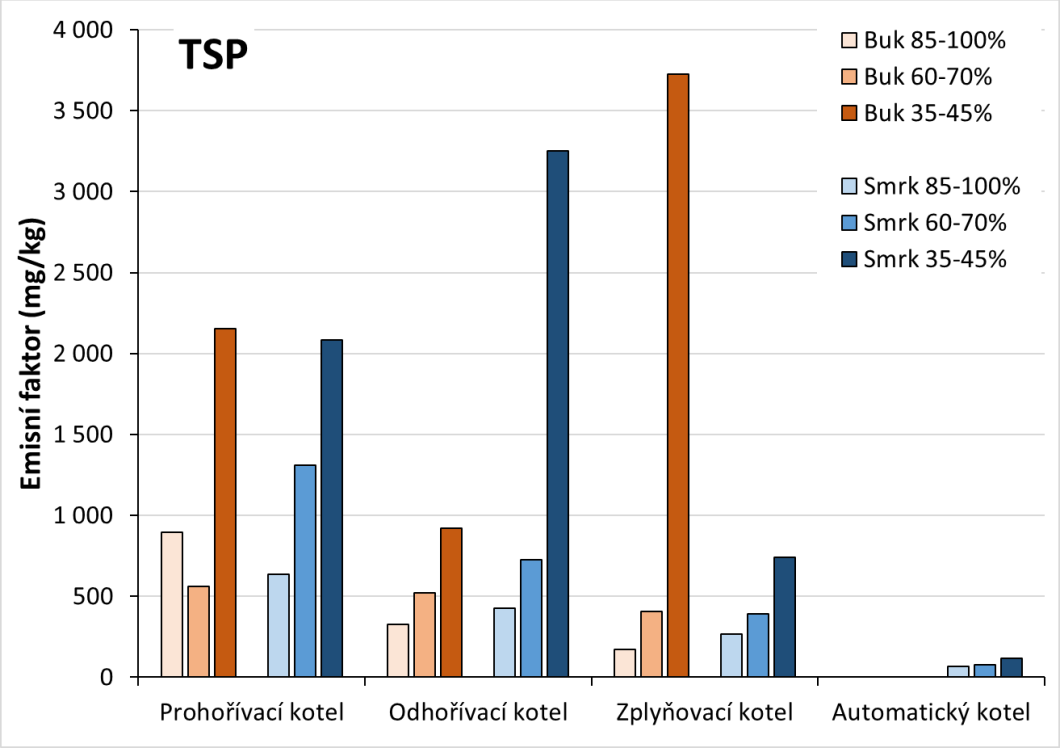

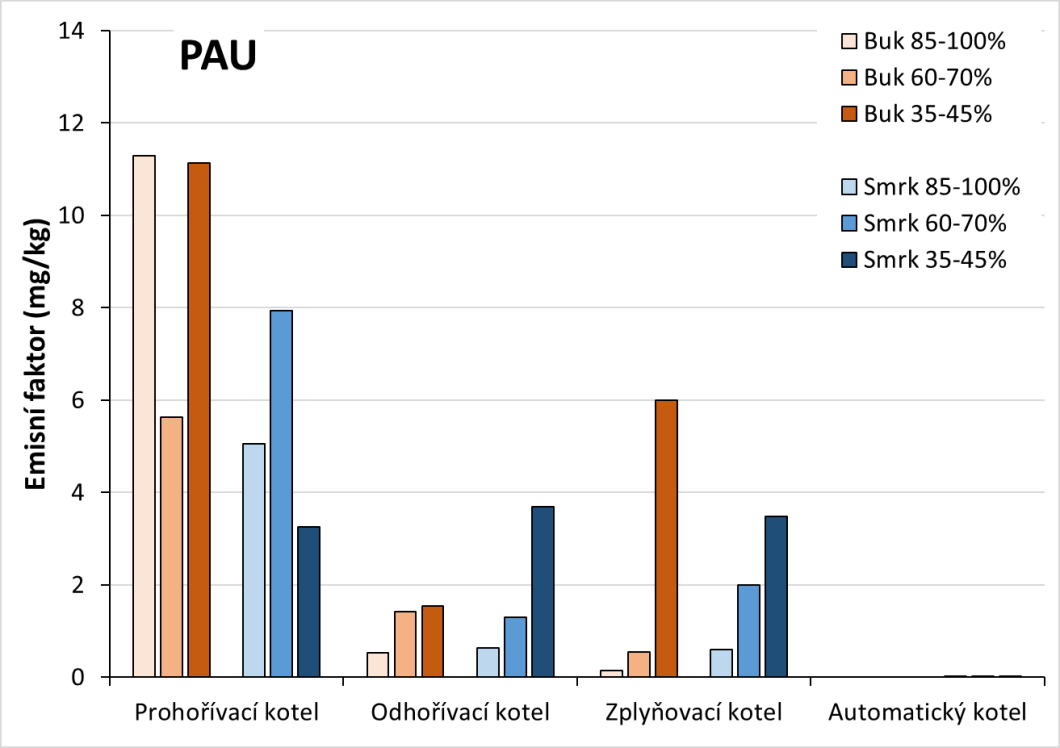

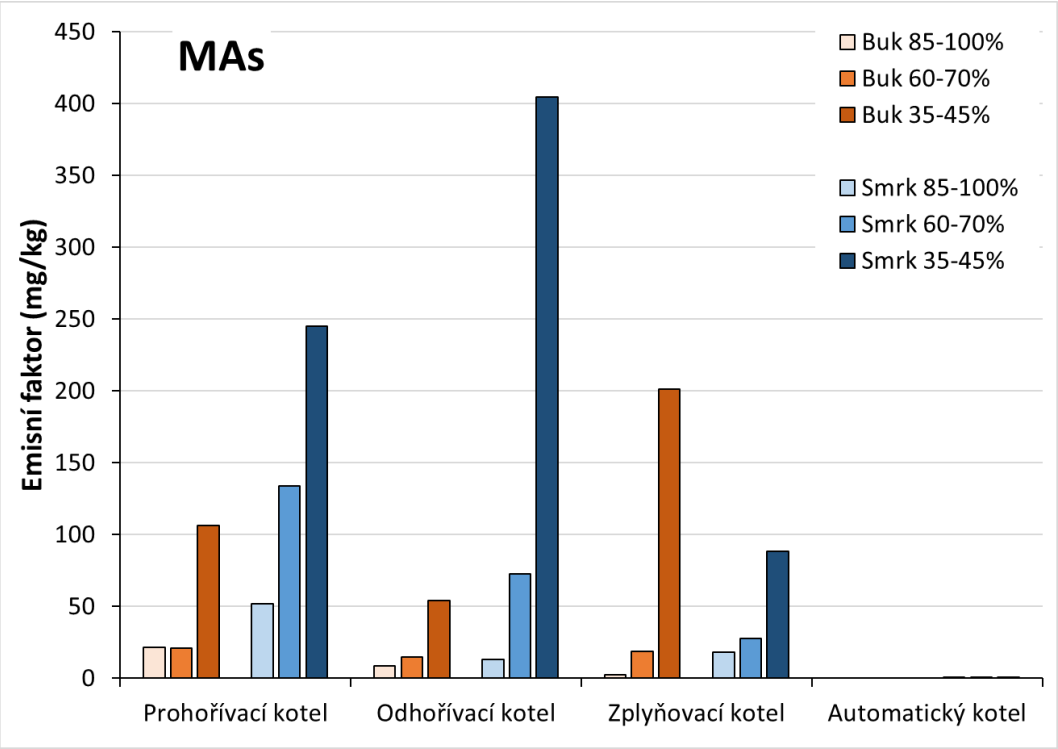

Obr. 1: Emisní faktory (mg/kg) pro TSP, PAU (polycyklické aromatické uhlovodíky), MAs (anhydridy monosacharidů) ze spalování paliv v kotlích při různých výkonech (%).

ZÁVĚR

Nejvyšší emisní faktory byly nalezeny při spalování v nejstarších typech kotlů pro všechna paliva. Kromě stanovení toxických PAU byla pozornost zaměřena na markery, pomocí kterých lze určit zdroj aerosolových částic na monitorované lokalitě.

PODĚKOVÁNÍ

Tato práce byla podporována výzkumným záměrem Ústavu analytické chemie AV ČR, v. v. i. (RVO:68081715), Grantovou Agenturou České republiky (503/20/02203S) a Ministerstvem školství, mládeže a tělovýchovy v rámci projektu ERDF/ESF (CZ.02.1.01/0.0/0.0/18_069/0010049).

LITERATURA

Brunekreef B., Holgate S. T., Air pollution and health, *Lancet*, 360, 1233-1242, (2002).

Křůmal K., Mikuška P., Večeřa Z., Využití organických markerů pro identifikaci zdrojů atmosférických aerosolů, *Chemické Listy*, 106, 95-103, (2012).

Křůmal K., Mikuška P., Večeřa Z., Polycyclic aromatic hydrocarbons and hopanes in PM1 aerosols in urban areas, *Atmospheric Environment*, 67, 27-37, (2013).

Mikuška P., Kubátková N., Křůmal K., Večeřa Z., Seasonal variability of monosaccharide anhydrides, resin acids, methoxyphenols and saccharides in PM2.5 in Brno, the Czech Republic, *Atmospheric Pollution Research*, 8, 576-586, (2017).

Mikuška P., Křůmal K., Večeřa Z., Characterization of organic compounds in the PM2.5 aerosols in winter in an industrial urban area, *Atmospheric Environment*, 105, 97-108, (2015).

PARALLEL DETERMINATION OF PARTICULATE AMMONIUM BY USING A CONTINUOUS AEROSOL SAMPLER AND CASCADE IMPACTOR

Lukáš ALEXA[1], Hana HLAVÁČKOVÁ[2], Hana CIGÁNKOVÁ[1], Pavel MIKUŠKA[1]

[1] Institute of Analytical Chemistry of the CAS, v. v i., Brno, Czech Republic, alexa@iach.cz
[2] Institute of Chemistry and Technology of Environmental Protection, Faculty of Chemistry, Brno University of Technology, Brno, Czech Republic

Keywords: Ammonium, Atmospheric aerosols, Online analysis, Cascade impactor

INTRODUCTION

Ammonia is a significant gaseous pollutant present in the atmosphere. As a neutralizing agent of acidic species ammonia forms particle-phase ammonium (NH_4^+) salts and contributes thus to formation of secondary atmospheric aerosols (Harrison and Jones, 1995). Aerosols (particulate matter, PM) are responsible for many negative effects on environments and health risks to human. The diameter of PM has significant impact on their environmental exposure, where the decreasing particle size increases the adverse health effects. The ultrafine particles hence play a major role in adverse impact on human health (Ryer-Powder, 1991).

Presented paper describes the use of the novel continuous aerosol sampler for online, and a commercial cascade impactor for offline, determination of NH_4^+ in ambient air.

EXPERIMENT SETUP

The aerosol sampling system consisted of cyclone inlet (2.5 μm cut-off diameter, 10 L min^{-1}), annular diffusion denuder for removing gaseous NH_3 and continuous aerosol sampler (CGU-ACTJU, Mikuška et al., 2018; Alexa and Mikuška, 2020) for collecting the aerosol particles into deionized water (1 mL min^{-1}). Subsequently the collected NH_4^+ was detected via analyser on the principle of continuous flow system (CFS) with fluorometric (FL) detection based on the reaction of NH_4^+ with o-phthaldialdehyde and sulphite in alkaline solution to form isoindol-1-sulphonate (Genfa et al., 1989). The concentrations were measured with a time resolution of 1 s.

The high-flow cascade impactor (100 L min^{-1}, 6 stages, model 131B, TSI) was chosen as a comparison method. Polycarbonate films (75 mm diameter) together with terminal quartz filter (90 mm diameter) were used for the sampling of PM. After sampling for 48 h the analytes were extracted by ultrasonication in deionized water and subsequently analysed by the CFS-FL analyser (NH_4^+) and an ion chromatography (fluorides, chlorides, nitrites, nitrates, sulphates, phosphates and oxalates).

The measurement of NH_4^+ in ambient air in Brno carried out during two campaigns. The summer campaign was going on 19. 7. – 5. 8. 2021 and the winter campaign 7.–24. 2. 2022 (Fig. 1). Both campaigns were performed on a terrace on the first floor of the Institute of Analytical Chemistry (UIACH) at Veveří Street. The particulate number concentration and size distribution of PM in the size range 7.64–299.6 nm were measured with the SMPS spectrometer (model 3936L72, TSI). The temperature, relative

humidity, wind speed and direction, irradiation and precipitations were measured using meteorological station (UIACH, roof).

RESULT AND CONCLUSION

The innovated continuous sampler CGU-ACTJU was optimized and used for online determination of NH_4^+ in urban air. Due to high sensitivity of FL detection (LOD = 3.52 ng m^{-3}) no preconcentration method is required. The online method was compared with the results obtained with the offline method based on aerosol sampling using cascade impactor and subsequent determination by CFS-FL analyser.

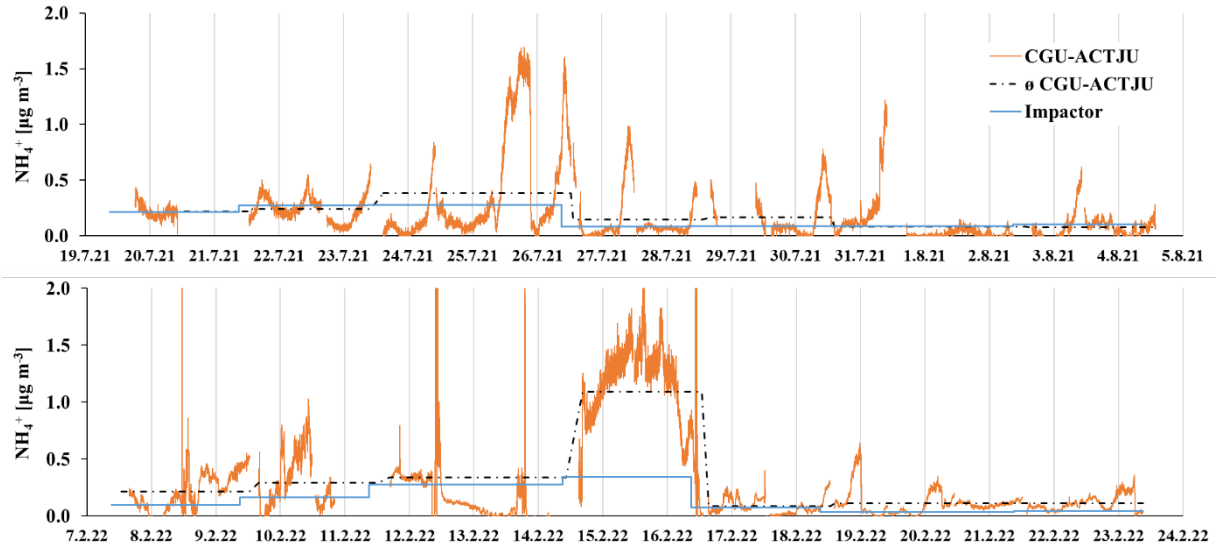

Fig. 1: Variations of NH4+ concentration in PM2.5 aerosol during winter and summer campaigns.

ACKNOWLEDGEMENT

This research was supported by the Grant Agency of the Czech Republic under project No. P503/20/02203S.

REFERENCES

Alexa, L. and Mikuška, P., Simultaneous Determination of Gaseous Ammonia and Particulate Ammonium in Ambient Air Using a Cylindrical Wet Effluent Diffusion Denuder and a Continuous Aerosol Sampler, *Anal. Chem.* 92, 15827-15836 (2020).

Genfa, Z., Dasgupta, P.K., Dong, S., Measurement of atmospheric ammonia, *Environ. Sci. Technol.* 23, 1467-1475 (1989).

Harrison, R., Jones, M., The chemical composition of airborne particles in the UK atmosphere, *Sci. Total Environ.* 168, 195-214 (1995).

Mikuška P., Čapka L., Večeřa Z., Aerosol sampler for analysis of fine and ultrafine aerosols, *Anal. Chim. Acta* 1020, 123-133 (2018).

Ryer-Powder, J.E., Health effects of ammonia, *Plant Oper. Progr.* 10, 228-232 (1991).

PRAKTICKÉ LIMITY OVĚŘENÍ FUNKCE FILTRŮ ČÁSTIC DÁLKOVÝM MĚŘENÍM

Michal VOJTÍŠEK[1], Martin PECHOUT[2]

[1] Centrum vozidel udržitelné mobility, Fakulta strojní, ČVUT v Praze,
michal.vojtisek@fs.cvut.cz, michal.vojtisek@mensa.cz
[2] Katedra vozidel a pozemní dopravy, Technická Fakulta, Česká zemědělská univerzita,
pechout@tf.czu.cz

Klíčová slova: Atmosférické aerosoly, Chemické složení, AMS, PM1

SUMMARY

The practical limitations of remote detection of defunct internal combustion engine particle filters are discussed in this work. Traditional cross-road sensing with open-path spectrometry is subject to very low absorbtion by ultrafine particles, necessitating sampling type measurement with particle counters, diffusion chargers or black carbon sensors, all being more limited by background concentrations than by instrument detection limit, offering a considerable opportunity for the use of low-cost non-optical instruments. Differentiating and discriminating particles from the measured vehicle from other sources, background and especially other vehicles remains to be a challenge and imposes limitations on spacing between measured vehicles.

ÚVOD

Příspěvek se zabývá praktickými limity dálkového měření výfukových emisí motorových vozidel, prováděného za účelem detekce vozidel bez funkčního filtru částic.

Motorová vozidla jsou považována za jeden z nejvýznamnějších zdrojů emisí částic, měřených dle celkové hmotnosti, v městských aglomeracích. Vzhledem k průměru primárních částic řádově deset nanometrů a jejich emisi nikoliv na vrcholu komína, ale v malé výšce uprostřed ulic, lze předpokládat, že mají hlavní podíl na celkovém dopadu emitovaných částic na lidské zdraví. Rozložení emisí podél trasy jízdy daného vozidla ani mezi vozidly není rovnoměrné, ale je podobné např. Lorenzově křivce (Lorenz, 1905). Relativně malá část vozového parku má tak značný, až dominantní, podíl na celkových emisích. Nejedná se pouze o stará vozidla, ale zejména o vozidla v nevyhovujícím technickém stavu; dobře udržované starší vozidlo tak může mít nižší emise částic, než vozidlo novější v neodpovídajícím technickém stavu. Automobily s naftovými motory měřené dálkově v Praze, které neměly funkční filtr částic, ač jej z výroby měly mít, vykazovaly průměrně vyšší emise částic než starší vozy bez filtru (Skácel a kol., 2018).

Vyhledávání vozidel s nadměrnými emisemi a motivace prozovatelů k jejich opravě nebo vyřazení z provozu, což lze považovat za časově, technicky i ekonomicky nejméně náročný způsob jak snížit celkové výfukové emise částic, by mělo být předmětem pravidelných technických kontrol. Ty jsou však v ČR v případě vznětových motorů dosud založeny na měření kouřivosti při volné akceleraci motoru (SAE, 1996), u zážehových motorů částice při pravidelných kontrolách nejsou měřeny vůbec (MDČR 2018). Účinnost pravidelných kontrol v ČR (v roce 2018 na emisích nevyhovělo 2,28 % vozidel oproti 6,6 % v SRN, ASEM 2021) je navíc sporná mimo jiné díky systematickým pochybením na velkém počtu stanic měření emisí (ASEM, 2021).

METODY MĚŘENÍ

Veškeré metody dálkového měření pracují se zředěnými výfukovými plyny, zanechanými po průjezdu vozidla. Tradiční dálkové měření spektrometrem s optickou dráhou napříč vozovkou (Bishop a kol., 1989) je velmi málo citlivé na částice o průměru řádově 10 nm, proto je uvažováno spíše vzorkování z jedoucího vozidla (chase vehicle, např. Canagaratna et al., 2004) nebo z okraje jízdní dráhy (Skácel a kol., 2018). Z poměru měřených koncentrací částic ku CO_2 jsou následně vypočteny emise na kg paliva nebo kWh výkonu. Emisním limitům Euro VI, 5 mg/kWh a 6 x 10^{11} částic/kWh, odpovídají, při spotřebě vzduchu řádově 5 m^3/kWh a zředění o tři řády, příspěvky ke koncentracím řádově 1 ug/m^3 a 100 nevolatilních částic/cm^3, z čehož v praktickém důsledku vyplývá, že téměř libovolný nárůst koncentrací elementárního uhlíku a/nebo nevolatilních částic, který lze průkazně rozlišit od „pouličního“ pozadí, a přiřadit konkrétnímu vozidlu, je důkazem absence funkčního filtru částic. Pro měření lze použít řadu „atmosférických“ přístrojů s rychlou odezvou, za zásadní lze považovat rozlišení příspěvku měřeného vozidla od ostatních vozidel a pozadí, což může představovat výrazná omezení zejména v rozestupech mezi vozidly.

PODĚKOVÁNÍ

Autoři práce děkují za podporu grantu H2020 814966 CARES – City Air Remote Emissions Sensing.

LITERATURA

ASEM. Asociace emisních techniků a opravářů. Statistika z Informačního systému technických prohlídek pro měření emisí za rok 2018. http://www.asem.cz/uploads/3/9/3/1/39314181/statistika_istp_sme.pdf, (2021).

Bishop, G.A.; Starkey, J.R.; Ihlenfeldt, A.; Williams, W.J.; Stedman, D.H.: IR long-path photometry: a remote sensing tool for automobile emissions. *Analytical Chemistry*, 61, 61 (10), 671A–677A, (1989).

Canagaratna, M. R., et al. Chase Studies of Particulate Emissions from in-use New York City Vehicles. *Aerosol Science & Technology*, 38, 555-573, (2004).

Lorenz, M. O. "Methods of measuring the concentration of wealth". Publications of the American Statistical Association. *Publications of the American Statistical Association*, Vol. 9, No. 70. 9 (70): 209–219, (1905).

MDČR. Autor neuveden. Metodický postup měření emisí vozidel ve stanicích měření emisí (SME) a ve stanicích technických control (STK). Ministerstvo dopravy ČR, čj. 1/2018-150-ORG3/18, Verze: 2018.01 rev.2, 24. září 2018, (2018).

SAE. Society of Automotive Engineers. J1667 Recommended Practice. Snap Acceleration Smoke Test Procedure for. Heavy-Duty Powered Vehicles. https://www.arb.ca.gov/enf/hdvip/saej1667.pdf, (1996).

Skácel, J., Vojtíšek, M., Beránek, V., Pechout, M. Black sheep - detecting polluting vehicles on the road using roadside particle measurement. Výroční konfence České aerosolové společnosti, (2018).

NMR AEROSOLOMICS STUDY OF WATER-SOLUBLE ORGANIC COMPOUNDS IN SIZE-RESOLVED PARTICULATE MATTER

Štěpán HORNÍK[1], Petr VODIČKA[1], Petra POKORNÁ[1], Jaroslav SCHWARZ[1], Vladimír ŽDÍMAL[1], Jan SÝKORA[1]

[1] Institute of Chemical Process Fundamentals of the CAS, Prague, Czech Republic, hornik@icpf.cas.cz

Keywords: NMR, Aerosolomics, WSOC, Organic composition, Source markers

INTRODUCTION

Organic aerosols (OA) account for a significant fraction (10 – 90%) of atmospheric particulate matter (Hallquist et al., 2009). The composition of organic aerosols is very complex and is usually characterized by their water solubility (Decesari et al., 2006). Water-soluble organic compounds (WSOC) constitute a large fraction of OA (10 – 80%) and consist of chemical species containing oxygenated functional groups such as hydroxyl, carboxyl, or carbonyl groups. NMR spectroscopy represents an alternative to commonly used techniques (gas chromatography-mass spectrometry, liquid chromatography-based techniques) for WSOC analysis. Our recently introduced method, called NMR aerosolomics, allows quantitative analysis of dozens of individual compounds from different aerosol samples (Horník et al., 2020).

An important part of the characterization of aerosols is their classification by particle size. The analysis of individual compounds in the size-resolved fractions of the WSOC class has been performed only in a few studies that focus mainly on a particular subclass of compounds or use multiple analytical techniques (Barbaro et al., 2019; Xu et al., 2020).

EXPERIMENTAL SETUP

Aerosol samples were collected in a suburb area of Prague-Suchdol in the campus of the Institute of Chemical Process Fundamentals (50° 7'39'' N, 14° 23'4'' E, 277 m a.s.l.). A homemade prototype of high-volume cascade slit impactor with five stages (flow rate 370 l/min) and a back-up filter was used for aerosol sampling. Four aerosol samples were separated into six different fractions: < 0.11 μm (1), 0.11 – 0.40 μm (2), 0.40 – 0.87 μm (3), 0.87 – 2.30 μm (4), 2.30 – 4.68 μm (5), and 4.68 – 20.0 μm (6). Impactor stages 1 – 4 correspond to the fine aerosol fraction, while stages 5 – 6 correspond to the coarse fraction. Two sample series were collected in summer 2015; the winter series were collected in two campaigns, one in 2017, the other in 2018. Three samples were collected as multi-day (2 – 8 days) samples, while one summer sample was collected on the same medium during several summer mornings and afternoons when new particle formation events could be collected, especially organics related to particle growth.

The sample medium was cut into pieces and extracted in 15 mL of deionized water. Extraction was performed for 30 minutes in an ultrasonic bath and for 2 hours on a shaker. The extract was then filtered and freeze-dried. Subsequently, the obtained material was dissolved in deuterated water (99.96% D) containing a known amount of DSS (dimethyl silapentane sulfonate, 0.8 mM) as a reference for chemical shift and line shape. Finally, after dissolution, the sample was transferred to a 5 mm NMR tube and

immediately inserted into the NMR spectrometer. Chenomx NMR Suite software was used to identify and quantify the compounds. In this approach, each compound in the ^{1}H NMR spectrum is identified based on the precise chemical shift of the individual signals.

RESULTS AND CONCLUSIONS

In this study, NMR aerosolomics was used to analyze WSOC in size-resolved particulate matter. Advanced analysis based on compound profiling in the ^{1}H NMR spectra allowed quantification of 31 – 45 compounds in each sample. A total of 73 individual compounds were assigned in the samples. The concentration data were subjected to multivariate statistical analysis, which revealed significant differences in chemical composition between the two seasons and in the main characteristics of the fine and coarse aerosols. Levoglucosan was identified as the major factor in group separation by season of sampling. Clustering based on particle size was mainly determined by the content of carbohydrates in the coarse aerosol fractions.

of the individual compounds showed that some of the compounds were present in all fractions in both the summer and winter samples, while some of the compounds were more specific to a particular season or to a particular particle size. The concentration profiles of the size-resolved aerosol showed an association of certain compounds across different classes that could be attributed to a common source or degradation pathway. A correlation of carbohydrates with trimethylglycine and choline was found in the coarse summer aerosol derived from various biogenic sources. Similar distribution profiles were observed for several compounds associated with solid fuel combustion (methylsuccinic acid, maleic acid, fumaric acid, phthalic acid, and imidazole) in the 2018 winter series with the highest concentration in the accumulation mode. A similar distribution profile in both winter series was found for glucose and levoglucosan, indicating a common origin, most likely biomass burning. Further details of this work were recently published in Horník et al. (2021).

ACKNOWLEDGEMENT

This work was supported by Technology Agency of the Czech Republic project (TK02010035); by the infrastructure project of the MEYS of the Czech Republic ACTRIS-CZ (grant No. LM2018122); and by the Czech Science Foundation, grant No. 20-08304J.

REFERENCES

Barbaro E., Feltracco M., Cesari D., Padoan S. et al., *Sci. Total Environ.*, 658, 1423–1439, (2019).

Decesari S., Fuzzi S., Facchini M.C., Mircea M. et al., *Atmos. Chem. Phys.*, 6, 375–402, (2006).

Hallquist M., Wenger J.C., Baltensperger U., Rudich Y. et al., *Atmos. Chem. Phys.*, 9, 5155–5236, (2009).

Horník Š., Sýkora J., Schwarz J., Ždímal V., *ACS Omega*, 5, 22750–22758, (2020).

Horník Š, Sýkora J., Pokorná P., Vodička P., Schwarz J., Ždímal V., *Atmos. Environ.*, 267, 118757, (2021).

Xu S., Ren L., Lang Y., Hou S. et al., *Atmos. Chem. Phys.*, 20, 3623–3644, (2020).

ZÁVISLOST AKTIVACE AEROSOLU NA METEOROLOGICKÝCH PODMÍNKÁCH

Naděžda ZÍKOVÁ[1], Petra POKORNÁ[1], Pavel SEDLÁK[2], Vladimír ŽDÍMAL[1]

[1] Ústav chemických procesů, AV ČR, Praha, Česká republika, zikova@icpf.cas.cz
[2] Oddělení meteorologie, Ústav fyziky atmosféry AV ČR, Praha, ČR

Klíčová slova: Atmosférické aerosoly, Aktivace, Meteorologické jevy

SUMMARY

Four intensive in-situ campaigns focused on aerosol-cloud interactions were performed in the autumn and spring months from Nov 2018 to Apr 2020 at Milešovka Mountain in Czechia to bring more insight into size-dependent aerosol activation and dependence on its origin for a wide variety of meteorological parameters. Most activated particles were larger than 100 nm, with a mode over 200 nm. For the description of the changes in the activation, no effect of photochemistry was found; in contrast, some dependence on relative humidity, temperature, wind speed, and liquid water content (LWC) proved to be useful. The strongest connection was found between activation and LWC. For LWC below 0.1 g/m^3, in the LWC-limited regime, the LWC values and variables effecting the LWC were the main factors influencing the activation, while different parameters could have played a role at LWCs over 0.1 g/m^3, in the LWC-independent regime.

ÚVOD

V šesté hodnotící zprávě IPCC byla nejvyšší hodnota aerosolového forcingu připsána tzv. nepřímému aerosolovému efektu, tedy interakci mezi atmosférickým aerosolem (AA) a oblačností (Arias a kol., 2021). Tato interakce závisí na množství aktivovaných oblačných jader, což je veličina, kterou je náročné měřit i modelovat. Proto byl zkoumán vliv velikostně diferencované aktivace AA na meteorologických veličinách a jevech.

METODY

Měření proběhla na stanici Milešovka (50°33'N, 13°55'E, 837 m. n. m), kde byla kompletní meteorologická měření a pozorování doplněna o početní velikostní distribuce (PVD) AA ve velikostech od 10 nm do 2.5 μm ze spektrometrů SMPS a APS. Vzorkování probíhalo pomocí dvou inletů, odběrových hlav – tzv. whole air inletu (WAI) a $PM_{2.5}$ hlavy, mezi kterými přepínal kulový kohout každých 5 minut.

Z rozdílů koncentrací naměřených dvěma odběrovými hlavami byly určeny koncentrace a PVD aktivovaného aerosolu (aPVD) každých deset minut. Z aPVD byla vypočtena aktivovaná část AA, tj. podíl aktivovaných jader z celkového počtu AA v dané velikosti. Z tohoto podílu pak byla proložením sigmoidální funkcí určena velikost D_{50}, tedy velikost AA, ze kterého je aktivováno 50 % částic (Obr. 1).

Měření probíhala v letech 2018 až 2020 v pěti intenzivních kampaních v jarních a podzimních měsících, kdy je na stanici nejvyšší pravděpodobnost výskytu nízké oblačnosti, kódované jako mlha. Celkově bylo ve 187 dnech měření nasbíráno přes 15 000

PVD, z toho 4000 vzorků s mlhou, které byly porovnávány s výsledky naměřenými bez pozorovaných meteorologických jevů.

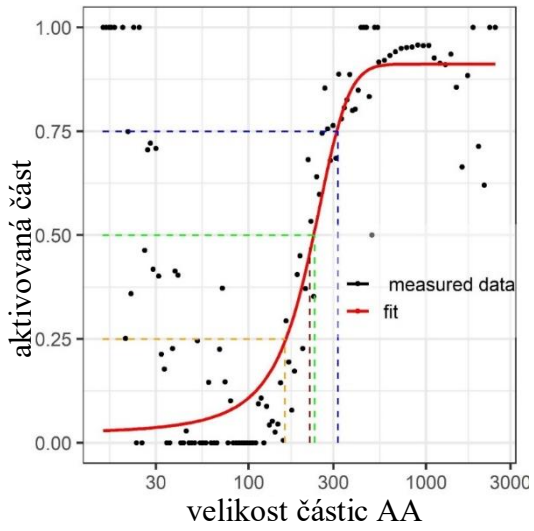

Obr. 1: Příklad jednoho SMPS a APS spektra (body) proloženého sigmoidální funkcí ke zjištění aktivované frakce (červená čára), ze které je určena velikost D_{50} v nm (zelená přerušovaná čára).

VÝSLEDKY, DISKUSE, ZÁVĚRY

Koncentrace neaktivovaného AA byly při výskytu mlhy nižší ve všech měřených velikostech v porovnání se situacemi bez mlhy (Zíková a kol., 2020).

Většina aktivovaného AA byla větší než 100 nm, s maximem aPVD přes 200 nm (Obr. 2). Rozdíl aPVD při výskytu mlhy a mrznoucí mlhy nebyl statisticky významný, a to ani ve tvaru, ani v celkové koncentraci aktivovaných jader. Mrznoucí mlha se lišila jen větší proměnlivostí přesycení nebo menší homogenitou AA – byl pozorován větší rozptyl hodnot parametru D_{50}. Během mrznoucí mlhy byl v porovnání s mlhou pozorován také menší efektivní poloměr kapek, což opět naznačuje odlišné podmínky přesycení vzduchu vodní parou.

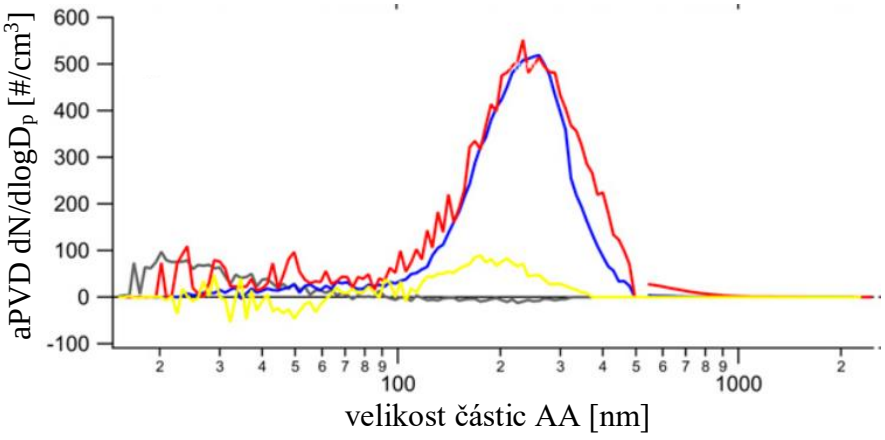

Obr. 2: aPVD naměřená při výskytu mlhy (modrá), mrznoucí mlhy (červená), mlhy současně s deštěm (žlutá) a při absenci výše uvedených jevů (šedá).

Aktivace AA byla zkoumána i za různých meteorologických podmínek. Spojitost s fotochemií nebyla prokázána – nebyl nalezen denní chod parametru D_{50}, který by ukazoval závislost na globálním záření. Naopak byla nalezena závislost na teplotě, relativní vlhkosti, rychlosti větru, a především na vodním obsahu oblaku (LWC, liquid water content) (Zíková a kol., 2021).

Při vyšší relativní vlhkosti byly aktivovány menší částice (klesala hodnota parametru D_{50}). Při nízké relativní vlhkosti stoupal význam proměnlivosti v přesycení vodní parou – šlo o režim řízený fluktuacemi v poli vodního obsahu oblaku. Podobný vliv byl pozorován i při vysokých rychlostech větru. Do rychlosti 10 m/s nebyl vliv větru na aktivaci pozorován, ale pro vyšší rychlosti se zvýšil rozptyl hodnot D_{50} z důvodu větší turbulence vzduchu, která souvisela s fluktuacemi v poli přesycení a/nebo s rozrušením teplotní inverze.

Nejsilnější závislost aktivace byla pozorována při změnách vodního obsahu oblaku, LWC. Pokud byl vodní obsah oblaku menší než 0.10 g/m^3, klesala hodnota parametru D_{50} o 35 nm při každém nárůstu LWC o 0.01 g/m^3 (Obr. 3). Pro vyšší vodní obsah v oblaku už se hodnota D_{50} se změnou vodního obsahu oblaku výrazněji neměnila. Pro hodnoty pod 0.1 g/m^3, kdy hovoříme o režimu omezeném vodním obsahem oblaku, byl vodní obsah oblaku rozhodujícím parametrem ovlivňujícím aktivaci AA. Při větším vodním obsahu oblaku pak byly důležitější jiné parametry než LWC.

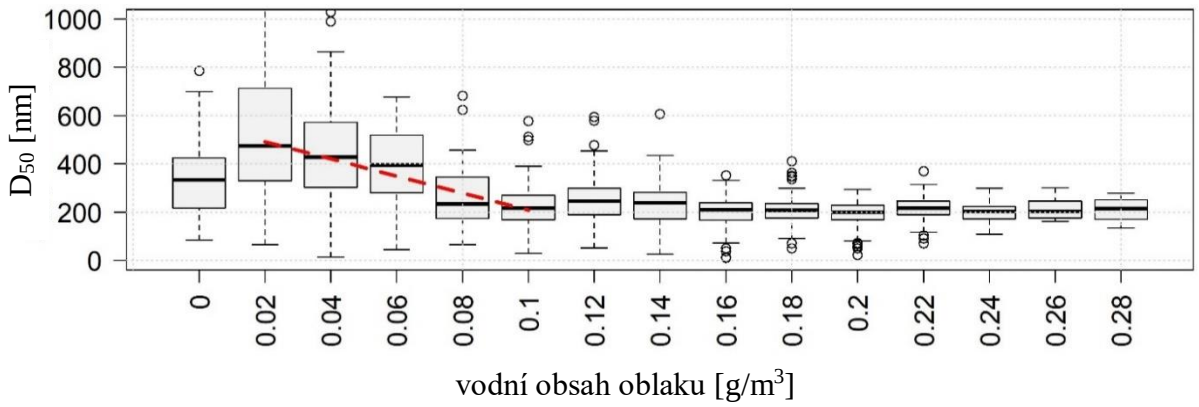

Obr. 3: Závislost pozice D_{50} na hodnotě vodního obsahu oblaku.

PODĚKOVÁNÍ

Příspěvek vznikl za finanční podpory GAČR v rámci projektu P209/18/15065Y a MŠMT v rámci projektu ACTRIS-CZ-LM2018122. ACTRIS IMP je podpořen EC Horizon 2020 programem H2020-INFRADEV-2019-2, Grant Agreement number: 871115.

LITERATURA

Arias, P. A., … Zickfeld, K. Technical Summary. In V. Masson-Delmotte, … , R. Yu, & B. Zhou (Eds.), Climate Change 2021: The Physical Science Basis. Contribution of Working Group I to the Sixth Assessment Report of the Intergovernmental Panel on Climate Change. Cambridge University Press (2021).

Zíková, N., Pokorná, P., Makeš, O., Rotrekl, J., Sedlák, P., Pešice, P., Ždímal, V. Variability in activation properties in relation to meteorological phenomena. *Journal of Hydrometeorology*, 22(10), 2565–2579, (2021).

Zíková, N., Pokorná, P., Makeš, O., Sedlák, P., Pešice, P., Ždímal, V. Activation of atmospheric aerosols in fog and low clouds. *Atmospheric Environment*, 230(April), 117490, (2020).

STANOVENÍ KONCENTRACE A VELIKOSTNÍ DISTRIBUCE RADIOAKTIVNÍCH AEROSOLOVÝCH ČÁSTIC

Petr OTÁHAL[1], Michaela KOZLOVSKÁ[1], Eliška FIALOVÁ[1,2]

[1] Státní ústav jaderné, chemické a biologické ochrany, v.v.i.
[2] Přírodovědecká fakulta, Masarykova univerzita Brno

Klíčová slova: Radioaktivní aerosolové částice, SMPS, Kaskádní impaktor

SUMMARY

Inhalation of radioactive aerosol particles is one of the possible exposure pathways that can significantly contribute to the total effective dose in how planned, existing, and so accidental exposure situations. Department of Nuclear Protection - SÚJCHBO, v.v.i. is mainly concerned with determining the total activity concentration of alpha emitters in the air and determining the concentration and size distribution of radon decay products at workplaces with material with an increased content of natural radionuclide (planned exposure situation). SUJCHBO also determines the concentration and size distribution of radon conversion products at workplaces with a possible increase in exposure from radon (existing exposure situation). Furthermore, the department's workplace is equipped with devices enabling the sampling and analysis of radioactive aerosol particles in accidental exposure situations.

ÚVOD

Inhalace radioaktivních aerosolových částic je jednou z možných expozičních cest, která může významně přispívat k celkové efektivní dávce jak při plánovaných, existujících i nehodových expozičních situacích. Odbor jaderné ochrany (OJO) - SÚJCHBO, v.v.i. se zabývá zejména stanovením celkové objemové aktivita zářičů alfa ve vzduchu a stanovením koncentrace a velikostní distribuce produktů přeměny radonu na pracovištích s materiálem se zvýšeným obsahem přírodního radionuklidu (plánovaná expoziční situace). SÚJCHBO dále stanovuje koncentrace a velikostní distribuce produktů přeměny radonu na pracovištích s možným zvýšením ozáření z radonu (existující expoziční situace). Dále je pracoviště odboru vybaveno zařízeními umožňujícími odběr a analýzu radioaktivních aerosolových částic při nehodových expozičních situacích.

METODY MĚŘENÍ

Pro potřeby stanovení celkové koncentrace (objemové aktivity alfa, beta, znalosti zvýšení koncentrace radioaktivních aerosolových částic ve vzduchu) radioaktivních aerosolových částic je odbor vybaven nízko-objemovými čerpadly QUICK TAKE 30 (objemový průtok 20 l/min), které spolu s vyhodnocovacím zařízením LB 124 SCINT-D umožňuje stanovit úroveň kontaminace vzdušniny přímo v terénu. Při znalosti isotopového složení aerosolových částic lze stanovit přímo koncentraci daného radionuklidu. Tuto metodu odběru aerosolových částic je vhodné využít zejména v případech nutnosti rychlého odhadu efektivní dávky kontaminovaných osob.

Druhým způsobem je možnost využití velkoobjemového vzorkovače VF NUCLEAR

VOPV-12, který vzorkuje v rozmezí 17 – 150 m^3/hod. Filtr, který slouží ke sběru aerosolových části (254 x 202 mm) je následně umístěn do měřící nádoby. Měření probíhá buď přímo v terénu s využitím měřícího zařízení RT-50 anebo laboratorně pomocí gamaspektrometru s vysokým rozlišením (Canberra). U takto odebraných vzorků je následně stanovována koncentrace radionuklidů emitujících záření gama.

V oblasti přírodního záření jsou v současnosti vyvíjeny metody stanovení velikostní distribuce pomocí kaskádního impaktoru Dekati ELPI+. Tento 15. stupňový impaktor je osazen vhodnou detekční a brzdící fólií. Toto uspořádání umožňuje stanovit velikostní distribuci produktů přeměny radonu. V současné době jsou finalizovány laboratorní experimenty, které mají prokázat vhodnost zvolené měřící a vyhodnocovací metody a byla již zahájena terénní měření za účelem stanovení velikostní distribuce produktů přeměny radonu na různých typech zejména podzemních pracovišť. V rámci laboratorních prací jsou výsledky stanovení velikostní distribuce srovnávány s výsledky stanovení získaných pomocí SMPS (Obr. 1).

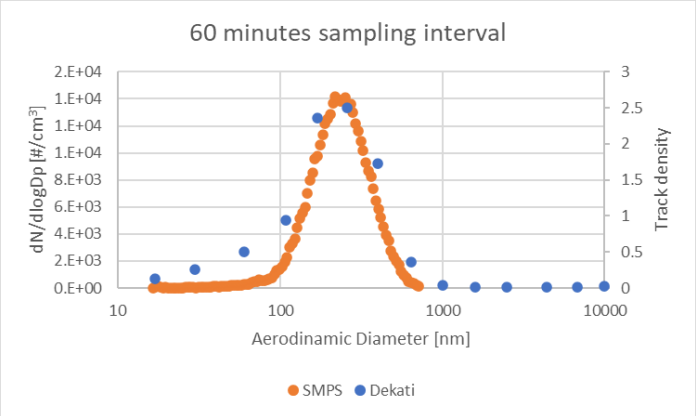

Obr. 4 Srovnání výsledků SMPS a Dekati ELPI+

PODĚKOVÁNÍ

Příspěvek vzniknul za podpory projektu Systém zpracování a vyhodnocování vzorků z terénních měření č. 54018.

LITERATURA

Zákon č. 263/2016 Sb., atomový zákon.
422/2016 Sb. - Vyhláška o radiační ochraně a zabezpečení radionuklidového zdroje.

AN IMPROVED METHOD FOR CALCULATION OF THE WET PARTICLE DIAMETER AND THE KAPPA PARAMETER FROM THE CCN DATA

Zdeněk WAGNER[1], Gaurav MISHRA[1], Pavel MORAVEC[1], Naděžda ZÍKOVÁ[1]

[1] Institute of Chemical Process Funtamentals of the CAS, Prague, Czech Republic, wagner@icpf.cas.cz

Keywords: Critical diameter, Wet particle diameter, CCN, Supersaturation

INTRODUCTION

The study of particle size distribution and hygroscopic growth is important for several reasons. Particle diameter is available experimentally, but the relationship of hygroscopic growth to cloud condensation nuclei (CCN) and AMS data can be modeled mathematically. In this paper, we present an improved algorithm for calculating the wet particle diameter and the κ parameter that is faster, more accurate, and more reliable than the algorithm used by other authors.

MATHEMATICAL METHOD

The basis for calculation is Köhler's theory. Petters and Kredenweis (2007) showed that water vapour saturation ratio s over an aqueous droplet is expressed by

$$s = \frac{D_{\mathrm{wet}}^3 - D_c^3}{D_{\mathrm{wet}}^3 - D_c^3(1-\kappa)} \exp\left(\frac{4\sigma_w M_w}{RT\rho_w D_{\mathrm{wet}}}\right) \qquad (1)$$

where D_{wet} is the wet particle diameter, D_c is the critical diameter of the dry particle, σ_w, ρ_w, M_w are the surface tension, density, and molar weight of water, and κ is a single parameter combining specific properties of aerosols such as molar weight, density, and van't Hoff factor. For given $s = 1 + S/100\%$, where S is a selected supersaturation, and D_c, it yields a single equation for two unknowns, namely D_{wet} and κ and has thus infinite number of solutions. Thus it is necessary to find D_{wet} that maximizes the saturation ratio while matching the selected supersaturation (Rose *et al.* 2010). To solve the problem they use nested minimization of $(-s)$ and $|s - 1 + S/100|$ by double application of the *fminsearch* function from Matlab. This approach has a serious drawback. The *fminsearch* function is an implementation of a Nelder-Mead algorithm designed for multidimensional optimization but used here in a single dimension. Since an absolute value is minimized, the method can find a false solution satisfying the minimization criterion but equation (1) is not satisfied.

When we examine the problem, we find that it is indeed a constrained optimization where the same equation plays both roles, it is both the criterion function and the constraint. The necessary condition for a local maximum is obtained by differentiation:

$$\frac{\partial s}{\partial D_{\mathrm{wet}}} = \frac{1}{D_{\mathrm{wet}}^3 - D_c^3(1-\kappa)} \left[\frac{3D_{\mathrm{wet}}^2 D_c^3 \kappa}{D_{\mathrm{wet}}^3 - D_c^3(1-\kappa)} - (D_{\mathrm{wet}}^3 - D_c^3)\frac{4\sigma_w M_w}{RT\rho_w D_{\mathrm{wet}}^2}\right] exp\left(\frac{4\sigma_w M_w}{RT\rho_w D_{\mathrm{wet}}}\right) = 0 \qquad (2)$$

Fig. 1 shows the values of the partial derivative of the saturation ratio with respect to the wet diameter for different values of supersaturation. For values slightly above the

diameter of the dry particle, the derivative is a decreasing function that reaches a minimum and then asymptotically approaches zero. The root of Eq. (2) can therefore be easily bracketed. D_{wet} and κ are then computed by nested solution of both equations using an algorithm we have implemented in GNU Octave that is always convergent.

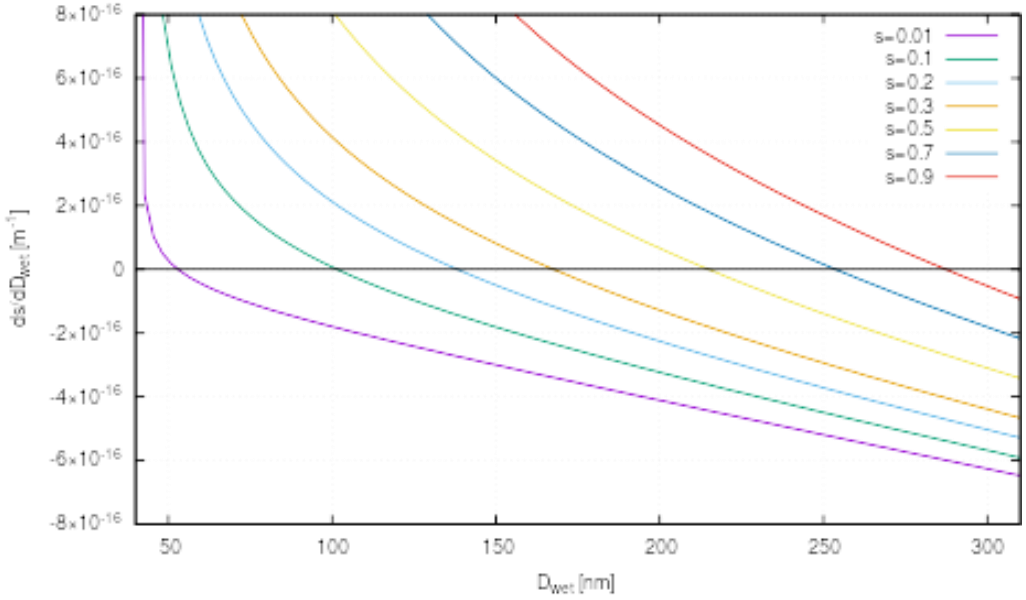

Fig 1: Dependence of partial derivative of saturation ratio with respect to the wet particle diameter for D_c = 40 nm and several values of supersaturation

CONCLUSIONS

The algorithm proposed here is based on a rigorous mathematical derivation and is implemented in GNU Octave. The procedure for solving a real equation with a single real variable is a combination of several algorithms that ensures that the iteration operator contracts in Banach space, i.e., the algorithm is always convergent provided that the root of the equation has odd multiplicity and can be bracketed. The method converges quickly and reliably even if the root is a turning point. The algorithm does not fall into a false solution at a very low supersaturation which is another advantage over using the *fminsearch* function, in addition to speed and precision.

ACKNOWLEDGEMENT

This work was supported by the ACTRIS-CZ-LM2018122 project.

REFERENCES

Petters M. D., Kreidenweis S. M., A single parameter representation of hygroscopic growth and cloud condensation nucleus activity, *Atmos. Chem. Phys.*, 7, 1961–1971, (2007).

Rose D., Nowak A., Achtert P., Wiedensohler A., Hu M., Shao M., Zhang Y., Andreae M. O., Pöschl U., Cloud condensation nuclei in polluted air and biomass burning smoke near the mega-city Guangzhou, China – Part 1: Size-resolved measurements and implications for the modeling of aerosol particle hygroscopicity and CCN activity, *Atmos. Chem. Phys.*, 10, 3365–3383, (2010).

PLANETARY BOUNDARY LAYER EFFECT ON VERTICAL TRANSPORT OF BLACK CARBON CONCENTRATION UNDER DIFFERENT METEOROLOGICAL CONDITIONS

Kajal JULAHA[1,2], Nadežda ZÍKOVÁ[1], Saliou MBENGUE[3], Vladimír ŽDÍMAL[1]

[1] Institute of Chemical Process Fundamentals of the CAS, Prague, Czech Republic, julaha@icpf.cas.cz
[2] Faculty of Mathematics and Physics, Charles University, Prague, Czech Republic
[3] Global Change Research Institute of the Czech Academy of Science, Brno, Czech Republic.

Keywords: PBL -eBC interaction, 250m-meteorological tower, Meteorology, Long-range transport

INTRODUCTION

The planetary boundary layer (PBL), the lowest part of the troposphere, has a higher aerosol concentration than the rest of the atmosphere because pollutants emitted from the surface are constrained in PBL. Among all aerosols, absorbing aerosols, mainly black carbon (BC), has the strongest interaction with PBL (Bond et al., 2013) and plays a vital role in modifying the diurnal evolution of PBL.

In the present study, we analyzed the impact of equivalent black carbon (eBC) aerosols at two different heights (4 m and 230 m) on the PBL height under different metrological conditions such as clear sky, foggy (visibility ≤ 1km), and hazy days (visibility ≤ 8km during the non-fog day), high relative humidity, temperature, and observational data; also, diurnal and seasonal variability was evaluated.

EXPERIMENTAL SETUP

The eBC concentration was measured from 1/2020 to 12/2020 by Sunset Analyzer simultaneously at 4 m and 230 m on a 250m-meteorological tower at National Atmospheric Observatory Košetice (NAOK; 49°35'N, 15°05'E), located at a rural background in the Czech Republic. The eBC concentrations were calculated from raw Sunset analyzers data according to Zíková et al. (2016). The PBL height has been taken from the ERA5 dataset (Hersbach H. et al., 2018).

RESULTS AND CONCLUSIONS

In this study, the mean eBC concentration was found the highest in winter (Dec-Feb), lower in spring (Mar-May) and autumn (Sep-Nov), and the lowest during the summer (Jun-Aug). In contrast, the average PBL height was the lowest in autumn, followed by summer and winter, and was measured the highest during the spring (*Figure 1*) due to the higher number of rainy days during the summer, resulting in lower PBL height. The eBC concentration at ground level showed peaks during mornings and evenings, likely due to local sources and the PBL diurnal evolution. At 230 m, eBC concentration displayed an opposite diurnal pattern similar to the diurnal pattern of the PBL height.

Several case studies were studied to find the impact of different meteorological conditions. The development of PBL was suppressed by fog and haze, further weakening the vertical mixing of aerosols, leading to higher eBC concentration at the ground. High RH (≈ 100%) with high temperature (28 °C) yields the highest PBL height and higher eBC concentration at 4m compared to 230 m.

Elevated eBC concentrations during noon and late-night have also been observed, driven by the transport of aerosols from distant sources. The long-range transport of aerosols was confirmed by air mass back trajectories using the HYSPLIT model. The eBC concentration was higher below the PBL height than above the PBL.

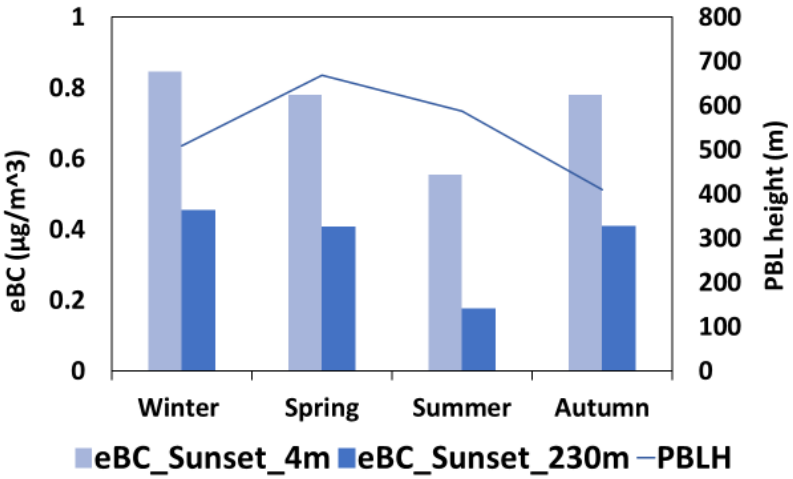

Fig. 1. Seasonal comparison of eBC concentration at two different heights and PBL height.

ACKNOWLEDGEMENT

This work was supported by MEYS of the Czech Republic under grants ACTRIS-CZ LM2018122.

REFERENCES

Bond, Tami C., Sarah J. Doherty, David W. Fahey, Piers M. Forster, Terje Berntsen, Benjamin J. DeAngelo, Mark G. Flanner et al., Bounding the role of black carbon in the climate system: A scientific assessment, *Journal of geophys. Res.: Atmospheres* 118, no. 11: 5380-5552, (2013).

Hersbach, H., B. Bell, P. Berrisford, G. Biavati, A. Horányi, J. Muñoz Sabater, J. Nicolas et al., ERA5 hourly data on single levels from 1979 to present, *Copernicus Climate Change Service (C3S) Climate Data Store (CDS),* [data set], (2018).

Zíková, Naděžda, Petr Vodička, Wolfgang Ludwig, Regina Hitzenberger, and Jaroslav Schwarz., On the use of the field Sunset semi-continuous analyzer to measure equivalent black carbon concentrations, *Aerosol Sci. Tech.,* 50, no. 3: 284-296, (2016).

THE IMPACT OF COVID-19 RESTRICTIONS ON CARBONACEOUS AEROSOLS AT RURAL BACKGROUND SITE: IMPORTANCE OF VERTICAL DISTRIBUTION

Saliou MBENGUE[1], Petr VODIČKA[2], Katerina KOMÍNKOVÁ[1], Jaroslav SCHWARZ[2], Nadezda ZÍKOVÁ[2], Roman PROKES[1,3], Lenka SUCHÁNKOVÁ[1,2], Kajal JULAHA[2], Jakub ONDRÁČEK[2], Ivan HOLOUBEK[1,3], Vladimir ŽDÍMAL[2]

[1] Global Change Research Institute of the Czech Academy of Sciences, Brno, Czech Republic, mbengue.s@czechglobe.cz
[2] Institute of Chemical Process Fundamentals of the CAS, Prague, Czech Republic,
[3] RECETOX, Faculty of Science, Masaryk University, Brno, Czech Republic,

Keywords: COVID-19, Vertical distribution, Organic – elemental carbon, Rural background site.

INTRODUCTION

Novel coronavirus disease 2019 (COVID-19) emerged in China in late 2019 and became a global outbreak in early 2020 (WHO, 2022). As in many other countries, Czech authorities took a number of preventive and control measures to prevent the spread of the disease, including city lockdowns and restrictions on numerous activities (traffic, economy, personal limitations). These measures led to a reduction in emissions from most anthropogenic sources, and improvements in air quality were observed in many megacities (Chauhan and Singh, 2020). However, little is known about the impact of COVID -19 on rural background site representing background air pollution. Atmospheric elemental (EC) and organic carbon (OC) are among the major constituents of ambient aerosols that have attracted growing interest due to their adverse effects on human health, atmospheric visibility, and climate warming (Mauderly and Chow, 2008; Bond et al., 2013). The objective of this study is to characterize the effects of COVID -19 lockdowns on carbonaceous aerosols at a rural background site using continuous in situ vertical distribution measurements.

EXPERIMENTAL SETUP

Ground-based (4 m a.g.l.) long-term monitoring of EC and OC has been initiated in 2013 at the National Atmospheric Observatory Košetice (NAOK; 49°35'N, 15°05'E) in the central Czech Republic using a semi-continuous thermal-optical OCEC analyzer (Sunset Laboratory Inc., USA). In late 2019, a second OCEC analyzer was installed at the top of the tower (230 m a.g.l.) and measurements were performed simultaneously with the ground from December 2019 to June 2021. Both instruments sampled with a time resolution of 4 h, including 20 min of OC /EC thermo-optical analysis according to the abbreviated EUSAAR-2 protocol (Cavalli et al., 2010; Mbengue et al., 2018). Sampling systems were equipped with a carbon parallel plate diffusion denuder (Sunset Lab) to avoid positive artifacts caused by absorption of volatile organic compounds on the quartz microfiber filter (Turpin et al., 2000). A total of 1955 pairs of OC/EC sampling points were measured during the campaign.

RESULTS AND CONCLUSIONS

In this study, EC and OC at 4 m elevation and EC at 230 m elevation showed a similar seasonal pattern with higher values in winter and lower values in summer. OC, measured at 230 m height showed an opposite behavior with slightly higher values in spring and summer, probably related to the increased contribution of secondary organic carbon (SOC). Concentrations were generally higher at 4 m, where there was also a better correlation between EC and OC, suggesting a greater influence of local sources near the surface. In contrast, measurements at 230 m may be more influenced by aged and long-range transported aerosols. These results are confirmed by source apportionment / receptor modeling (Conditional Bivariate Probability Function the Potential Source Contribution Function).

To examine the impact of Covid lockdowns, ground-level measurements of OC and EC from the pre-Covid period (2017-2019) were compared to the values recorded during the Covid period (2020-2021). The results show that the restrictions during the COVID lockdowns did not systematically lead to a decrease in the values of OC and EC at the rural background site. This is particularly true for the second lockdown for EC in the spring and for OC in all seasons (Fig. 1).

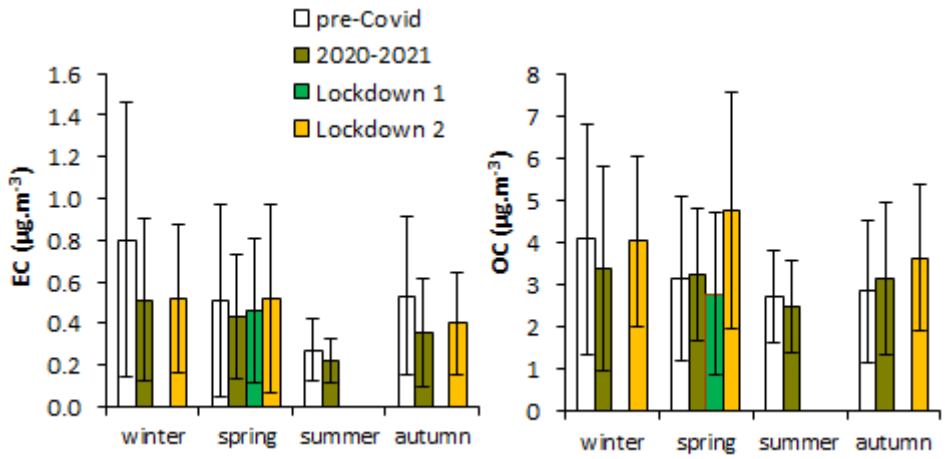

Fig. 1: Seasonal mean concentrations of OC, EC, measured at 4 m a.g.l. during pre – COVID (from 2017–2019) and COVID (2020-2021) periods.

The effect of the COVID-related lockdowns could be better observed by examining the correlation of EC and OC between 4 m and 230 m (Fig. 2). Indeed, the correlation coefficient which was around 0.20 during the pre-lockdown, especially for EC, increased steeply during the two controlled periods (up to 0.85 and up to 0.70 during lockdown 1 and 2, respectively). The higher correlation during the lockdowns suggests that aerosols collected at 4 m and 230 m were influenced by common sources and/or transported simultaneously at the sampling site. Because the COVID restrictions resulted in reduced emissions from local anthropogenic sources, the receptor site was influenced primarily by aged aerosols transported over long distances. This is consistent with the increased concentration of SOC, which follows the same behavior observed for OC during the second lockdown.

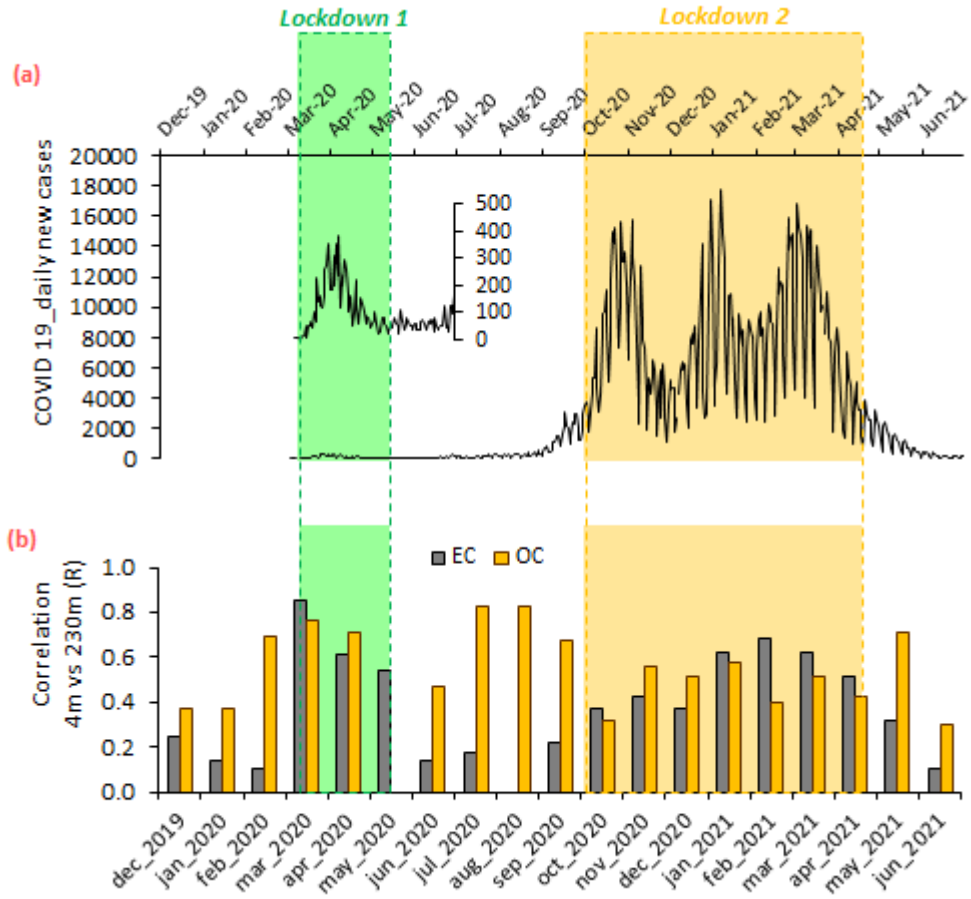

Fig. 1: Time series of a) Number of coronavirus COVID_19 daily new case in Czechia, and b) monthly correlation coefficient between EC and OC at 4 m and those at 230 m from December 2019 to Jun 2021.

ACKNOWLEDGEMENT

The research leading to these results was funded by the National Research Infrastructure Support Project - ACTRIS Participation of the Czech Republic (ACTRIS-CZ LM201822), supported by the Ministry of Education, Youth and Sports of the Czech Republic.

REFERENCES

Bond, T.C., Doherty, S.J., Fahey, D.W., et al., Bounding the role of black carbon in the climate system: a scientific assessment. J. Geophysical Research, Atmos. 118, 5380–5552 (2013).

Cavalli, F., Viana, M., Yttri, K.E., Genberg, J., Putaud, J.P., Toward a standardized thermal-optical protocol for measuring atmospheric organic and elemental carbon: the EUSAAR protocol. Atmos. Meas. Tech. 3, 79–89 (2010).

Chauhan, A., Singh, R.P., Decline in PM2.5 concentrations over major cities around the world associated with COVID-19. Environ. Res. 187, 109634 (2020).

Mauderly, J.J., Chow, J.C., Health effects of organic aerosols. Inhal. Toxicol. 20, 257-288 (2008).

Mbengue, S., Fusek, M., Schwarz, J., Vodička, P., Šmejkalová, A.H., Holoubek, I., Four years of highly time resolved measurements of elemental and organic carbon at a rural background site in Central Europe. Atmos. Environ. 182, 335–346 (2018).

Turpin, B.J., Saxena, P., Andrews, E., Measuring and simulating particulate organics in the atmosphere: problems and prospects. Atmos. Environ. 34, 2983–3013 (2000).

WHO, COVID-19 Weekly Epidemiological Update. Edition 99 published 6 July (2022).

HARMONIZED UFP NUMBER AND SIZE DISTRIBUTION MEASUREMENTS ACCEPTED BY ACTRIS, EMEP AND NATIONAL MONITORING NETWORKS

Lucia BUSTIN[1], Torsten TRITSCHER[1], Sebastian H. SCHMITT[1], Andrea J. TIWARI[2], Jürgen SPIELVOGEL[1], Thomas KRINKE[1], Oliver F. BISCHOF[1]

[1] TSI GmbH, Neukoellner Str. 4, 52068 Aachen, Germany, lucia.bustin@tsi.com
[2] TSI Inc., 500 Cardigan Road, 55126 Shoreview, MN, USA

Keywords: Atmospheric aerosols, UFP monitoring, ACTRIS

INTRODUCTION

For many years, mass-based particulate matter PM2.5 and PM10 measurements have been standardized and represented the cornerstone for the regulatory quantification and characterization of particles in ambient air. In the past decade the measurement of ultrafine particles (UFP) has gained importance outside the field of atmospheric research. Studies like the one by de Jesus et al. (2019) have highlighted the world-wide need to address UFP concentrations due to their potential risks for human health. UFP particle number concentrations (PN) and particle number size distributions (PSD) have been measured by scientifically motivated projects and networks (e.g. ACTRIS, GAW, GUAN) for years (Birmili et al. 2016).

While number-based measurements of atmospheric aerosol have been made, it has been difficult to meaningfully compare data gathered internationally. This difficulty is due to the fact that particle measuring sites were sometimes using different sampling, conditioning, and particle measurement instrumentation. “Harmonizing” these aspects is key to comparing data and drawing conclusions relevant to all the fields relevant to ambient aerosols, including emissions regulations, public health, and climate.

In an effort to harmonize the continuous measurement of UFP in terms of their PN and PSD in ambient air, the European Committee for Standardization (CEN) published technical specifications CEN/TS 16976 for Condensation Particle Counters (CPC) and CEN/TS 17434 for Mobility Particle Size Spectrometer (MPSS) or Scanning Mobility Particle Sizer (SMPS). These normative documents describe a standardized method by defining a set of requirements for the instrument, its sampling system, the measurement procedure and the reporting of measurement results.

We will introduce the recent customization of our established CPC and SMPS instruments with dedicated sampling and dilution options to meet these CEN/TS specifications. We will show results from several weeks of ambient measurement of the urban aerosol in a light industrial area in Aachen, Germany.

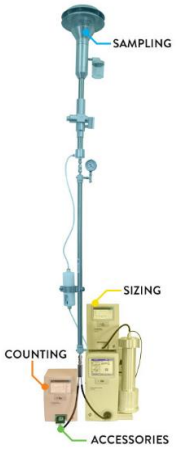

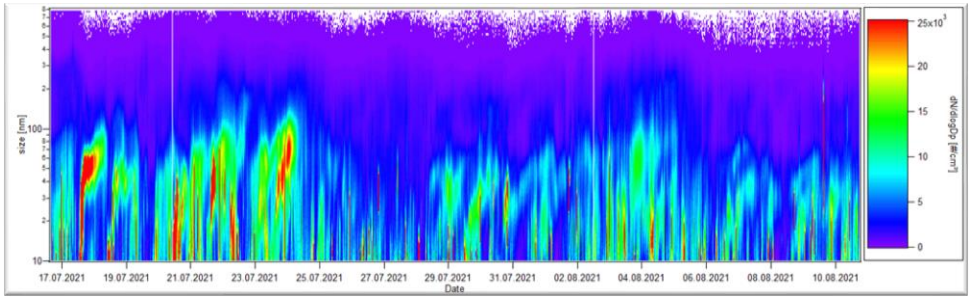

Fig. 1: Full CEN-compliant solution including sampling inlet, PN and PSD measurements .
Fig. 2: The data shows 24 days @ 5min time resolution close to UFP sources. The sampling site was at TSI GmbH Aachen.

A full-flow butanol-based CPC (Model 3750-CEN, TSI Inc., Shoreview, USA) is calibrated independently at the World Calibration Center for Aerosol Physics (WCCAP) in Leipzig, in addition to the manufacturer's calibration. The same is done for the new wide-range SMPS (Model 3938W50-CEN, TSI Inc.), so it fully complies with the CEN/TS 17434 guideline. An optimized sampling inlet system with dryer, RH/T control and an optional diluter were used to enable standardized measurements. A further advantage of this complete UFP monitoring solution is its comprehensive data output, which permits a transfer to the EBAS database and other data protocols.

REFERENCES

de Jesus, A.L., Rahman, M.M., Mazaheri, M., et al. (2019). Ultrafine particles and PM2.5 in the air of cities around the world: Are they representative of each other? Environment International, Vol. 129, 118-135. DOI: https://doi.org/10.1016/j.envint.2019.05.021

Birmili, W., Weinhold, K., Rasch, F., et al. (2016). Long-term observations of tropospheric particle number size distributions and equivalent black carbon mass concentrations in the German Ultrafine Aerosol Network (GUAN), Earth Syst. Sci. Data, 8, 355–382, DOI: https://doi.org/10.5194/essd-8-355-2016Earth Syst. Sci. Data

CEN/TS 16976. (2016). Ambient air - Determination of the particle number concentration of atmospheric aerosol.

CEN/TS 17434. (2020). Ambient air - Determination of the particle number size distribution of atmospheric aerosol using a Mobility Particle Size Spectrometer (MPSS).

TSI Instrumentation for measuring atmospheric particles according to CEN/TS 16976:2016 and 17434:2020 a Buyer's guide to CEN compliance. (2021). P/N 5002757 Rev. A-(A4), TSI Inc. ,https://tsi.com/getmedia/032b5f18-8f5f-4160-bb72-7dd55dce6d05/CEN_SMPS_Buyers_Guide_5002757A-A4-web?ext=.pdf.

SMOKEMANOVO DESATERO SPRÁVNÉHO TOPIČE – AUDIOVIZUÁLNÍ VERZE

Jiří HORÁK[1], František HOPAN[1]

[1] VŠB – Technická univerzita Ostrava, Centrum energetických a environmentálních technologií, Výzkumné energetické centrum, 17. listopadu 15/2172, Ostrava-Poruba, smokeman@vsb.cz

Klíčová slova: Vytápění pevnými palivy, Kotle, Kamna, Pevná paliva

SUMMARY

SMOKEMAN's Ten Rules for a Good Heater attempts to point out in a simple and entertaining way the basic parameters and principles that, if followed, will allow us to get more heat and less smoke from our chimneys. SMOKEMAN, as a trained miner, never liked theoretical discussions unless it was clear what their practical application was.

ÚVOD

SMOKEMANovo desatero správného topiče se snaží jednoduchou a zábavnou formou ukázat na základní parametry a zásady, které uživateli, pokud se jimi budeme řídit, umožní, aby se více ohřáli, a přitom se z jejich komínů méně kouřilo. SMOKEMAN jako vyučený horník nikdy neměl zalíbení v teoretických rozborech, pokud nebylo jasné, jaké je jejich praktické využití.

VÝSLEDKY, DISKUSE, ZÁVĚRY

Série SMOKEMANových videí vychází z „Desatera správného topiče“ (Obr. 1) a snaží se zábavnou i poučnou formou oslovit co nejširší skupinu provozovatelů spalovacích zařízení na pevná paliva a přiblížit jim správné praktiky spalování pevných paliv. Videa jsou představena formou tří plylistů. První plylist obsahuje „hranou“ část, do které je vsunuta „vysvětlující“ (animovaná) část, která danou problematiku podrobněji vysvětluje. Další dva playlisty prezentují zvlášť „hranou“ a „vysvětlující“ část. Názvy jednotlivých epizod:

TRAILER 1 – Stechiometrie spalování jako vztah mezi mužem a ženou
TRAILER 2 – Zrození SMOKEMANa
01/10 - TOP TAK, JAK CHCEŠ, ABY TOPIL TVŮJ SOUSED
02/10 - SUŠ DŘEVO MINIMÁLNĚ JEDEN, LÉPE DVA ROKY
03/10 - NESPALUJ ODPADKY
04/10 - NEDUS OHEŇ
05/10 - JAK ČASTO A KOLIK PŘIKLÁDAT
06/10 - CO A JAK ČISTIT
07/10 - POUŽÍVEJ MODERNÍ KOTEL ČI KAMNA
08/10 - UDRŽUJ OPTIMÁLNÍ TEPLOTU SPALIN
09/10 - NEVYHAZUJ TEPLO OKNEM
10/10 - CO OVLIVNÍ TVŮJ KOUŘ

PODĚKOVÁNÍ

Projekt LIFE IP – Zlepšení kvality ovzduší (LIFE18 IPE/SK/000010) podpořila Evropská unie v rámci programu LIFE. Projekt je také spolufinancován Ministerstvem životního prostředí ČR.

ODKAZY

Smokemanovo desatero správného topiče:
playlist dlouhých videí (spojena “hraná” a “vysvětlující” část) ,
https://www.youtube.com/playlist?list=PLZCEJpckSlpV3TGeEixJU73JVH1J2mi62 nebo
https://estav.tv/porad/smokemanovo-desatero/
Playlist “hraných” částí:
https://www.youtube.com/playlist?list=PLMYSdf0zSP5aDdtT61EyvrVHi04sVPZks
Playlist “vysvětlujících” (animovaných) částí:
https://www.youtube.com/playlist?list=PLMYSdf0zSP5YgkX0AVdnFy6-ydEW8w5l1

Obr. 1: Smokemanovo desatero správného topiče.

ENDOSKOPICKÉ ZÁKROKY V DOBĚ COVID-19

Martin WASSERBAUER[1], Štěpán HLAVA[1], Raden KEIL[1]

[1] Interní klinika FN Motol, Praha

SUMMARY

Onemocnění COVID-19 bylo, je a pravděpodobně i nadále bude vážný celosvětový zdravotní problém. V součinnosti s Akademií věd ČR byl vytvořen experimentální model, který simuloval podmínky přítomné během endoskopických procedur horní části zažívacího traktu (např. gastroskopie). Cílem naší práce bylo prokázat počet potenciálně infekčních částic přítomných během endoskopických procedur a najít účinné nástroje k eliminaci rizik infekce COVID-19 při jejich provádění. Z tohoto důvodu jsme navrhli a testovali prototyp ochranného krytu pro ovládací část endoskopu, abychom zabránili uvolňování a šíření těchto částic tekutin z pracovního kanálu endoskopu. Provedli jsme měření s ochranným krytem ovládací části endoskopu i bez něj. Bylo zjištěno, že kapalina procházející pracovním kanálem endoskopu při přítomnosti vložených instrumentárií generuje tekutinové partikule s průměrem v rozmezí 0,1–1,1 mm. Bylo zjištěno, že speciální ochranný kryt navržený naším týmem na ovládací část endoskopu, vyrobený z prodyšného materiálu (chirurgická čepice), eliminuje uvolňování potenciálně infekčních částic tekutin.

PHYSICOCHEMICAL PROPERTIES AND ORIGIN OF PM_1 MEASURED AT A RURAL BACKGROUND SITE

Petra POKORNÁ[1], Naděžda ZÍKOVÁ[1], Petr VODIČKA[1], Radek LHOTKA[1,2], Saliou MBENGUE[3], Adéla HOLUBOVÁ ŠMEJKALOVÁ[4], Véronique RIFFAULT[5], Jakub ONDRÁČEK[1], Jaroslav SCHWARZ[1], Vladimír ŽDÍMAL[1]

[1] Institute of Chemical Process Fundamentals of the CAS, Prague, Czech Republic, pokornap@icpf.cas.cz
[2] Institute for Environmental Studies, Faculty of Science, Charles University, Prague, Czech Republic
[3] Global Change Research Institute of the Czech Academy of Sciences, Brno, Czech Republic
[4] Czech Hydrometeorological Institute, Prague, Czech Republic
[5] IMT Nord Europe, Institut Mines-Télécom, Université de Lille, Centre for Energy and Environment, Lille, France

Keywords: Atmospheric aerosol, Aerosol mass spectrometer, Chemically speciated mass size distribution, Density, Shape, Cluster analysis.

INTRODUCTION

Measurements at rural background sites representative of wider areas are important to study the influence of regional and long-range transport as well as the long-term trends in PM characteristics (Putaud et al., 2010; Schwarz et al., 2016; Poulain et al., 2020). The National Atmospheric Observatory Košetice (NAOK), officially classified as a central European rural background site, participates in the European Monitoring and Evaluation Programme (EMEP), Aerosol, Clouds, and Trace Gases Research Infrastructure Network (ACTRIS), and Global Atmosphere Watch (GAW) network. Several studies were conducted at the NAOK site however, detailed work focused on the seasonal variability in PM chemical composition data with high temporal and spatial resolutions is still lacking. Therefore, the focus of this study was to characterise individual episodes of high mass and number concentrations based on highly-time resolved measurement and linked to different air mass types, thereby offering insights into the physicochemical properties and sources of aerosol particles arriving at a rural background site.

MEASUREMENT AND METHODS

Two intensive campaigns (July 2019 and January – February 2020) were conducted. Size-resolved PM chemical composition, as well as particle number size distribution in the size range 10 – 800 nm were measured every 5-min by a compact time of flight aerosol mass spectrometer (C-ToF-AMS, Aerodyne) and a Mobility Particle Size Spectrometer (MPSS, IFT TROPOS, Leipzig, with CPC 3772, TSI). 1-min PM_1 equivalent black carbon (eBC) concentrations were determined by aethalometer (AE33, Magee Scientific) simultaneously with 4-h PM2.5 organic and elemental carbon concentrations (Sunset Laboratory Inc.). Besides, PM_1 were collected for 12 h by a sequential sampler (LVS-3, Sven Leckel Ingenieurbüro) for subsequent chemical analyses (water-soluble ions and monosaccharide anhydrides). Finally, 1-h $PM_{2.5}$ mass concentrations (Environnement SA,

MP101M) and meteorological parameters were also recorded.

The standard data processing procedure of AMS was carried out by running the Squirrel v1.62 programme in Igor Pro data analysis software (WaveMetrics, Inc.).

The statistical data treatment was performed using R version 3.6.1 with the ggplot2 (Wickham, 2016) and Openair (Carslaw and Ropkins, 2012) packages.

To determine the collection efficiency (CE; Drewnick et al., 2005) in the AMS, PM_1 filter sampling with subsequent ion chromatography (IC) analysis was conducted in parallel with the AMS measurements.

The effective density (ρ_{eff}) and material density (ρ_m) was estimated along with the dynamic shape factor (χ) inferred from the two densities.

96 h backwards trajectories were calculated using the Hybrid Single-Particle Lagrangian Integrated Trajectory (HYSPLIT) model (Rolph et al., 2017) with a 500 m a.g.l. (above ground level) starting position and Global Data Assimilation System (GDAS) Archive Information at a resolution of 1° x 1° as input data. The calculations were initialized every 6 h for the cluster analysis. For the episodes of high mass concentrations, the trajectory ensemble option with calculation initialized every hour and a total duration of 72 h was utilized. The trajectories were further clustered using Hysplit4 software based on the total spatial variance. From HYSPLIT, the planetary boundary layer height data were extracted. For the planetary boundary layer height calculations, the 0.25° x 0.25° Global Forecast System (GFS) dataset was used as input data to obtain a 3 h temporal resolution.

RESULTS AND CONCLUSIONS

The average PM_1 concentration (sum of NR-PM_1 and eBC) was 8.6 ± 3.7 $\mu g \cdot m^{-3}$ and 10.1 ± 8.0 $\mu g \cdot m^{-3}$ for summer and winter, respectively. NR-PM_1 was mainly composed of organics during both campaigns, followed by either SO_4^{2-} (summer) or NO_3^- (winter). The size distribution of NR-PM_1 species was dominated by the accumulation mode in both seasons, with larger particles for all species in winter as a result of aerosol ageing. Organics showed the smallest modal diameter from all NR-PM_1 chemical species, which suggests its condensation on pre-existing particles (Tab. 1).

Tab. 1: Mode diameter of mass distributions of species measured by AMS (D_p corresponds to the vacuum aerodynamic diameter (D_{va})) for the summer and winter campaigns.

	Org	SO_4^{2-}	NO_3^-	NH_4^+
Summer D_{va} (nm)	334	377	401	497
Winter D_{va} (nm)	413	501	547	517

Since the winter aerosols were less oxidized than the summer ones (comparing m/z 44 and 43), the importance of local sources in the cold season was to be considered. Although aged continental air masses from the south-east (SE) were rare in summer (7 %), they were related to the highest concentrations of PM_1, eBC, and all NR-PM_1 species, especially SO_4^{2-} and NH_4^+. In winter, slow continental air masses from the south-west (SW) (44 %) were linked to inversion conditions over central Europe and were associated with the highest concentrations among all NR-PM_1 species as well as PM_1 and eBC (Fig. 1). The average PM_1 material density (ρ_m) corresponded to higher inorganic contents in both seasons (summer: ~1.30 $g.cm^{-3}$ and winter: ~1.40 $g.cm^{-3}$). The dynamic shape factors (χ)

decreased slightly with particle mobility diameter (D_m) in both seasons.

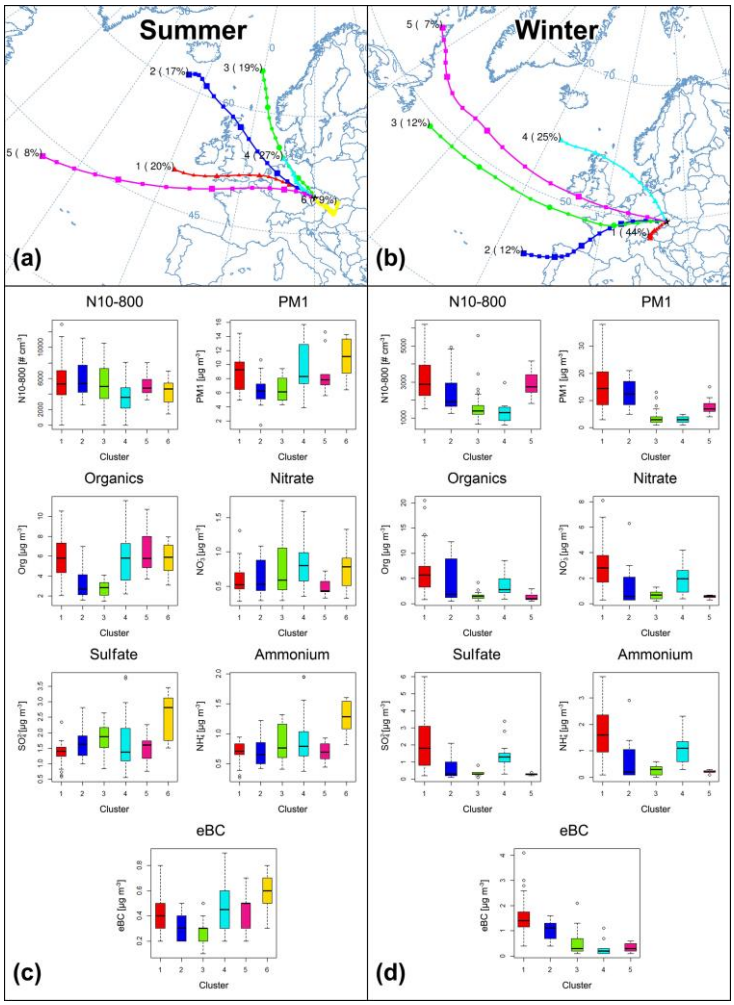

Fig. 1: Geographical locations of the means of the clusters observed in summer (a) and winter (b) along with boxplots of the PM_1, N10–800, organic, nitrate, sulfate, ammonium, and eBC concentrations in individual clusters measured during the summer (c) and winter (d) campaigns. The boxes are color coded as the clusters, the black horizontal line is the median, the boxes border the 25th and 75th percentiles, and the whiskers represent 1.5 x IQR.

By examining individual episodes of high mass and number concentrations, we show that the seasonal differences in the physicochemical properties of aerosol particles were caused by the diversity of sources and were related to the different air masses and meteorological conditions during summer and winter season. We also confirmed the relation between particle size and age reflected both in its oxidation state and shape factor. The results of these specific properties (density, shape, and oxidation state of particles) have general validity and thus transcend the regional character of this study.

ACKNOWLEDGEMENT

This work was supported by the GACR under grant P209/19/06110Y and by the MEYS of the Czech Republic, within the project for support of the national research infrastructure ACTRIS–CZ (LM2018122) and under grant LTAUSA19006 as well as by COST Action COLOSSAL (CA16109) within STSM.

REFERENCES

Carslaw, D.C., Ropkins, K., Openair – an R package for air quality data analysis, *Environ. Model. Software* 27–28:52–61, (2012).

Drewnick, F., Jayne, J. T., Canargaratna, M., Worsnop, D. R., Demerjian, K. L., Measurement of ambient aerosol composition during the PMTACS-NY 2001 Using and Aersosol Mass Spectrometer. Part II: Chemically speciated mass distribution, *Aerosol Sci. Tech.*, 38:104–117, (2004).

Poulain, L., Spindler, G., Grüner, A., Tuch, T., Stieger, B., van Pinxteren, D., Petit, J.-E., Favez, O., Herrmann, H., Wiedensohler, A., Multi-year ACSM measurements at the central European Research station Melpitz (Germany) – Part 1: Instrument robustness, quality assurance, and impact of upper size cutoff diameter, *Atmos. Meas. Tech.*, 13:4973–4994, (2020).

Putaud, J.P., Van Dingenen, R., Alastuey, A., Bauer, H., Birmili, W., Cyrys, J., Flentje, H., Fuzzi, S., Gehrig, R., Hansson, H.C., others, A European aerosol phenomenology — 3: physical and chemical characteristics of particulate matter from 60 rural, urban, and kerbside sites across Europe, *Atmos. Environ.*, 44:1308–1320, (2010).

Rolph, G., Stein, A., Stunder, B., Real-time environmental applications and display sYstem: READY, *Environ. Model. Software* 95:210–228, (2017).

Schwarz, J., Cusack, M., Karban, J., Chalupníčková, E., Havránek, V., Smolík, J., Ždímal, V., $PM_{2.5}$ chemical composition at a rural background site in Central Europe, including correlation and air mass back trajectory analysis, *Atmos. Res.* 176–177:108–20, (2016).

Wickham, H., ggplot2: Elegant Graphics for Data Analysis, *Springer-Verlag, New York*, ISBN 978-3-319-24277-4, (2016).

THREE YEARS OF EXPERIENCE WITH MEASUREMENT OF CLOUD CONDENSATION NUCLEI CONCENTRATIONS USING CLOUD CONDENSATION NUCLEI COUNTER CCN-200

Pavel MORAVEC[1], Radek LHOTKA[1], Vladimír ŽDÍMAL[1]

[1] Institute of Chemical Process Fundamentals of the CAS, Prague, Czech Republic, moravec@icpf.cas.cz

Keywords: Atmospheric aerosols, CCN, CCN concentration measurement, CCN-200

INTRODUCTION

Aerosol particles in the atmosphere that allow water vapor to condense and form cloud droplets are called Cloud Condensation Nuclei (CCN). Elevated concentrations of CCN tend to increase the concentration and decrease the size of droplets. This can lead to suppression of precipitation in shallow and short-lived clouds and to greater convective overturning and more precipitation in deep convective clouds, Rose et al. (2010). The response of cloud properties and precipitation processes to increasing anthropogenic aerosol concentrations represents one of the largest uncertainties in the current understanding of climate change. One of the fundamental challenges is to determine the ability of aerosol particles to act as CCN under relevant atmospheric conditions. Knowledge of the spatial and temporal distribution in the atmosphere is essential to incorporate the effects of CCN into meteorological models of all scales, Huang et al. (2007). Long-term CCN measurements are performed at aerosol monitoring sites such as those forming ACTRIS (Aerosols, Clouds and Trace Gases Research Infrastructure) network. In this paper, we present the three-year experience of measuring CCN concentrations over the National Atmospheric Observatory Košetice (NAOK), a rural background site in the Czech Republic. The first results of these measurements were presented by Mishra et al. (2022).

EXPERIMENTAL SETUP

The instrument used for the CCN concentration measurements was a Dual Column Cloud Condensation Nuclei Counter (CCN-200) purchased from Droplet Measurements Technologies, USA. The DMT CCNC operates on the principle that heat conduction in air is slower than diffusion of water vapor (Roberts and Nenes, 2005). The CCNC operates by maintaining a positive temperature difference between the top and bottom of the column. Inside the column, the supersaturated water vapor condition is caused by diffusion of water vapor from the warm, moist column wall toward the centerline, at faster rate than heat. In order to obtain homogeneous data sets with high quality CCN measurements, a standard operating procedure (SOP) has been defined within the ACTRIS-2 project (WP3-NA3). The SOPs are defined for both polydisperse and monodisperse measurements. The CCN dual column counter we use allows us to make two simultaneous measurements of CCN concentrations. Different combinations of supersaturations (SSs) can be used in each column, so that data for multiple SSs can be collected during one measurement cycle. Another option is to perform the CCN measurement in one column in a polydisperse manner and in the other in a monodisperse manner. The advantage of monodisperse CCN

concentration measurement is that fractions of activated aerosol particles can be obtained on each SS for several particle sizes, so that two-dimensional CCN concentration spectra can be obtained during one measurement cycle. In our measurements, we mostly used the same SS in both columns during the measurement cycle, but in one measurement period (No. 3 in Table 1) we used different SS in columns A and B. An overview of the measurement campaigns can be found in Table 1.

Tab 1: SS settings of measurements in different time periods. No 1 - period from 24. 6. 2019 to 26. 2. 2020, No. 2 - period from 24. 6. 2020 to 21. 9. 2020, No. 3 - period from 21. 9. 2020 to 14. 10. 2020, No. 4 - period after WiIN10 System Upgrade from 14. 4. 2021 until now.

No. 1	SS [%]	0.1	0.15	0.2	0.3	0.5	1
	Time [min]	10	6	6	7	8	8
No. 2	SS [%]	0.1	0.2	0.3	0.5	1	
	Time [min]	20	10	10	10	10	
No. 3	SS_A [%]	0.15	0.2	0.25	0.5	0.7	
	SS_B [%]	0.1	0.2	0.3	0.5	1	
	Time [min]	20	10	10	10	10	
No. 4	SS [%]	0.1	0.2	0.3	0.5	1	
	Time [min]	10	7	7	8	8	

Apart from the above-mentioned advantages, the CCN-200 also has some disadvantages compared to the single-column CCN-100. They arise from the fact that the same size box can accommodate two instruments instead of one. As a result, the replacement of some spare parts (sheath flow filters, Nafion, etc.) is more complicated due to the poor access to these parts. Another problem occurs during the transition period from the highest to the lowest SS. The amount of heat that must be removed from the cover is twice as large and it takes longer to stabilize the temperatures for new SS than for the CCN-100 single-column instrument. This must be taken into account when setting the time for the measurement cycle overlay. Unfortunately, there is no reference to this phenomenon in the CCN-200 instruction manual. The water consumption is also twice that of the CCN-100, which is not insignificant when measuring in remote locations. Therefore, we have replaced the original 0.5-liter bottles with 2-liter bottles, which allows 8 days of continuous operation of the CCN-200.

INTERCOMPARISON AND CALIBRATION WOKSHOP

In March 2020, we participated in an intercomparison and calibration workshop at TROPOS in Leipzig, Germany, where calibration of flow rates and SSs as well as intercomparison measurements with our CCN-200 and four other CCN-100 instruments were performed. On this occasion we also found out the problem with the cooling of the optical detector. The results are shown in Fig. 1a. We can see that the temperature T_1 is almost constant and the temperatures T_2 and T_3 change up and down quite rapidly when SS changes. T_{Opc} also increases rapidly but decreases very slowly. This is due to the fact

that the optical cell is heated but not cooled. In fact, at the end of the 10-minute measurement interval for SS 0.1%, T_{Opc} is still about 6 °C above T_3 (the correct value for $T_{Opc\ Set}$ in the CCN-200 software is T_3 + 2 °C). Of course, T_{Opc} should be higher than T_3 to prevent fogging of the optical cell, but too high T_{Opc} leads to evaporation of condensed water and loss of droplets. Studies with DMT have shown (Operator Manual, 2018) that T_{Opc} can be up to 5 °C above T_3 without decreasing concentration. At a T_{Opc} of 7 °C above T_3, there is a 20% loss of droplets, which is similar to the case of our measurements with 10 min interval for SS 0.1%. After adjusting the measurement interval at SS 0.1% to 20 minutes, see period No. 2 in Table 1, the difference between T_{Opc} and T_3 at the end of the

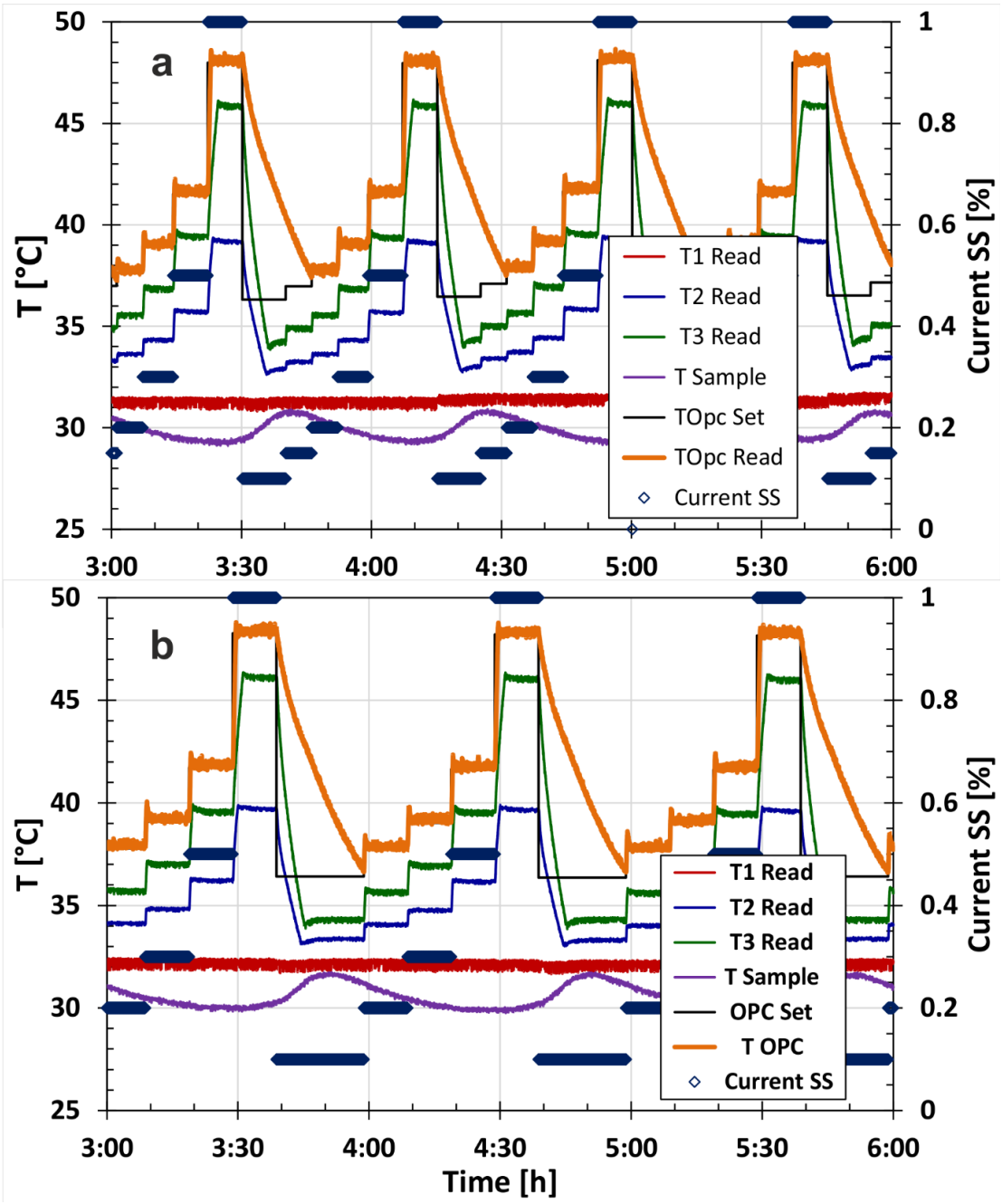

Fig. 1a, b: Time dependences of temperatures at CCN-200 for 45 and 60 minutes measuring cycles. T_1, T_2 and T_3 - temperatures at column top, middle and bottom, T_{Sample} - temperature in the inlet manifold, T_{Opc} and Opc Set - measured and set temperature in the optical cell.

measurement interval did not exceed 5 °C, see Fig. 1b, so we can consider the measurements in period No. 2 to be correct.

CCN-200 – WIN10 SYSTEM UPGRADE

At the end of 2020, we accepted a quote from DMT for CCN-200 - WIN10 System Upgrade. The upgrade included: WIN10 Electronic System Hardware Upgrade, WIN10 Operating Software & Driver Installation, Win10 CCN-200 Software Installation and regular maintenance, factory calibration and door-to-door logistics. We were told that the functionality of the unit after the upgrade was the same as before, but that was not the case. Water consumption is now about 15% higher, so the 2-liter supply bottle is used up in 7 days instead of 8. The main difference, however, is in the setting of the SSs. In the Win7 CCN-200 software, the length of the measurement time for each SS was exactly the same as specified by the user in the SS settings table, regardless of whether the temperatures were stabilized or not, so the times for each SS and for the entire measurement cycle were precisely defined. In the WIN10 CCN-200 software, the measurement time for each SS consists of two parts: the unknown time required to stabilize all temperatures, including T_{0pc}, and the time defined by the user for the measurement itself in the SS settings table. Temperatures are considered stabilized when the difference between the set temperature and the measured temperature is ≤ 0.4 °C. The sum of unknown times for each SS during the measurement cycle is almost 20 minutes, mainly for the transition from the highest SS to the lowest. Originally, this time was even longer, but it was significantly shortened by using a new insulation of the optical cell. From the above, it is obvious that we cannot specify exact times for individual SS or for the entire measurement cycle. Another novelty of the upgrade is that the user can choose between two measurement modes: System Stability and Individual Stability. In system stability, the SSs and time intervals in both columns must be the same. The measurements in both columns are then synchronized, i.e. the measurement cycles in both columns start and end at the same time. In Individual Stability mode, the user can set different SSs and different time intervals in each column, but the measurement cycles in each column are different in length and the measurements are not synchronized.

Even with Win7 system, CCNC would occasionally reboot spontaneously, with a frequency of reboots every month or two. This was strange, but acceptable. However, after the system upgrade, the frequency of reboots gradually increased, eventually ending in a cyclic reboot and eventual system collapse. As a result, we sent CCNC back to DMT for warranty repair and were surprised to find that the problem was resolved very quickly. We were told to use UPS for the CCNC power supply to avoid voltage fluctuations. However, this did not work. After about two months, the problem repeated itself with spontaneous reboots and the system breaking down. The diagnosis made by our employee from IT together with technicians from DMT revealed that the problem was most likely a damaged PC of the CCNC. Initially, we thought we would have to buy a new PC and replace it ourselves. However, we were pleasantly surprised. DMT staff (sales manager and technicians) visited our institute and replaced the damaged PC, helped calibrate the flow rates, and accompanied us to NAOK to see the installation of the CCNC at a remote site. Since then (November 16, 2021), the CCN-200 has been working properly with no spontaneous reboots.

RESULTS AND CONCLUSIONS

We have been collecting CCN concentration data through NAOK since June 2019. Until October 2020, we used the Dual CCN.exe program running on WIN7 operating system. This data is almost ready to be submitted to the EBAS database. However, the data set from June 2019 to February 2020 contains CCN concentrations at SS 0.1%, which were underestimated by 10 - 20% due to the short measurement interval and T_{Opc} being too high. Data collected after CCN-200 - WIN10 SYSTEM UPGRADE have an undefined measurement cycle length. For these data, the procedure for submission to the EBAS database still needs to be worked out and approved by NILU.

ACKNOWLEDGEMENT

This work was supported from European Regional Development Fund-Project "ACTRIS-CZ RI" (No. CZ.02.1.01/0.0/0.0/16_013/0001315) and by the infrastructure project of the MEYS of the Czech Republic ACTRIS-CZ – LM2015037.

REFERENCES

Huang Y., Chameides W.L., Dickinson R.E., Direct and indirect effects of anthropogenic aerosols on regional precipitation over east Asia, *J. Geophys. Res.* 112, D03212, doi:10.1029/2006JD007114 (2007).

Mishra G., Moravec P., Ždímal V., Fist surface measurements of variation in Cloud Condensation Nuclei concentrations over a rural background site of the Czech Republic, IAC 2022, Athens, Greece, 4-9 September 2022.

Operator Manual for Dual-Column CCN, DOC-0128 Revision F, Chapter 12.2.2.1, p. 67, DMT 2018.

Roberts G.C., Nenes A., A continuous-flow streamwise thermal-gradient CCN chamber for atmospheric measurements, *Aerosol Sci. Technol.*, 39, 206-221 (2005).

Rose D., Nowak A., Achtert P., Wiedensohler A., Hu M., Shao M., Zhang Y., Andreae M.O., Pöschl U., Cloud condensation nuclei in polluted air and biomass burning smoke near the mega-city Guangzhou, China – Part 1: Size-resolved measurements and implications for the modeling of aerosol particle hygroscopicity and CCN activity, *Atmos. Chem. Phys.*, 10, 3365-3383 (2010).

WP3- NA3: In-situ chemical, physical and optical properties of aerosols. Deliverable D3.13: Standardized protocol for CCN measurements, http://fp7.actris.eu/Portals/97/deliverables/PU/WP3_D3.13_M24.pdf

ANALÝZY ATMOSFÉRICKÝCH AEROSOLŮ POMOCÍ SVAZKU URYCHLENÝCH IONTŮ

Vladimír HAVRÁNEK[1]

[1] Ústav jaderné fyziky AV ČR v.v.i., Husinec-Řež, Česká Republika, havranek@ujf.cas.cz

Klíčová slova: Aerosoly, Prvkové složení, Jaderné analytické metody, Iontová mikrosonda

SUMMARY

Energetic ions of MeV energies supplied mainly by electrostatic accelerators are nowadays for a long period of time successfully used for the aerosol elemental characterization by PIXE, RBS, PESA and PIGE methods worldwide. Laboratory of nuclear analytical method at NPI AV CR in Řež near Prague has more than thirty years' experience in utilizing these methods for the aerosol analysis as well. Two experimental vacuum target chambers are available in beam lines of 3MV TANDETRON 4130MC accelerator. One designated for broad beam measurement simultaneously by above mentioned techniques and second for microbeam measurement with lateral resolution of about 1μm and scanning area of 1-2mm^2.

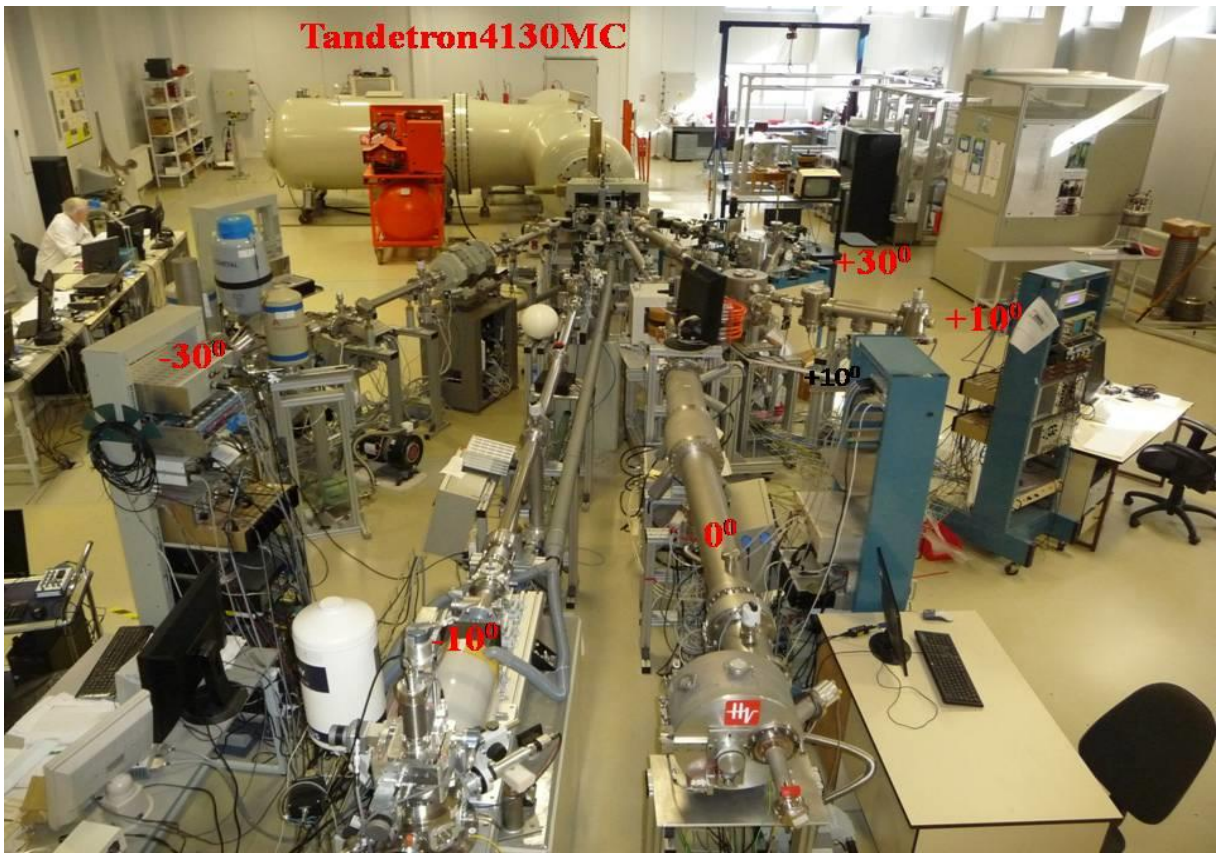

Obr. 1: Uspořádání iontových tras na Tandetronu 4130MC. Iontová mikrosonda je umístěna na trase -10°, komora pro simultánní analýzy PIXE, PIGE,RBS a PESA na -30°.

METODY, URYCHLOVAČ A VZORKY

Jaderné analytické metod vyžívající energetické ionty s energiemi o oblasti jednotek MeV, nejčastěji urychlenými pomocí elektrostatických urychlovačů, jsou již dlouhou dobu úspěšně využívány také k prvkovým analýzám vzorků atmosférických aerosolů. Kombinací metod PIXE (částicemi buzená rentgen fluorescence), RBS (rutherfordův zpětný rozptyl), PIGE (částicemi buzená emise gama záření) a PESA (elastický rozptyl protonů) lze za vhodných podmínek a vhodně zvolené podložky k depozici aerosolu pokrýt prakticky celé spektrum prvků periodické soustavy včetně analýz vodíku. V současnosti naše laboratoř disponuje elektrostatickým urychlovačem tandemového typu (Tanderton 4130 MC od firmy HVEE) s terminálovým napětím 3MV schopným urychlovat většinu iontů na energie od stovek keV do jednotek až nižších desítek MeV. Pro analýzu aerosolů jsou nejvhodnější protony s energiemi mezi 1-4MeV, případně částice alfa (jádra He) mírně vyšších energií. K analýze aerosolů jsou k dispozici dvě terčíkové komory na trasách -30st. (mnohoúčelová komora s možností simultánních analýz PIXE, PIGE, RBS a PESA s možností umístění dalších detektorů podle požadavku experimentu) a -10st. (iontová mikrosonda s laterálním rozlišením okolo 1μm a skenovanou plochou do 1-2 mm^2 s možností analýz PIXE, RBS, STIM s možností rozšíření o další metody).

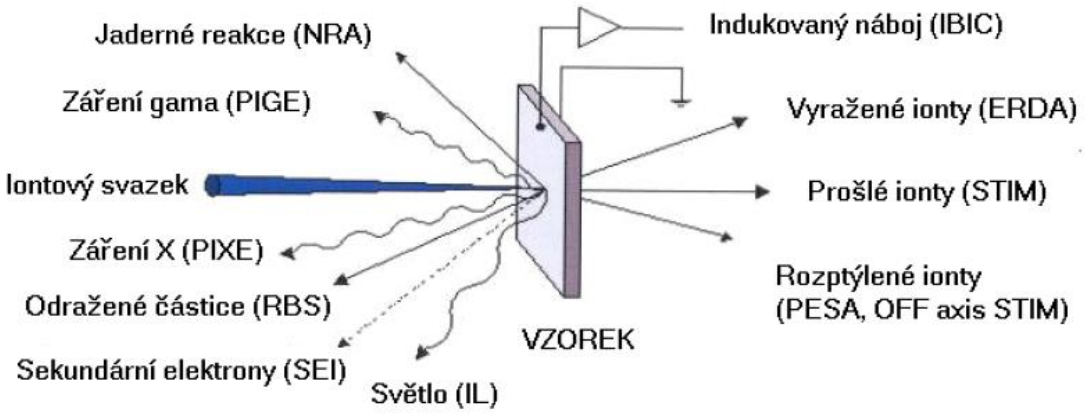

Obr. 2: Základní procesy vyvolané svazkem urychlených iontů ve zkoumaném vzorku. K analýze aerosolů se využívají především metody, PIXE, PIGE, RBS a PESA.

Pro co nejlepší výsledky analýz je potřeba správně volit odběrové zařízení i složení odběrových fólií s nízkým obsahem stopových znečisťujících prvků (blankem). Pro analýzu vodíku jsou vhodné tenké teflonové filtry. Pro tloušťku fólie je vhodné volit co nejtenčí k potlačení pozadí od sekundárních elektronů. Při volbě tlustších substrátů nebo tlustších depozitů z kaskádních impaktorů je často nezbytné provést korekce na tloušťku depozitu. V případě dostatečného množství odebraného aerosolu je také možné volit vzorky v podobě tenkých lisovaných tablet.

PODĚKOVÁNÍ

Autoři práce děkují za podporu projektu CANAM LM2015056 za podporu experimentů.

TRANSPORT OF PLASMA REACTIVE SPECIES INTO AEROSOLS VS. BULK WATER

Mostafa Elsayed HASSAN[1], Mário JANDA[1], Zdenko MACHALA[1]

[1] Division of Environmental Physics, Faculty of Mathematics, Physics and Informatics, Comenius University, Mlynská Dolina, Bratislava 842 48, Slovakia
machala@fmph.uniba.sk

Keywords: Non-thermal plasma, Electrospray, Aerosol microdroplets, Transport of gaseous species, Henry's law solubility

INTRODUCTION

Atmospheric non-thermal plasmas produce mixtures of reactive oxygen and nitrogen species (RONS). The plasma–water interaction enables the transport of these RONS to the liquid water, which is significantly enhanced by converting bulk water to aerosol microdroplets [1]. Having different Henry's law solubility coefficients (k_H) under the equilibrium conditions, the expected solubility of various RONS is very different. We investigate the transport of RONS into the water aerosol microdroplets, under nonequilibrium conditions characteristic of plasma–water interactions.

EXPERIMENTAL SETUP AND METHODS

The transport of gaseous H_2O_2, HNO_2, NO_2, NO, and O_3 into the bulk water and the aerosol of electrosprayed (ES) and nebulized microdroplets is investigated. Gaseous H_2O_2, HNO_2, NO_2, NO, and O_3 species are first provided by external sources (liquid H_2O_2 or HNO_2, NO_2 and NO mixtures from pressure tanks, ozone generator). UV-Vis spectroscopy colorimetric methods are used for the chemical analysis of the dissolved species (H_2O_2, NO_2^-, NO_3^-, and O_3) in water. The concentrations of gaseous H_2O_2, NO, and O_3 are measured using electrochemical gas sensors, while HNO_2 and NO_2 are measured by UV-Vis absorption spectroscopy.

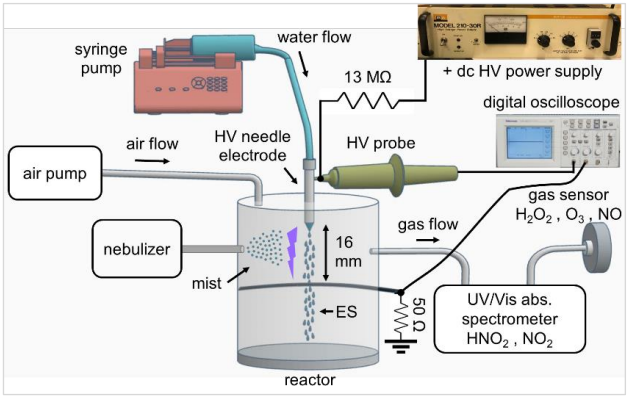

Fig. 1: Schematic of the experimental setup of plasma discharge interacting with electrosprayed or nebulized water aerosols.

Figure 1 shows the schematic diagram of the experimental setup with the streamer corona plasma discharge in contact with water aerosols. The solvation of RONS in water is compared in two types of microdroplets: charged microdroplets produced by electrospray (ES), and nebulized non-charged microdroplets.

RESULTS AND CONCLUSIONS

Figure 2 shows the total molar number of the dissolved aqueous RONS within 1 min plasma treatment at 0.5 ml/min water flow rate. The solvation of the gaseous H_2O_2, HNO_2, NO_2, NO, and O_3 into water is enhanced by the increasing gas-water interface surface area obtained during the ES or nebulizing aerosolization compared to the transport of RONS into the bulk with a fixed surface area. H_2O_2 was solvated in water 4 orders of magnitude more efficiently than O_3, despite the 7 orders of magnitude larger k_H. This is because H_2O_2 is completely depleted from the gas, unlike O_3 molecules. HNO_2 is well solvated into the water, producing aqueous NO_2^-, with 3 orders of magnitude higher efficacy than O_3, which correlates with their ratio of k_H. NO_2 and NO are solvated in water also making aqueous NO_2^-, with 2 orders of magnitude higher efficacy than O_3, despite similar k_H.

The amount of H_2O_2 and NO_3^- dissolved in the nebulized microdroplets is higher compared to that in the ES microdroplets due to larger plasma–water interface area in nebulized microdroplets (~5 μm). On the other hand, the production of NO_2^-(aq), mainly from HNO_2 [2], is higher in the charged ES microdroplets, despite their larger size (~20-100 μm). The microdroplet size distribution was measured by using high speed camera in parallel with our novel laser/LED attenuation technique [3].

Our results lead to a better understanding of the transport mechanism of plasma-generated gaseous RONS into the water and enable optimization of the plasma-liquid systems for multiple applications in biomedicine, environment, and agriculture.

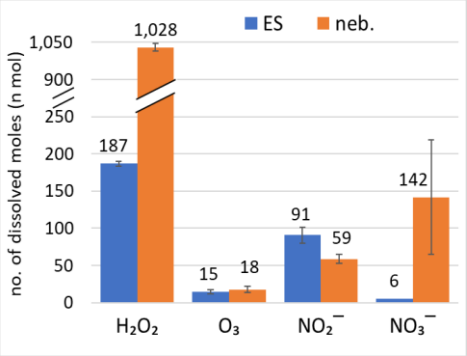

Fig. 2: Amount of dissolved aqueous RONS formed by streamer corona discharge in electrosprayed vs. nebulized water aerosol.

ACKNOWLEDGEMENT

This work was supported by Slovak Research and Development Agency APVV-17-0382 and Grant agency of the Slovak Ministry of Education VEGA 1/0596/22 and Comenius University grant UK/141/2022.

REFERENCES

Hassan M.E., Janda M., and Machala Z., Transport of Gaseous Hydrogen Peroxide and Ozone into Bulk Water vs. Electrosprayed Aerosol, *Water* 13, 182 (2021).

Janda M., et al. The role of HNO2 in the generation of plasma activated water by air transient spark discharge, *Appl. Sci.* 11, 7053 (2021).

Janda M., et al. In-situ monitoring of electrosprayed water microdroplets using laser and LED light attenuation technique: Comparison with ultra-high-speed camera imaging, *J. Appl. Phys*. 129, 183305, (2021).

CHANGE IN SIZE-RESOLVED FILTRATION EFFICIENCY OF RESPIRATORS AFTER DECONTAMINATION/DISINFECTION TREATMENTS

Jakub ONDRÁČEK[1], Lucie ONDRÁČKOVÁ[1], Michal DŘEVÍNEK[2], Petr OTÁHAL[2], Josef VOŠÁHLÍK[2]

[1] Department of Aerosol Chemistry and Physics, ICPF of the CAS, Prague, Czech Republic, ondracek@icpf.cas.cz
[2] Nuclear Protection Department, NINCBP, Kamenná, Czech Republic

Keywords: Respirators, size-resolved FE, decontamination, MPPS, pressure drop

INTRODUCTION

The COVID pandemic increased the global interest in high quality respirators or generally any Personal Protective Equipment (PPE) of respiratory tract. In order to assess the quality of the used PPE it is important to know the filtration efficiency (FE) and pressure drop (breathing resistance) of the PPEs.

Currently used filtration efficiency standards, such as EN149, were not developed to test the PPE FE against particles in sizes of viruses (i.e. < 200 nm). On top of this, the result of EN149 standard filtration efficiency testing is a single number, which could be described as an average filtration efficiency of the tested PPE over large size range of potentially dangerous aerosol particles. The penetration of these particles through the filtration material is a function of their size. Unfortunatelly, the size of "naked" SARS-CoV-2 virus particles (i.e. 80-150 nm) is in the size range, where the main physical mechanisms have very small effect on particle deposition inside the filtration material. Therefore, it is important to know ideally the size-resolved filtration efficiency of the PPE in order to obtain the information about the real protection efficiency of the PPE against the relevant dimensions of the dangerous particles. Such measurement also allows to find the size of the particles penetrating with the highest percentage through the material of PPE (MPPS), which is a crucial parameter to estimate the protection level of the PPE against specific agents, including e.g. SARS-CoV-2 virus particles.

Furthermore, during COVID pandemic many people were using the PPEs for longer time than it was suggested by the manufacturer or tried to use home-made or web community recommended decontamination/disinfection/antiviral treatments. Such treatments may severely destroy the structure of the filtration material and alter the filtration properties as compared to the original piece of the PPE and thus not protect the wearer properly against harmful particles. This work aims to estimate the change in the size-resolved filtration efficiency of different respirators after application of selected decontamination/disinfection treatments.

EXPERIMENTAL SETUP

The size resolved penetration through the material of PPEs (circular sample) was measured using filter testing system developed at LACP ICPF CAS. The simplified schematics of measurement apparatus can be seen on Fig. 1. The measurement was conducted with the flow rate of 8.7 l/min, corresponding to face velocity of 10.6 cm/s

across the sample of the material with active diameter 42 mm given by filter holder geometry. This face velocity is derived from a required flow rate of 95 l/min (according to EN149 standard) through the recommended cross-section of a respirator (facemask) of 150 cm^2. The challenging aerosol was generated by a nebulizer (AGK-2000, Palas) by dispersion of salt solution of $(NH_4)_2SO_4$ having concentration of 1 g/l. The generated aerosol was dried in the diffusion drier containing silica-gel, after that the Boltzmann charge distribution on aerosol particles was achieved by passing through a neutralizer with ^{85}Kr and then the treated aerosol continued into an electrostatic classifier (Electrostatic Classifier, EC Goliath, Research Workshop of ICPF CAS). The monodisperse fraction of the generated aerosol, selected in the classifier by corresponding voltage on the inner electrode, was diluted in the mixing volume so, that the required flow rate through the tested sample was reached. The number concentration of aerosol particles of given size was determined at the same time upstream and downstream the tested filtration material by two CPCs (Condensation Particle Counter).

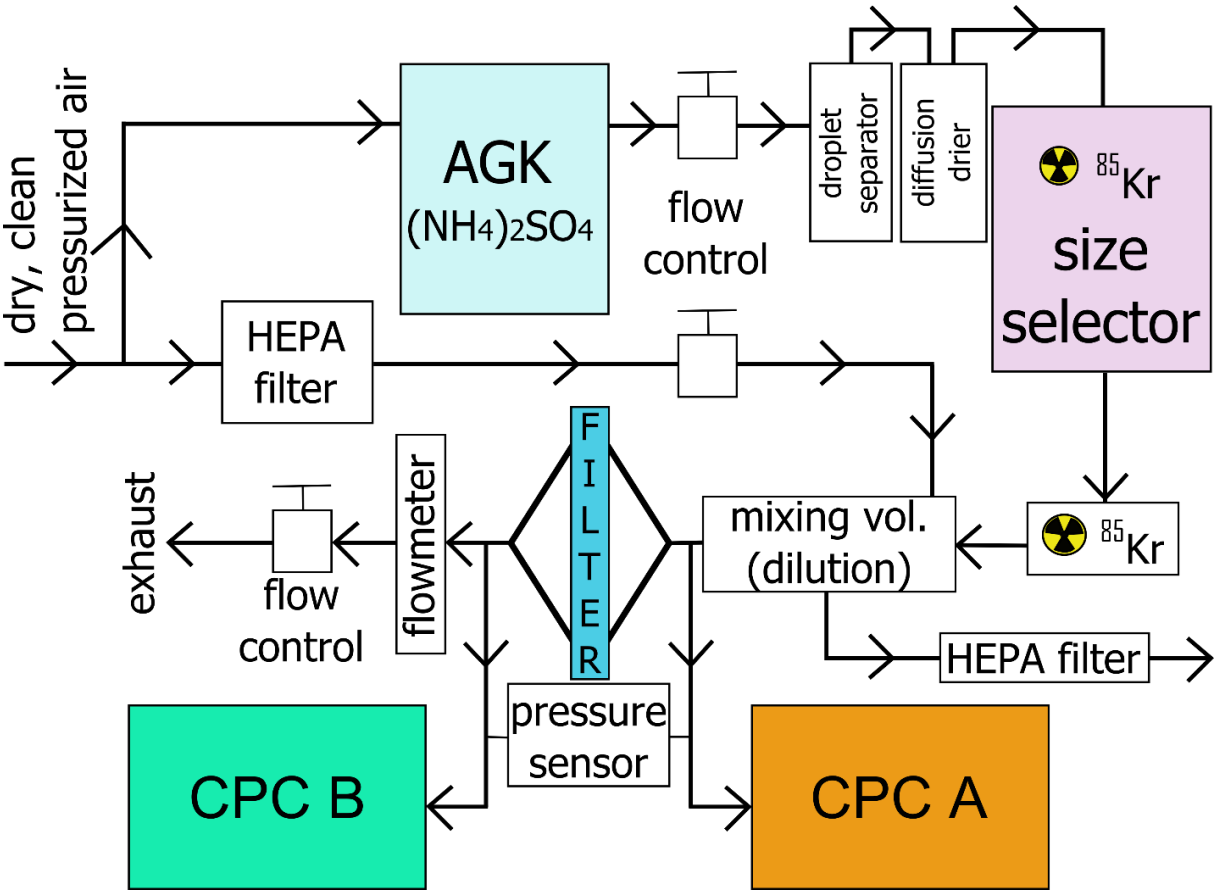

Fig. 1: Schematics of measurement set-up.

The position of the two CPCS was alternated for every selected size of the particles using the pair of electromagnetic valves. The valve switching allows avoiding any errors in measurement due to possible differences in the measurement of both counters. The changes in filtration material properties during the measurement (e.g. filter loading by challenging aerosol) were monitored by the measurement of pressure drop across the filter.

This approach has several advantages as compared to EN149 standard. It has to be considered that the EN 149 standard uses polydisperse aerosol and the method itself is

different from our approach. Moreover, the EN 149 is burdened with many artifacts, which are in most of the cases overestimating the filtration efficiency, and is not very suitable for judging the efficiency of the filtration materials against particles in the sizes from tenths to hundreds of nanometers (the size of SARS-CoV-2 particles was estimated to vary between 80 to 150 nm).

The EN 149 standard uses as a challenge aerosol so called polydisperse aerosol (mixture of sodium chloride particles covering the particle size range 20 nm – 2 μm with mass median diameter at 600 nm and corresponding count median diameter at 360 nm). In most of the cases, the modern filtration materials are having very good filtration efficiency at 360 nm, which is the size of the highest concentration of the challenging aerosol according to EN 149. However, the real MPPS of these materials is usually bellow 100 nm. Furthermore, the detection method giving the information about particle concentration in EN 149 is size dependent – i.e. the larger particles (hundreds of nanometers to units of micrometers) give much more intense signal and these particles are removed by the material with very high efficiency, therefore the resulting filtration efficiency is distorted towards higher numbers.

Several different types of respirator were chosen for the measurements in order to cover a part of the commonly used respirators available on the market (Tab. 1).

Tab. 1: List of tested respirator types.

Type **(Name)**	Manufacturer	EN 149 class
ADD **Air Active** 5500	Air Active	FFP3 NR
G&W GDGP3	Guandong Tengsheng	FFP3 NR
General Public Protection	General Public	FFP3 NR
PHARMAWEX Ro1	PHARMAWEX	FFP2 NR
Refil 750	Refil	FFP3 NR
SpurTex V100	SPUR	FFP2 NR

Tab. 2: List of applied decontamination/disinfection treatments.

Abbreviation	Decontamination treatment	Repetitions
T1	Thermal	1x
T3	dry heat 70°C	3x
T10	60 min	10x
E1	Ethanol	1x
E3	75% bath	3x
E10	15 min	10x
CH1	Chlorine based	1x
CH3	0.6% NaClO bath	3x
CH10	30 min	10x
PV1	Peroxyacetic acid	1x
PV3	saturated vapours	3x
PV10	atmosphere	10x

The decontamination/disinfection treatments were selected to cover part of available approaches (Tab. 2). The treatments were repeated once, 3 and 10 times to see the effect of repeated procedure on the size-resolved filtration efficiency of the respirator materials.

RESULTS AND CONCLUSIONS

Most of the small changes in FE after different decontamination/disinfection treatments is most probably caused rather by the differences in the filtration efficiency of the original material – piece to piece variability in filtration material quality (see Fig.2). Most of the PPEs originally meet their declared EN149 class (checking @CMD=360 nm, which should correspond to MMAD=600 nm according to EN149). And all the materials have MPPS < 100 nm.

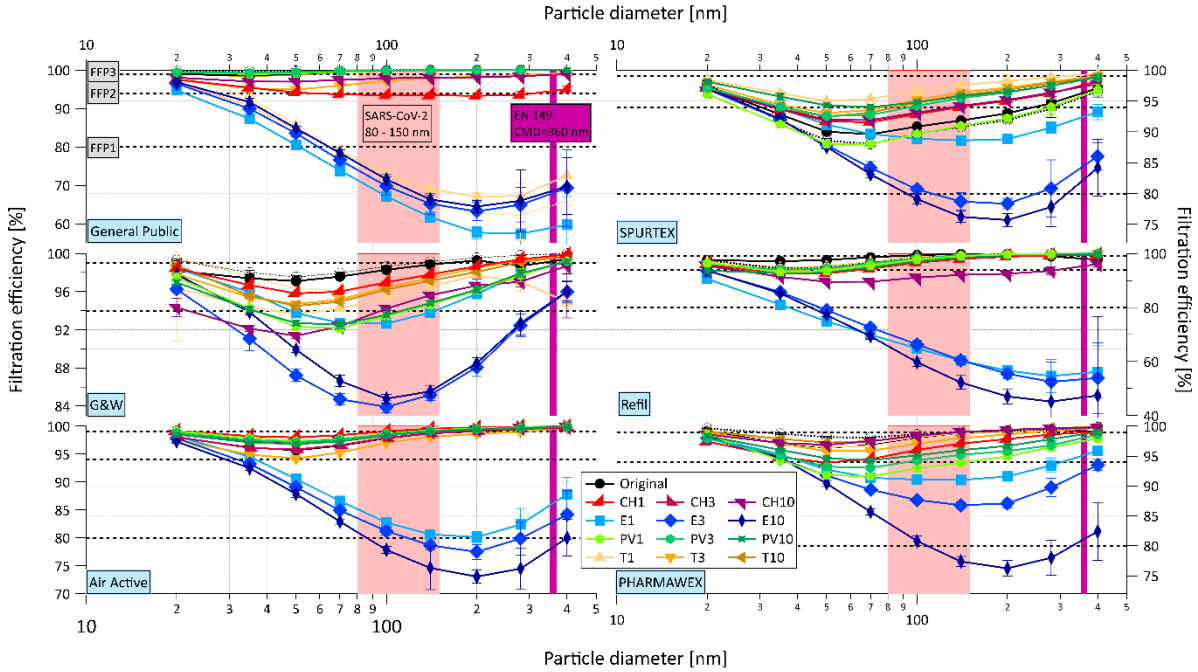

Fig. 2: Size-resolved filtration efficiency for different PPEs after application of various decontamination/disinfection treatments.

However, some more pronounced negative effects can be seen after applying the ethanol bath (for all the respirator types). This effect can be twofold. The removal of the electrostatic charge, originally enhancing the filtration efficiency of the PPE material, by the application of liquid can be one reason for lowered filtration efficiency. The other negative effect can be partial destruction of the structure of filtration material by ethanol (i.e. dissolution of the glues or other damage caused by the interaction of ethanol with the filtration material).

ACKNOWLEDGEMENT

This work was supported by the Ministry of Interior of the Czech Republic under the project no. VI04000048.

THE FLOW OF INHALED FIBRES IN A MODEL OF THE FIRST BIFURCATION IN HUMAN AIRWAYS UNDER TRANSIENT CONDITIONS

František LÍZAL[1], Matouš CABALKA[2], Milan MALÝ[1], Miloslav BĚLKA[1], Ondrej MIŠÍK[1], Jan JEDELSKÝ[1]

[1] Dpt. of Thermodynamics and Environmental Eng., Faculty of Mechanical Engineering, Brno University of Technology, Brno, the Czech Republic, lizal@fme.vutbr.cz
[2] Institute of Mathematics, Faculty of Mechanical Engineering, Brno University of Technology, Brno, the Czech Republic, Matous.Cabalka@vutbr.cz

Keywords: Fibrous aerosols, Fibres, Human airways

INTRODUCTION

Inhaled fibres are known to induce various adverse health effects due to their ability to penetrate deep into the lower regions of the human lungs. This behaviour, however, could potentially be used for delivery of therapeutic drugs to alveoli. Such conversion of originally adverse behaviour to a beneficial and health-improving solution would be not only witty but also potentially commercially attractive. The reason why this potential has not been exploited so far grounds, besides other factors, also in the fact that our current mathematical or computational models are unable to precisely predict the delivered dose for a specific patient. Experimental data on the flow, orientation and "flips" of fibres are needed to improve the current mathematical models. This contribution presents the experimental setup and statistically evaluated data on the behaviour of rigid micrometre-sized fibres in the replica of the first bifurcation in human airways under transient conditions.

EXPERIMENTAL SETUP

The fibres prepared from a glass wool Supafil® Loft (Knauf Insulation GmbH, Simbach am Inn, Germany) were used for the experiment. The wool was crushed by a mechanical press to produce fibres.

The fibres were introduced into a 1.5 m tube of the diameter corresponding to the diameter of the human trachea which was equipped with the 3D-printed realistic airway bifurcation (Lizal et al. 2022). The diameter of the fibres was 4 to 6 μm and the length was 30 to 50 μm. A FASTCAM SA-Z high-speed camera (Photron, Japan) with long-distance microscope 12X Zoom lens (NAVITAR, New York, USA) composed of 2X F-mount adapter (type 1-62922) and 12 mm F.F zoom lens (type 1-50486) was used to record the fibre flow. The image spatial resolution was 1.5 μm per pixel, and image maximal dimensions were 1.5 ×1.5 mm for 1024×1024 px. The flow was illuminated by background light using a pulse LED light model HPLS-36DD18B (Lightspeed Technologies, USA). The light pulse duration was 400–800 ns.

Fig. 1: Positions of measuring points upstream and downstream of the replica of the first bifurcation in the human airways.

RESULTS

The recordings allowed us to evaluate orientations of fibres in areas upstream and downstream of the bifurcation and observe the changes during the flow through the measuring window. Also, trajectories and the nature of "flips" (sudden changes from perpendicular to parallel orientation of fibre to the streamlines) were analyzed.

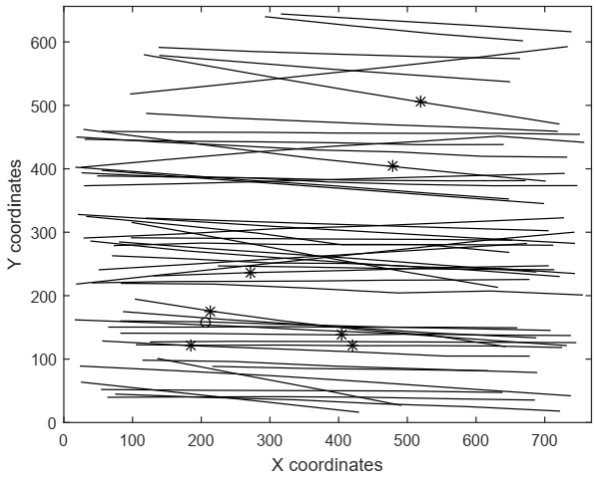

Fig. 2: Trajectories and flips of fibres during transient inhalation flow downstream of the bifurcation. The asterisks denote flip from perpendicular to parallel orientation to the streamlines, the circles the opposite.

ACKNOWLEDGEMENT

This work was supported by the Czech Science Foundation under the grant GA22-20357S.

REFERENCES

LIZAL, F., M. CABALKA, M. MALY, J. ELCNER, et al. On the behavior of inhaled fibers in a replica of the first airway bifurcation under steady flow conditions. *Aerosol Science and Technology*, Mar 2022, 56(4), 367-381.

ON PARTICLE COAGULATION IN ELECTROSTATIC PRECIPITATOR

Oleksandr MOLCHANOV[1], Kamil KRPEC[1], Jiří HORÁK[1], František HOPAN[1]

[1] Energy Research Center, Technical University of Ostrava, Czech Republic,
smokeman@vsb.cz

Keywords: Electrostatic precipitator; Particulate matter; Pollution control; Coagulation

SUMMARY

The particle concentration in the electrostatic (ESP) precipitator is expected to evolute under electrostatic removal and enhanced coagulation by the charge on the particle, applied electric field and turbulence induced in gas flow by ionic wind can. In the present work, the contribution of coagulation is reasoned and confirmed by experimental measurements carried out at the ESP used to control emissions from a 90-kW boiler with biomass combustion. ESP was operated in two operating modes to ensure different coagulation conditions, and the changes in the particle concentrations were predicted and measured. It was found that coagulation can be responsible for up to 5 % removal efficiency depending on ESP operation parameters.

INTRODUCTION

Modern small-scale boilers generate emissions of ultrafine particles ranging from 50 to 200 nm. The worldwide distribution of such boilers and the hazards of these emissions to public health make this issue of global interest. Appropriate technology can suppress these emissions.

The usual Electrostatic precipitator consists of the discharge and collection electrodes and uses an electric field generated between electrodes to charge and precipitate particles. The corona discharge occurs in ESP ionising gaseous medium, then generated ions charge with particles. The electric field forces charged particles to move towards the electrodes removing them from the gas flow. The electric field also induces an ion movement-the ionic wind, which causes the gas flow pattern to become turbulent enough to affect the particle movement. A weak charge, typical for fine particles, makes this turbulence particularly essential for the precipitation of submicron particles.

The Deutsch precipitation model (Deutsch, 1922) for predicting ESP removal efficiency suggests that the particle distribution is uniform in the ESP cross-section and does not consider the effect of ion-generated turbulence. Consequently, some calculation inaccuracy is involved in predictions of ESP removal efficiency, which become noticeable for precipitation of ultrafine particles in small-scale ESPs with short residence time and weak electric parameters. So, for accurate technical ESP modelling, these processes must be respected.

Some accurate complex software, such as FLUENT or COMSOL, are known based on solving the Navier-Stokes equation. However, such methods request appropriate skills and are not always available to boiler producers; therefore, their usage in the usual engineering practice is limited. This work aims to develop a simplified method for ESP modelling.

PREDICTION METHOD

In the present work, the particle concentration of particles of specific size is assumed to reduce in ESP by i) electrostatic removal defined by the Deutsch method:

$$\left(\frac{dC}{dt}\right)_{ESP} = -\frac{A}{Q} C_0 w_f \quad (1)$$

Where A-is an ESP collecting area and Q- is a gas flow.
and ii) loss of specific particles by coagulation, specified by the Smoluchowski equation (Smoluchowski 1916).

$$\left(\frac{dC}{dt}\right)_C = -K_R {C_0}^2 \quad (2)$$

The particle coagulation in the present work is considered monodisperse: particles of each specific size are suggested to coagulate to a target 1-μm - outside the size range of interest. Consequently, the resulting evolution in concentration $\left(\frac{dC}{dt}\right)$ for particles of a specific size (d_p) is considered as further

$$\frac{dC}{dt} = -K_R {C_0}^2 - \frac{A}{Q} C_0 w_f \quad (3)$$

Electrostatic precipitation

The critical parameter in the operation of ESP is the particle drift velocity w_f, which is strictly depends on electric field strength E_{av}, the medium viscosity μ and particle size d_p and charge Q_p:

$$w_f = \frac{E_{av} Q_p e}{3\pi\mu d_p} \cdot C_{Cu} \quad (4)$$

Fuchs and Sutugin propose to evaluate a charging rate for an ultrafine particle with respecting the image forces (Fuchs and Sutugin, 1971):

$$\frac{dQ_p}{dt} = \pi\overline{\langle v \rangle} \frac{{d_p}^2}{4} N \left(1 + \sqrt{\frac{e^2}{4\epsilon_0 d_p k_b T}}\right) \quad (5)$$

Particles concentrations reduced by precipitation C_E can be defined by the analytical solution of Equation (1):

$$C_E = C_0 e^{-\frac{A}{Q} w_f} \quad (6)$$

Coagulation

The Brownian motion of aerosol particles in an undisturbed medium inevitably results in arbitrary continuous coagulation, which kernel can be found:

$$K_B = 4\pi d D_d C_{Cu} \quad (7)$$

Where C_{Cu} −Cunningham correction factor, D_d- Particle diffusion coefficient

However, the coagulation problem becomes more complex under corona discharge in energised ESP. So, further coagulation mechanisms should be discussed

Turbulent coagulation

Ions in the electric field are influenced by concentration/temperature gradient and the applied external field; therefore, secondary narrow jet-like flows of ionic wind are formed in the ionised gas. The velocity of ionic wind increase can achieve a value of the same order of magnitude as the velocity of the main gas flow. The turbulent coagulation kernel (Saffman and Turner, 1956) defines as.

$$K_T = \varsigma \sqrt{\frac{8\pi\varepsilon}{15\upsilon}} d^3 C_{Cu} \quad (8)$$

Gradient coagulation

The formula (4) shows that the velocity of charged particles towards the electrodes is individual for each particle size. The drift velocity of the studied particles in the experimental ESP ranged by a few centimetres per second. This velocity gradient is negligible and cannot affect the particles' behaviour, so gradient coagulation is not

considered.

Shear coagulation

The particle inertia and following the turbulent flow eddies are ignored, so the motion of charged particles is regarded for newly arrived particles as transversal laminar shear causing the coagulation. The monodisperse shear coagulation kernel K_{Sh} is related to Brownian K_B kernel as follows (Sinajskij et al., 2002):

$$K_{Sh} = \frac{d^3 w_f \mu}{2k_b T} K_B \tag{9}$$

Electrically affected coagulation

Fuchs (Fuchs, 1955) defines the effect of particle charge by the kernel for charged particle coagulation K_{Ch} as Brownian coagulation kernel K_B multiplied by the factor β. Since the particles charg in ESP is predominantly unipolar, the electrostatic dispersion in the present work is respected, so the coagulation factor β for monodisperse particles with unipolar charge was determined here as (Green and Lane, 1964):

$$\beta = \frac{y}{e^y - 1} + y, \; y = \frac{(eQ_p)^2}{4\pi\epsilon_0 k_b T d_p} \tag{10}$$

The coagulation kernel K_F respecting the effect of the ESPelectric field was obtained as follows (Lianze et al., 2005):

$$K_F = \frac{2d_p E_{av}}{3\mu} \cdot C_{Cu} \tag{11}$$

Effective coagulation kernel

The effective kernel K_E of coagulation in energised ESP is obtained by summing the kernels for the above mechanisms:

$$K_E = K_T + K_{Sh} + K_{Ch} + K_F \tag{12}$$

Particle concentration, reduced by coagulation C_C during electrostatic precipitation, was defined by the analytical solution of Equation (2):

$$C_C = \frac{C_0}{K_E t C_0 + 1} \tag{13}$$

EXPERIMENTAL APPARATUS AND METHODS

The contribution of coagulation was investigated in an experimental set-up shown in Fig. 2.

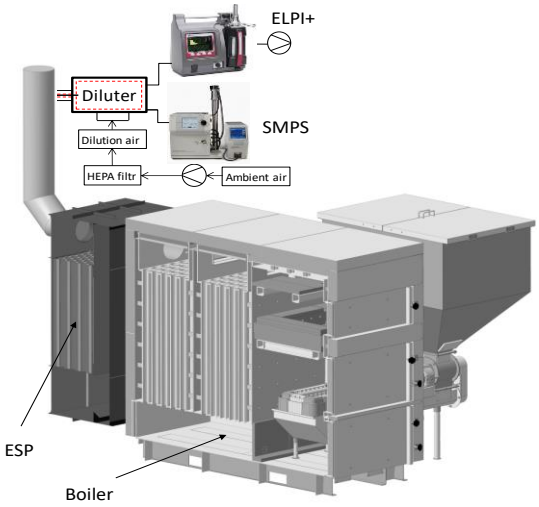

Fig. 2 Experimental set-up

The typical automatic 90-kW boiler with wood pellets combustion was used. The measurements were undertaken when boiler operation was stabilised: CO concentration,

combustion gas temperature negative pressure of 15 Pa in the boiler stuck were constant.

Combustion gases were cleaned from particles in the vertical honeycomb ESP. The ESP was operated in two modes: at high voltage 9 and 12.5 kV, ensuring a corona current of 10 and 40 mA, respectively. All tests were repeated five times for each ESP operating mode.

The removal efficiency was estimated by comparing the particle concentration with ESP on/off. The changes in numerical particle concentrations caused by ESP operation were measured simultaneously by The Dekati Electrical Low-Pressure Impactor (ELPI) and TSI Electric Mobility Spectrometer (SMPS), composed of serially working a differential mobility analyser (DMA) and TSI Condensation Particle Counter Model 3775 (CPC). To adopt samples to the capacity of measuring equipment, a two-stage Dekati fine particle sampler FPS-4000 was used to dilute the flue gas.

The SMPS mobility equivalent diameter was approximated to the Stokes diameter, and the ELPI results were recalculated to Stokes diameter using the fly ash particles density at 2 g/cm3. Obtained concentrations were normalised to the volume unit of dry gas at 101.325 kPa, 0 °C, and reference O2 of 10%.

RESULTS AND DISCUSSION

Experimental conditions and ESP parameters. The ESP operation parameters and conditions of the experiments are presented in Tab. 2.

Tab. 2: Average experimental parameters of the ESP

Parameter	Unit		ESP regime	
			A	B
Gas temperature,	°C	85		
Gas flow Q **	m^3/h	556		
Residence time in ESP, t	s	2.5		
Specific collecting area	$m^2/(m^3/s)$	136		
Electric current in ESP, I	mA		40	5
Voltage on ESP, U	kV		12.5	9
Electric field strength, Eav	$\times 10^5$ V/m		2.8	1.8
Concentration of ions, N	$\times 10^{14}$ ions/m^3		2.3	0.7

* in dry flue gas (0 °C, 101.3 kPa); at reference O2 = 10 % vol.

** effective value, valid at the given actual temperatures and actual atmospheric pressures.

Coagulation mechanisms

Fig. *3* compares the Brownian coagulation kernel with kernels for coagulation due to studied mechanisms at operation regimes of ESP.

The values of turbulent K_T, charge K_{Ch} and electric field K_F coagulation kernels were calculated for both ESP operation regimes and compared as ratios to the Brownian coagulation kernel.

Intensified parameters of the ESP demonstrate the growing importance of the electric field for coagulation: the excess over Brownian coagulation becomes more significant for finer particles. The relatively low effect of turbulence on coagulation was observed: the low Reynolds number of about 1200 can explain this.

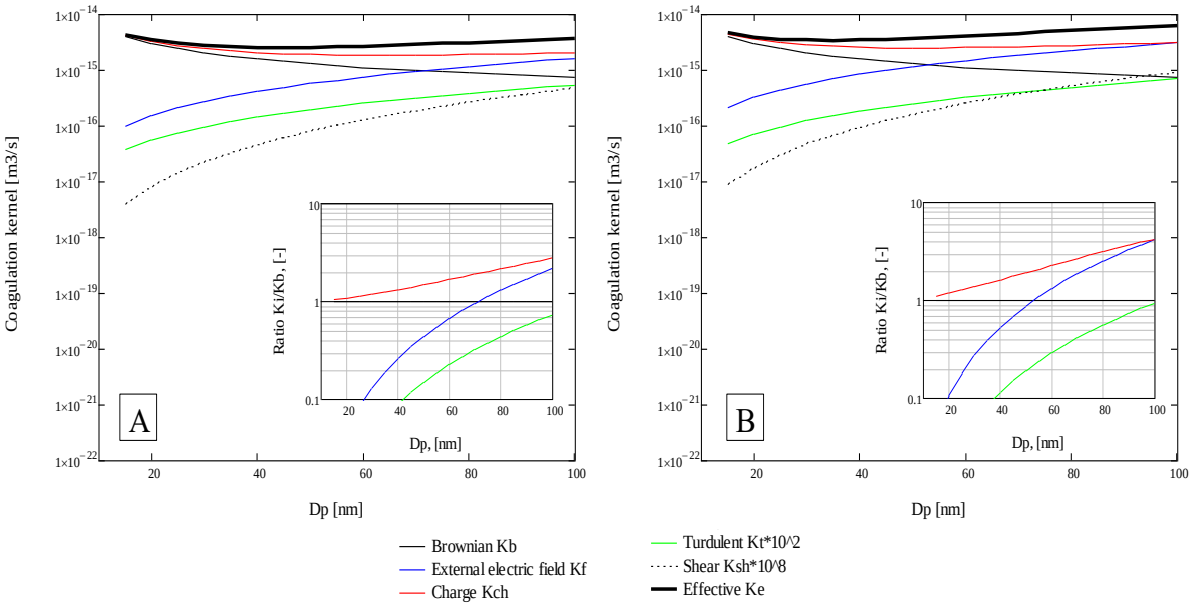

Fig. 3: Coagulation kernels for discussed coagulation mechanisms

Particle size distribution

For particles of interest, the ELPI and SMPS demonstrated similar measurement results for particles of interest for all ESP regimes (see

Fig. *4*). Predicted with considered coagulation results appear closer to measuring results than calculations involving electrostatic precipitation purely. Because enhancement in electric field strength and enrichment in ion concentration are much more supportive for particle charging and removal than for coagulation through discussed mechanisms, the coagulation effect was less significant with an increased ESP efficiency.

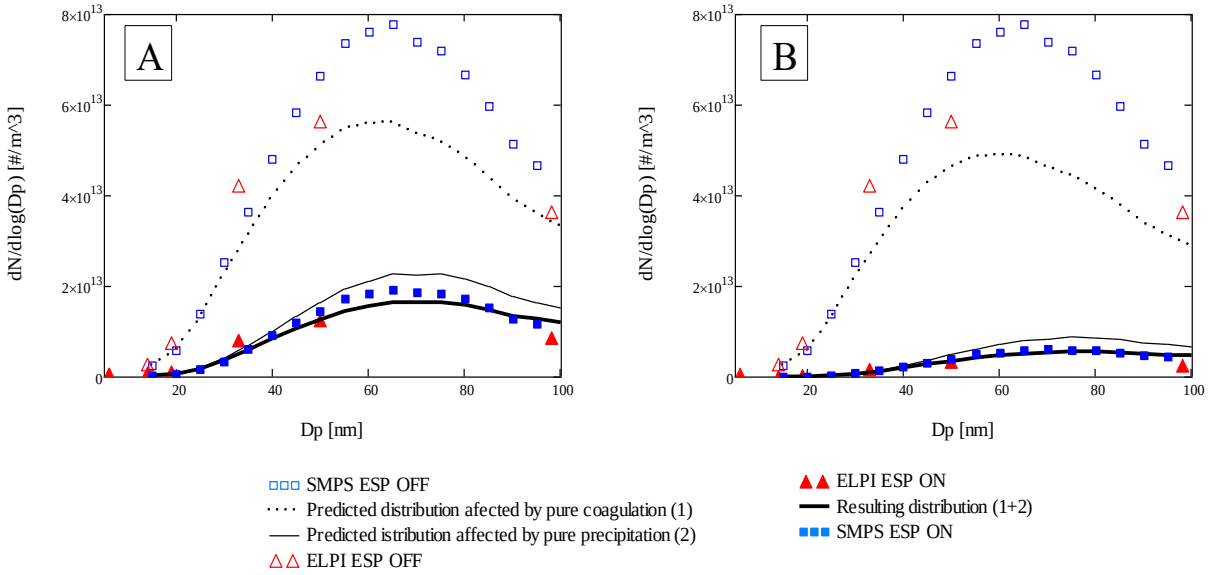

Fig. 4 Measured and predicted particle size distribution

The maximal contribution of coagulation was stated at about 5% for particles with a diameter of 70 nm. The coagulation effect is least pronounced for partially charged

particles with a diameter of less than 40 nm. Thus, enhanced coagulation can explain the increase in removal efficiency observed for partially charged particles with intensification from the electrical parameters of the ESP encountered in (Zhuang et al., 2000).

CONCLUSIONS

Coagulation in the corona discharge field was studied in the experimental ESP used to control PM emissions from a 160-kW automatic boiler with wood pellets combustion. Two operation con condition of ESP was studied.

The evolution of particle concentration and size distribution was predicted respecting the electrostatic removal and coagulation enhanced in energised ESP. Particle size distribution was obtained by measurements and compared to the theoretically predicted one.

The particle charge and the external electric field have the most substantial effect on coagulation, while the effects of turbulence and shear were negligible. The resulting coagulation can contribute to ESP removal efficiency by up to 5% and explain the discrepancy between theoretical prediction for ESP removal efficiency and measurement results. The accuracy of ESP removal efficiency for ultrafine particles can be ensured by respecting coagulation.

ACKNOWLEDGEMENTS

This work was supported by the project „Enhancing the implementation of Air Quality Management Plans in Slovakia by strengthening capacities and competencies of regional and local authorities and promoting air quality measures“ LIFE18 IPE/SK/000010, and The Real-Life emissions project LIFE 20 PRE/FI/000006.

REFERENCES

Deutsch, W., Bewegung und Ladung der Elektrizitätsträger im Zylinderkondensator. Ann. Der Physik, 68, (1922).

Fuchs, N.A., Mechanika aerozolej. Moskwa, (1955).

Fuchs, N.A., Sutugin, A.G., HIGH-DISPERSED AEROSOLS, in: Hidy, G.M., Brock, J.R. (Eds.), Topics in Current Aerosol Research. Pergamon, p. 1, (1971).

Green, H.L., Lane, W.R., Particulate clouds: dusts, smokes, and mists; their physics and physical chemistry and industrial and environmental aspects. Van Nostrand, (1964).

Lianze, W., Xiangrong, Z., Keqin, Z., An analytical expression for the coagulation coefficient of bipolarly charged particles by an external electric field with the effect of Coulomb force. Journal of Aerosol Science 36(8), 1050-1055, (2005).

Saffman, P.G., Turner, J.S., On the collision of drops in turbulent clouds. Journal of Fluid Mechanics 1(1), 16-30, (1956).

Sinajskij, E., Lapoga, E., Yajcev, Y., Separation of Multiphase Multicomponent Systems. Nedra, (2002).

Smoluchowski, M., Drei vortrage uber diffusion, brownshe molekularbewegung und koagulation von kolloidteilchen. Phys. Zeits. 17, 557-571, (1916).

Zhuang, Y., Kim, Y.J., Lee, T.G., Biswas, P., Experimental and theoretical studies of ultra-fine particle behavior in electrostatic precipitators. Journal of Electrostatics 48(3-4), 245-260, (2000).

DEKATI® OXIDATION FLOW REACTOR DOFR™ FOR SECONDARY AEROSOL FORMATION STUDIES

Markus NIKKA[1], Elmeri LAAKKONEN[1], Anssi ARFFMAN[1], Oskari VAINIO[1]

[1] Dekati Ltd., Kangasala, Finland, markus.nikka@dekati.fi

Keywords: Oxidation flow reactor, Secondary aerosol, Potential aerosol mass

INTRODUCTION

Unlike primary aerosols, secondary aerosols (SA) are formed long after the emission into the atmosphere through gas-particle conversion processes. SA are divided into secondary inorganic aerosols (SIA) and secondary organic aerosols (SOA) based on their chemical composition. SA and SOA have significant contribution to global PM and hence affecting climate, air quality and health (Hallquist et al., 2009). In urban areas, organic aerosol fraction from the submicron PM can be over 50 % and 2/3 of it can be SOA (Nault et al., 2021).

Gaseous compounds that produce SA are called precursors. These precursors go through reactions in the atmosphere which may increase their particle formation potential. SIA precursors and their reaction are well known making modelling of the SIA particle formation possible. However, vast number of different SOA precursors and their complex reaction make modelling on SOA particulate formation very difficult. (Hallquist et al., 2009) SOA precursors are volatile or semivolatile organic compounds that will undergo oxidation in the atmosphere producing compounds with sufficiently low equilibrium vapor pressure for nucleation or condensation, this process is also referred to as aging (Kanakidou, 2005).

Formation of secondary aerosols have been studied using environmental chambers and oxidation flow reactors (OFR). In both cases, sample is introduced to the chamber where humidity, ozone concentration and UV-irradiation are accurately monitored and controlled. OFR's are compact constant flow reactors that provide fast aging of the sample. Processes that would take days in atmosphere are achieved in a time scale of minute inside of the OFR. Dekati has brought to the market Dekati® Oxidation Flow Reactor DOFR™ which is based on the TSAR (TUT Secondary Aerosol Reactor), an OFR designed and introduced by Tampere University (formerly known as Tampere University of Technology) (Simonen et al., 2017). DOFR has 12 UVC lamps with wavelength of 254 nm to produce hydroxyl radicals inside the reactor. UVC intensity can be modified by activating or deactivating any number of these lamps. Integrated ejector diluter is used to produce and maintain constant flow through the reactor and provide high volume output for multiple instruments.

EXPERIMENTAL SETUP

We have carried laboratory and field tests to characterize and demonstrate the performance of the DOFR™ with both laboratory and field tests.

Maximum aging power of the reactor was tested using carbon monoxide as marker gas and measuring the decrease of carbon monoxide concentration inside the reactor with

varying aging conditions. Residence time distribution and laminarity of the flow through the reactor were determined using salt particles and two condensation particle counters.

To verify performance with a real-world emission source, potential aerosol mass from an idling TSI gasoline engine was measured. Sample was first diluted with particle free pressurized air and then introduced through a Nafion humidifier. After humidification, ozone generated with separate generator was introduced to the sample. Sample was then introduced to DOFR™, where aging conditions were modified mainly by increasing the UVC-intensity inside the reactor. After the reactor, Dekati® High resolution ELPI®+ was used as an aerosol instrument to measure produced secondary aerosol mass.

RESULTS AND CONCLUSIONS

Decrease of carbon monoxide concentration inside the reactor is converted to equivalent age in the atmosphere using following equations:

$$[OH]_{exp} = \frac{1}{k_{OH,CO}} * \ln\left(\frac{[CO]_0}{[CO]_f}\right) \quad (1)$$

$$t_{ekv} = \frac{[OH]_{exp}}{1.5*10^6\ molec./cm^3 s} \quad (2)$$

Where, 1.5e6 molec./cm3*s equals the average hydroxyl radical reactivity in the atmosphere. Figure 1 presents results as equivalent age while using maximum UVC intensity and different ozone concentration and relative humidity levels.

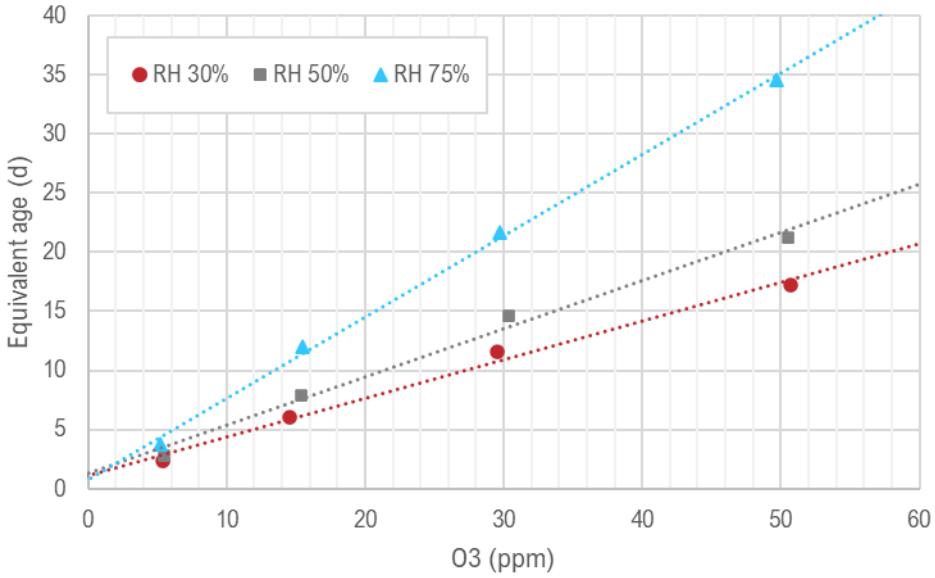

Fig. 1: Equivalent aging time of DOFR™ with varying humidity and ozone concentration.

As can be seen, equivalent aging time of 1 month can be achieved with suitable reactor parameters.

Figure 2. presents secondary aerosol mass size distributions from a 1.4 liter TSI gasoline engine.

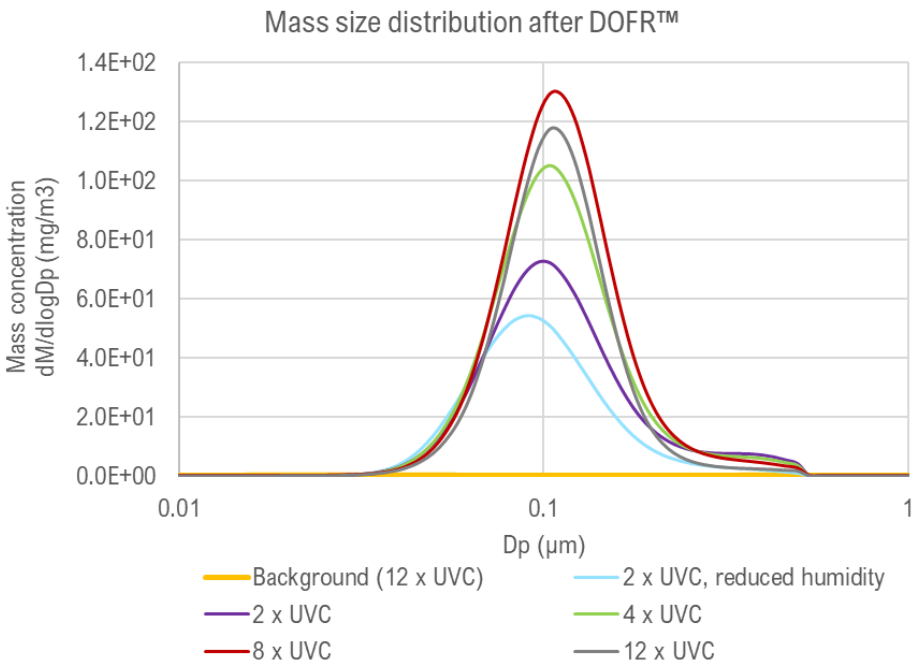

Fig. 2: Secondary aerosol mass size distributions from a 1.4 liter TSI engine with varying aging conditions.

Different lines represent different aging conditions. UVC-intensity was the main parameter for aging control. With increasing UVC intensity (number of active UVC-lamps), produced SA increases, reacing maximum with 8 active lamps. With futher increase of UVC intensity, the produced SA mass starts to decrease which is typical for secondary aerosol processes.

REFERENCES

Hallquist, M., Wenger, J. C., Baltensperger, U., Rudich, Y., Simpson, D., Claeys, M., Dommen, J., Donahue, N. M., George, C., Goldstein, A. H., Hamilton, J. F., Herrmann, H., Hoffmann, T., Iinuma, Y., Jang, M., Jenkin, M. E., Jimenez, J. L., Kiendler-Scharr, A., Maenhaut, W., McFiggans, G., Mentel, Th. F., Monod, A., Prévôt, A. S. H., Seinfeld, J. H., Surratt, J. D., Szmigielski, R., and Wildt, J.: The formation, properties and impact of secondary organic aerosol: current and emerging issues, *Atmos. Chem. Phys.,* 9, 5155–5236, (2009).

Nault, B. A., Jo, D. S., McDonald, B. C., Campuzano-Jost, P., Day, D. A., Hu, W., Schroder, J. C., Allan, J., Blake, D. R., Canagaratna, M. R., Coe, H., Coggon, M. M., DeCarlo, P. F., Diskin, G. S., Dunmore, R., Flocke, F., Fried, A., Gilman, J. B., Gkatzelis, G., Hamilton, J. F., Hanisco, T. F., Hayes, P. L., Henze, D. K., Hodzic, A., Hopkins, J., Hu, M., Huey, L. G., Jobson, B. T., Kuster, W. C., Lewis, A., Li, M., Liao, J., Nawaz, M. O., Pollack, I. B., Peischl, J., Rappenglück, B., Reeves, C. E., Richter, D., Roberts, J. M., Ryerson, T. B., Shao, M., Sommers, J. M., Walega, J., Warneke, C., Weibring, P., Wolfe, G. M., Young, D. E., Yuan, B., Zhang, Q., de Gouw, J. A., and Jimenez, J. L.: Secondary organic aerosols from anthropogenic volatile organic compounds contribute substantially to air pollution mortality, *Atmos. Chem. Phys.,* 21, 11201–11224, (2021).

Kanakidou, M., Seinfeld, J. H., Pandis, S. N., Barnes, I., Dentener, F. J., Facchini, M. C., Van Dingenen, R., Ervens, B., Nenes, A., Nielsen, C. J., Swietlicki, E., Putaud, J. P., Balkanski, Y., Fuzzi, S., Horth, J., Moortgat, G. K., Winterhalter, R., Myhre, C. E. L., Tsigaridis, K., Vignati, E., Stephanou, E. G., and Wilson, J.: Organic aerosol and global climate modelling: a review, *Atmos. Chem. Phys.*, 5, 1053–1123, (2005).

Simonen, P., Saukko, E., Karjalainen, P., Timonen, H., Bloss, M., Aakko-Saksa, P., Rönkkö, T., Keskinen, J., Dal Maso, M., A new oxidation flow reactor for measuring secondary aerosol formation of rapidly changing emission sources, *Atmos. Meas. Tech*., 10, 1519–1537, (2017).

ASSESSMENT OF THE SOURCES' IMPACT ON PM10

Tomasz OLSZOWSKI[1]

[1] Opole University of Technolgy, Poland, t.olszowski@po.edu.pl

Keywords: Atmospheric aerosol; Elements; PX-375; XRF analysis; Rural area

INTRODUCTION

The sources of particulate matter in the atmosphere which are then enriched with toxic elements or compounds have been widely investigated in many Works (Rodríguez et al., 2004; Rogula-Kozłowska et al., 2015). In several papers it was remarked that, in the cold season, the principal source of PM emission is associated with the combustion of conventional fuels (maliny hard coal) in domestic heating systems (Kaczmarek et al., 2017; Olszowski, 2019). However, a precise determination of the types of contamination sources is difficult. Aerosol particle concentrations in local air reservoirs are also influenced by meteorological parameters, which are responsible for e.g. the transport of particles from polluted urban or industrial areas and from distant natural sources (Khedairia and Khadir, 2012).

The main purpose of the study was to examine whether data averaging has an impact on the determination of pollutant emission sources. In addition PM10 mass concentration and concentration of PM10-bound elements were examined.

EXPERIMENTAL SETUP

As the receptor, the measurement point in the northern part of the village was selected, which is situated near a moderately inhabited rural area (Kotórz Mały, Opolskie Voivodeship) surrounded by meadows, farmlands low shrubs and trees (50^{o}73'66.02" N;18^{o}05'06.80" E, 162 m. a. s. l., 968 inhabitants). Continuous particle monitor + energy dispersive X-ray fluorescence (CPM+EDXRF; PX-375 Horiba®, Japan) technique were used to examine PM10 concentrations and their chemical composition (Al, Ca, Cr, Cu, Fe, K, Mn, Ni, Pb, Zn). The device operated in automatic mode, providing data every single hour.

Certified standard material, SRM 2783 (air particulate matter on filter media), was used to assess the elemental quantification of X-ray spectra and to get a quality control measure. The lowest detection limits (LLD as a double the standard deviation of blank analyzed) were Al (56.7 ng/m^3), Ca (1.1 ng/m^3), Cr (2.05 ng/m^3), Cu (1.85 ng/m^3), Fe (7.00 ng/m^3), K (4.8 ng/m^3), Mn (1.45 ng/m^3), Ni (0.9 ng/m^3), Pb (1.05ng/m^3), Zn (1.25 ng/m^3).

Sampling and weather condition measurements were carried out for 14 consecutive days during the winter period (February 2019).

For further analysys of recievied records, the raw data were scaled according to the fomula (1).

$$X' = \frac{(X - X_{min})}{(X_{max} - X_{min})} \quad (1)$$

The principal component analysis (PCA) was applied to assess the correlations between different PM10-bound elements and identify the main sources of PM10. In addition, to detect structures in the data, the results were analyzed using cluster analysis (CA). The results were analyzed for daily and hourly concentrations. The variability of the intensity of emission sources in different periods of the day was checked.

RESULTS AND CONCLUSIONS

Figure 1 shows the profiles of PM10 and PM10-bound elements concentration. The twenty-four-hour concentrations of PM10 in Kotórz Mały ranged from 6.9 to 178.6 μg/m^3. The mean PM10 concentration for the entire measurement period was equal to 51.5 μg/m^3. It was above the daily PM10 concentration limit established by the European Commission (50 μg/m^3; not to be exceeded on more than 35 days per year). Generally, the lowest concentrations of PM10 were recorded between 00.00-06.00 a.m. and the highest between 04.00 p.m.-10.00 p.m.

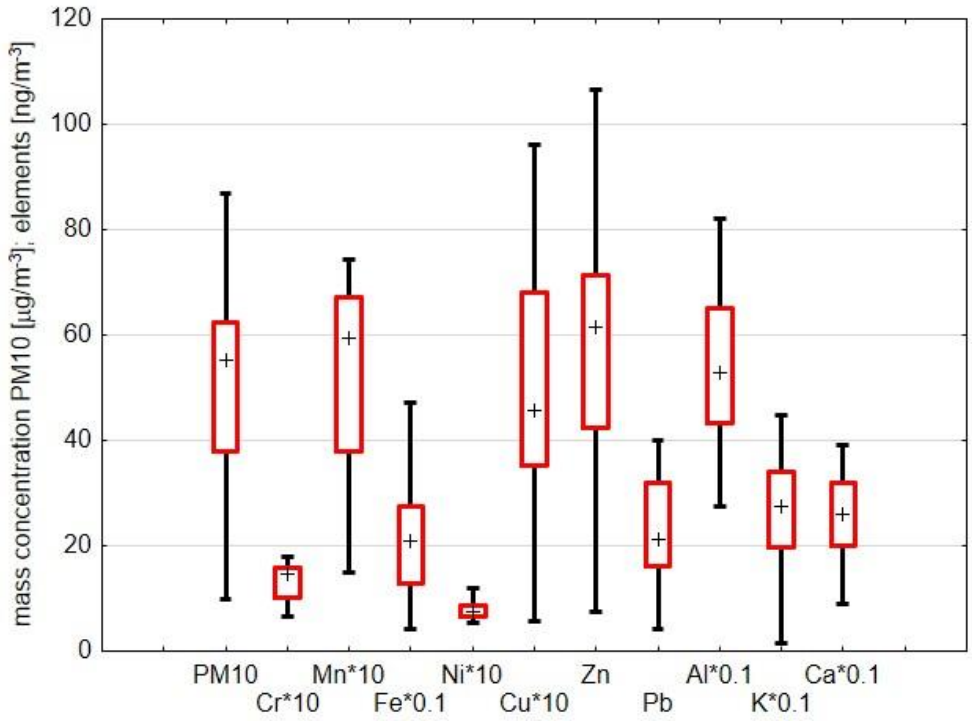

Fig 1. PM10 and PM10-bound elements concentration ranges. The whiskers extend from the edge of the box to the 5th and 95th percentiles of the data. The squares inside indicate median values.

The mean concentrations of the selected PM10-bound elements fluctuated within wide limits and took values from 0.95 ng/m^3 (Ni) to 1406.3 ng/m^3 (Al). PM10-bound elements collectively accounted on average for 1% of the PM10 mass. Al, Ca and, K were the most abundant among the determining elements. On average, during the entire two-weeks measurement period, the elements related to PM10 tested in the study can be arranged in the following order: Al>Ca>K>Fe>Zn>Pb>Mn>Cu>Cr>Ni. The concentrations of PM10-bound K, Al, Fe, Ca and Mn were determined by natural sources. This is indicated

by Enrichment Factor (EF) values which, regardless of the time of day, do not exceed 10 during the entire measurement period. K, Al, Fe and Ca are typical crustal elements, therefore it can be assumed that they were derived from the resuspension of crustal and soil matter (Majewski and rogula-Kozłowska, 2016). The concentrations of the remaining PM10-bound elements, i.e. Cu, Pb, Ni, Zn, and Cr were strongly influenced by anthropogenic sources (EFx> 10). The elements came from the combustion of fuels, abrasion of vehicle components (wheels, brakes) and road surfa ces surfaces, the influx of polluted air masses from urban areas.

The main aim of the study was realized with the use of PCA and CA analysys. Both analyses were conducted for data averaged up to 24 hours (D), all hourly data (H), and for periods divided into morning (M; 6 a.m.-10 p.m.), midday (MD; 11 a.m.-3 p.m.), afternoon/evening (AE; 4 p.m.-10 p.m.) and night (N; 11 p.m.-5 a.m.).

In the PCA analysis, two principal components (PC) were extracted for data (D), which explained about 83% of the variation in the original data. Based on the factor coordinates of the variables, it is not possible to indicate which source was dominant. Both elements from natural and anthropogenic sources (with the exception of Cu) were concentrated in the first principal component (69% of the total variance).

In the case of the analysis of hourly measurement data (H), three principal components were identified, which explained about 72% of the variability in the original data. Seven of ten elements were strongly correlated with PC1. The vast majority of these elements were of natural origin. Clear groups were identified indicating that soil resuspension and mechanical abrasion processes of crustal materials were the main sources of contamination (Al, K, Ca, Mn, Fe). Additional sources were fuel combustion and traffic (Pb, Zn, Ni, Cu).

For the morning (M) and afternoon/evening (AE) hours, the PCA resulted in two PCs (71% (M) and 72% (AE) of the total variance). The results indicated that the main source of pollution was related to the use of individual heating systems (PC1 43% (M) and 53% (AE); Zn, Pb and Cr). Also, the "natural origin" of pollutants played a key role (PC2 18% (M) and 14% (AE); Al, K, Ca, Mn, Fe).

For the midday (MD) and nighttime (N) hours, the analysis showed significant similarity to the daily and hourly results, respectively. Three principal components were identified for (MD) (84% of the variation in the original data) and two (70%) for (N), respectively.

Table 1 provides information on the results of the cluster analysis.

Tab. 1: Hierarchy of clusters of elements for the analyzed periods of data averaging (clusters for: 100·Distance/Max. distance <40).

D	H	M	MD	AE	N
Cr-Mn	Mn-Fe	Cu-Ca	Mn-Fe	Zn-Pb	Mn-Fe
Fe-Ca	Zn-Pb	Mn-Fe	Zn-Pb	Al-K	Al-K
Zn-K	Cu-Ca		Al-K	Mn-Fe	Zn-Pb
Al-K	Al-K			Cu-Ca	
Mn-Fe					
Zn-Pb					

The results in Table 1 show a similarity in the occurrence of the same pairs of elements regardless of the period of data analyzed. The largest "mix" occurs for results

averaged up to 24 hours of observation (n=14), which captures the essence of the difficulty of unambiguously identifying the dominant source of pollution. For other periods, the clustering results are more unambiguous and seem to confirm the PCA results.

The final conclusions are as follows:

- averaging the results to 24 hrs leads to greater uncertainty in determining the origin of pollution, i.e., the likely types of sources can be determined, but there is a problem in indicating the dominant source,
- anthropogenic emissions are the leading source during the morning and evening hours, while natural emissions occur around the clock, with intensification occurring in the middle of the day,
- in order to fully assess the impact of aerosol emission sources, it is necessary to analyze meteorological conditions (preferably hour by hour).

ACKNOWLEDGEMENT

This work was supported by private initiative.

REFERENCES

Kaczmarek, K., Zajusz Zubek, E., Mainka, A. PM10 composition in urban and rural nursery schools in Upper Silesia, Poland: a trace elements analysis. International Journal of Environment and Pollution 61, 98 (2017).

Khedairia, S.; Khadir, M.T. Impact of clustered meteorological parameters on air pollutants concentrations in the region of Annaba, Algeria. *Atmos. Res.*, *113*, 89–101 (2012).

Majewski, G.; Rogula-Kozłowska, W. The elemental composition and origin of fine ambient particles in the largest Polish conurbation: first results from the short term winter campaign. Theor. Appl. Climatol. 125, 79–92 (2016).

Olszowski, T. Influence of individual household heating on PM2.5 concentration in a rural settlement. Atmosphere 10, 16–21 (2019).

Rodríguez, S., Querol, X., Alastuey, A., et al. Comparative PM10-PM2.5 source contribution study at rural, urban and industrial sites during PM episodes in Eastern Spain. Sci Total Environ 328, 95–113 (2004).

Rogula-Kozłowska, W., Majewski, G., Czechowski, P.O. The size distribution and origin 901 of elements bound to ambient particles: a case study of a Polish urban area. Environ Monit Assess 187 (2015).

KONCENTRÁCIA A ANORGANICKÁ ELEMENTÁRNA ANALÝZA PEVNÝCH ČASTÍC V PROSTREDÍ CESTNÉHO TUNELA

Dušan JANDAČKA[1], Daniela ĎURČANSKÁ[1]

[1] Žilinská univerzita v Žiline, Stavebná fakulta, Katedra cestného a environmentálneho inžinierstva, Žilina, Slovensko, dusan.jandacka@uniza.sk, daniela.durcanska@uniza.sk

Kľúčové slová: Tuhé častice, Emisie bez výfukových plynov, Chemický prvok, Prostredie tunela, Cestná doprava, Faktorová analýza

SUMMARY

Particulate matter (PM) originates from the exhaust and non-exhaust processes of road traffic (brake wear, tire wear, road surface wear, and road dust resuspension). This study deals with the specification of non-exhaust PM emissions in a tunnel environment where the primary source is road traffic. PM measurements took place in the "Považský Chlmec" highway tunnel with a length of 2118 m, directly in the tunnel tube and near the tunnel portal. PM measurements were performed using gravimetric and optical methods. PM chemical analyses were performed using energy-dispersive X-ray fluorescence (EDXRF). Using EDXRF, the main chemical elements Al, Br, Ca, Cl, Cr, Cu, Fe, K, Mg, Mn, Na, P, Si, S, Ti, and Zn were identified in the PM.

ÚVOD

Emisie tuhých častíc (PM) z cestnej dopravy pochádzajú z dvoch primárnych zdrojov: výfukových procesov a degradácie častí vozidiel a povrchu vozoviek. Ten druhý, ktorý zahŕňa všetky emisie častíc vo vzduchu vytvárané vozidlami, opotrebovanie vozovky a resuspenziu cestného prachu, je definovaný ako emisie tuhých častíc – nevýfukové emisie. Podiel emisií PM z nevýfukových zdrojov sa v posledných rokoch rýchlo zvýšil v dôsledku výrazného zníženia emisií zo spaľovania a v súčasnosti predstavuje približne 90 % všetkých emisií PM z cestnej dopravy (OECD, 2020; Rexeis & Hausberger, 2009; Timmers & Achten, 2016). Častice z nevýfukových procesov, ktoré sa usadili na povrchu vozovky, môžu byť tiež resuspendované turbulenciou v cestnej premávke (US-EPA, 2011). Nevýfukové emisie PM možno rozdeliť na priame emisie z opotrebovania (opotrebenie bŕzd, pneumatík a vozovky) a resuspenziu cestného prachu. PM z nevýfukových procesov sú hlavnou zložkou hrubej frakcie $PM_{2,5-10}$ (Harrison a kol., 2021; OECD, 2020).

V rámci nášho výskumu boli vykonané merania PM_{10} a $PM_{2,5}$ a ich elementárna chemická analýza v prostredí tunela. Merania sa robili súčasne na dvoch miestach: vo vnútri tunela a vonku pri portáli tunela.

METÓDY MERANIA

Merania PM boli realizované v prostredí tunela, vo vnútri tunela a v blízkosti portálu tunela (západný portál) v meste Žilina, tunel Považský Chlmec. Merania PM boli realizované na stanovenie koncentrácií PM_{10} a $PM_{2,5}$ priamo v tunelovej rúre ($PM_{2,5}$_IN, PM_{10}_IN) a portálovej časti ($PM_{2,5}$_OUT, PM_{10}_OUT) a ich elementárneho chemického zloženia (prítomnosť chemických prvkov v PM). Merania PM sa robili počas dvoch období:

pred údržbou tunela (1. – 7. októbra 2020) a po údržbe tunela (12. – 20. októbra 2020). Merania sa uskutočňovali celkovo počas 16 dní.

Na meranie PM_{10} a $PM_{2,5}$ boli použité dve metódy: referenčná gravimetrická (4x prístroje Leckel LVS3) a optická metóda (Fidas 200S a APM-2). Vo vnútri tunela boli použité 2x prístroje Leckel a prístroj APM-2. V blízkosti portálu tunela boli použité 2x prístroje Leckel a prístroj Fidas 200S.

Anorganické prvky sa detegovali pomocou spektrometra ARL™ QUANT'X EDXRF. Vzorky sa analyzovali pomocou EDXRF spektrometrie vo vákuovej atmosfére.

VÝSLEDKY, DISKUSIA, ZÁVERY

Priemerné koncentrácie všetkých frakcií PM boli nižšie v portálovej časti tunela ako v tunelovej rúre. Zaznamenané poklesy boli 53,3 % pre PM_{10} a 44,2 % pre $PM_{2,5}$. Maximálna 24-hodinová koncentrácia PM_{10} 54,06 µg/m^3 bola nameraná v tunelovej rúre dňa 20.10.2020 a maximálna 24-hodinová koncentrácia $PM_{2,5}$ 24,69 µg/m^3 bola nameraná v tunelovej rúre dňa 19.10.2020, kedy sa nezaznamenali žiadne zrážky.

Distribúcia PM v tunelovej rúre predstavovala zloženie PM_{10} frakciami $PM_{2,5}$_IN 51 % a $PM_{2,5\text{-}10}$_IN 49 %. V blízkosti portálovej časti $PM_{2.5}$_OUT 59 % a $PM_{2.5\text{-}10}$_OUT 41 %, v tomto poradí. Hrubá frakcia $PM_{2,5\text{-}10}$ dosahovala až 50 % celkovej frakcie PM_{10}.

Závislosť PM nameraných v tunelovej rúre a portálovej časti tunela bola skúmaná pomocou lineárnej regresnej analýzy. Jemná frakcia $PM_{2,5}$ vykazovala vyššiu závislosť častíc produkovaných v tunelovej rúre od častíc nameraných v portálovej časti (koeficient determinácie R^2 = 0,57, korelačný koeficient r = 0,75, významnosť p = 0,005647). Pre hrubú frakciu PM2,5-10 nebol vzťah medzi časticami nameranými v tunelovej rúre a v portálovom úseku taký významný ako pre $PM_{2,5}$ (R^2 = 0,27, r = 0,52, p = 0,038899).

Chemické analýzy PM odhalili prítomnosť niektorých chemických prvkov. Analyzovaných bolo 64 vzoriek PM, z toho 32 vzoriek PM_{10} a 32 vzoriek $PM_{2,5}$. V PM boli identifikované nasledujúce chemické prvky: Al, Br, Ca, Cl, Cr, Cu, Fe, K, Mg, Mn, Na, P, Si, S, Ti, Zn, Ni, Mo, Pb, Rb, Sb Se, Sr, V a Zr (Obr. 1). Celková koncentrácia prvkov na filtroch bola v priemere 365,8 mg/m^2 PM_{10}_IN, 85,4 mg/m^2 $PM_{2,5}$_IN, 142,5 mg/m^2 PM_{10}_OUT a 48,2 mg/m^2 $PM_{2,5}$_OUT.

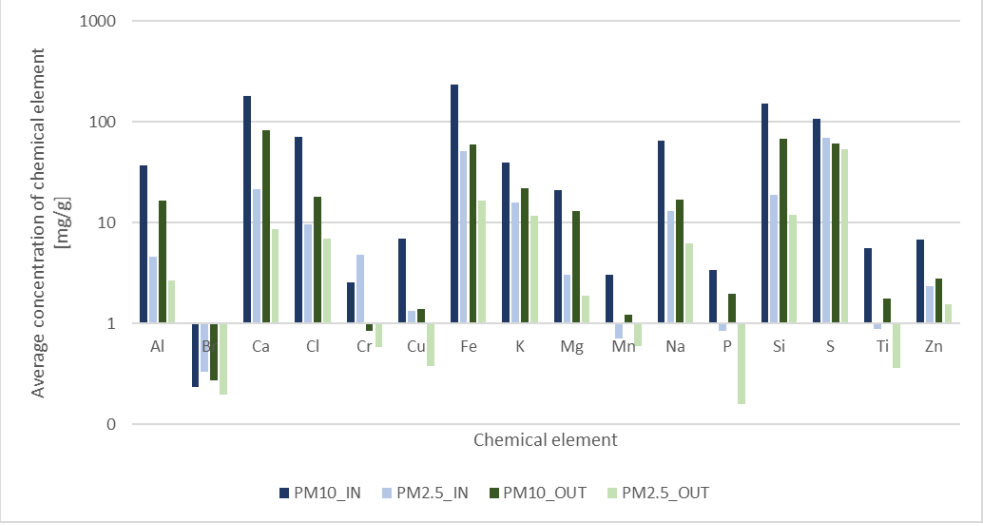

Obr. 1: Priemerná koncentrácia chemických prvkov v PM (miligramy prvku na gram PM) počas meraní v tuneli Považský Chlmec.

Skúmali sme aj zastúpenie jednotlivých chemických prvkov v $PM_{2,5}$ a $PM_{2,5-10}$. $PM_{2,5-10}$ predstavuje hrubú frakciu PM_{10} a jeho zdrojom je najmä mechanický proces. Vo frakcii $PM_{2,5-10}$ boli vo väčšej miere zastúpené chemické prvky Al, Ca, Cl, Cu, Fe, K, Mg, Mn, Na, P, Si, Ti, Zn ($PM_{2,5-10}/PM_{2,5}$ >1). Na druhej strane Br, Cr, S, K - vonku a Zn - vonku boli viac zastúpené v $PM_{2,5}$ (pomer $PM_{2,5-10}/PM_{2,5}$ <1).

Korelačná analýza odhalila v PM_{10} dve skupiny chemických prvkov s významnou vzájomnou koreláciou (r> 0,7, p<0,05): Skupina 1, Al, Ca, Cu, Fe, K, Mg, Mn, Si, Ti a Zn; a Skupina 2, Na a Cl. V $PM_{2,5}$ signifikantne korelovali Al, Ca, Mg, Si, Cu, Fe, Na a Cr. Vo frakcii $PM_{2,5}$ neboli chemické prvky tak výrazne viazané ako vo frakcii PM_{10}. Preto sa predpokladalo, že hrubá frakcia $PM_{2,5-10}$ bola dôležitá vo významných koreláciách medzi chemickými prvkami. Preto sa táto frakcia skúmala oddelene. Významné korelácie tvorili prvky podobné frakcii PM_{10} (Obr. 2). Z hľadiska prepojenia chemických prvkov bola v tomto prípade pre celkovú frakciu PM_{10} významná hrubá frakcia $PM_{2,5-10}$.

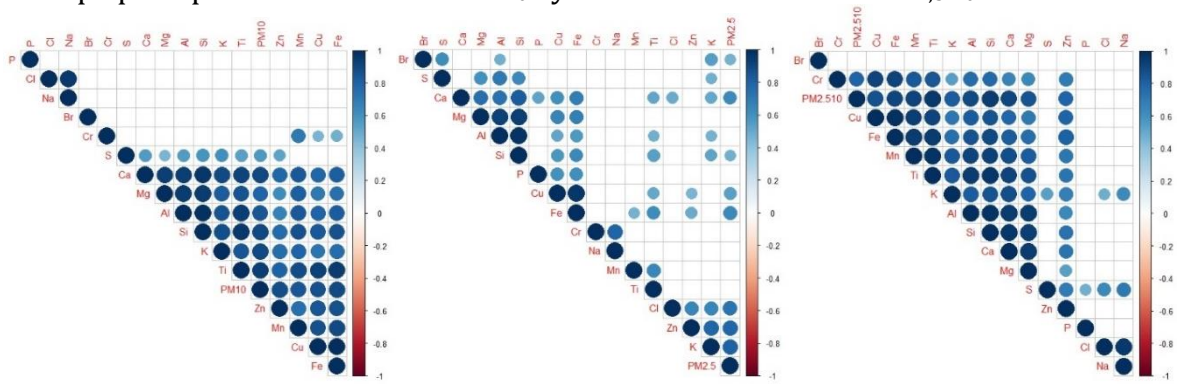

Obr. 2: Výsledky korelačnej analýzy koncentrácie chemických prvkov v PM získaných pri meraniach v tuneli Považský Chlmec.

Prezentovaný výskum sa zaoberal meraním a analýzou koncentrácií PM_{10} a $PM_{2,5}$ a ich chemického zloženia v prostredí tunela. Miestom merania bol tunel Považský Chlmec nachádzajúci sa v Žiline na Slovensku. Merania sa uskutočnili vo vnútri tunelovej rúry a vonku v blízkosti portálu tunela, čím sa líši od iných štúdií (Cui a kol., 2016; Hao a kol., 2019). Priemerná koncentrácia PM_{10} v tuneli bola o 53 % vyššia a $PM_{2,5}$ o 44 % vyššia ako vonku v blízkosti portálu tunela. Koncentrácie boli významne ovplyvnené zrážkami počas merania. Vplyv primárneho zdroja cestnej dopravy sa prejavil najmä počas pracovných dní zvýšením koncentrácií PM, ktoré sa zvýšili v období bez zrážok. Regresná analýza koncentrácií PM vo vnútri tunela a vonku v blízkosti portálu tunela ukázala prepojenie týchto PM; to znamená, že veľká časť PM v portáli pochádzala priamo z tunela (PM_{10} - R^2 = 0,43, $PM_{2,5}$ - R^2 = 0,57). $PM_{2,5-10}$ tvorili až 50 % z celkovej frakcie PM_{10}, čo je vyššia hodnota ako u mestských aerosólov (Samara & Voutsa, 2005).

Chemická analýza PM_{10} a $PM_{2,5}$ pomocou EDXRF odhalila prítomnosť nasledujúcich chemických prvkov v PM: Al, Br, Ca, Cl, Cr, Cu, Fe, K, Mg, Mn, Na, P, Si, S, Ti a Zn. Celková koncentrácia prvkov na filtroch bola v priemere pre PM_{10}_IN 365,8 mg/m^2, $PM_{2,5}$_IN 85,4 mg/m^2, PM_{10}_OUT 142,5 mg/m^2 a $PM_{2,5}$_OUT 48,2 mg/m^2. Tieto chemické prvky boli hmotnostne zastúpené v PM_{10}_IN (31,4 %), $PM_{2,5}$_IN (14,4 %), PM_{10}_OUT (27,7 %) a $PM_{2,5}$_OUT (15,4 %). Podobné výsledky zloženia PM v tuneloch boli získané v niektorých štúdiách (Brito a kol., 2013; Cui a kol., 2016; Handler a kol., 2008; Hao a kol., 2019; He a kol., 2008). Koncentrácie chemických prvkov dosahovali vyššie hodnoty vo vnútri tunela ako vonku, v blízkosti portálu tunela.

POĎAKOVANIE

Tento príspevok vznikol za podpory grantu VEGA 1/0337/22 „Analýza vplyvu textúry povrchu vozovky na šmykové trenie, bezpečnosť jazdy a potenciál resuspenzie tuhých častíc“

LITERATÚRA

Brito, J., Rizzo, L. v, Herckes, P., Vasconcellos, P. C., Caumo, S. E. S., Fornaro, A., Ynoue, R. Y., Artaxo, P., & Andrade, M. F. (2013). Atmospheric Chemistry and Physics Physical-chemical characterisation of the particulate matter inside two road tunnels in the São Paulo Metropolitan Area. *Atmos. Chem. Phys*, *13*, 12199–12213.

Cui, M., Chen, Y., Tian, C., Zhang, F., Yan, C., & Zheng, M. (2016). Chemical composition of PM2.5 from two tunnels with different vehicular fleet characteristics. *Science of the Total Environment*, *550*, 123–132.

Handler, M., Puls, C., Zbiral, J., Marr, I., Puxbaum, H., & Limbeck, A. (2008). Size and composition of particulate emissions from motor vehicles in the Kaisermühlen-Tunnel, Vienna. *Atmospheric Environment*, *42*(9), 2173–2186.

Hao, Y., Deng, S., Yang, Y., Song, W., Tong, H., & Qiu, Z. (2019). Chemical Composition of Particulate Matter from Traffic Emissions in a Road Tunnel in Xi'an, China. *Aerosol and Air Quality Research*, *19*(2), 234–246.

Harrison, R. M., Allan, J., Carruthers, D., Heal, M. R., Lewis, A. C., Marner, B., Murrells, T., & Williams, A. (2021). Non-exhaust vehicle emissions of particulate matter and VOC from road traffic: A review. *Atmospheric Environment*, *262*, 118592.

He, L. Y., Hu, M., Zhang, Y. H., Huang, X. F., & Yao, T. T. (2008). Fine particle emissions from on-road vehicles in the Zhujiang Tunnel, China. *Environmental Science and Technology*, *42*(12), 4461–4466.

OECD. (2020). *Non-exhaust Particulate Emissions from Road Transport*. OECD.

Rexeis, M., & Hausberger, S. (2009). Trend of vehicle emission levels until 2020 – Prognosis based on current vehicle measurements and future emission legislation. *Atmospheric Environment*, *43*(31), 4689–4698.

Samara, C., & Voutsa, D. (2005). Size distribution of airborne particulate matter and associated heavy metals in the roadside environment. *Chemosphere*, *59*(8), 1197–1206.

Timmers, V. R. J. H., & Achten, P. A. J. (2016). Non-exhaust PM emissions from electric vehicles. *Atmospheric Environment*, *134*, 10–17.

US-EPA. (2011). *AP-42, 5th Edn., Vol. 1, Chapter 13 Miscellaneous Sources., Section 13.2.1 Paved Roads.*

IMPACTS OF VARIOUS PARAMETERIZATIONS ON ORGANIC AEROSOL MODELLING IN CENTRAL EUROPE

Lukáš BARTÍK[1], Peter HUSZÁR[1], Ondřej VLČEK[2], Kryštof EBEN[3]

[1] Department of Atmospheric Physics, Faculty of Mathematics and Physics, Charles University, Prague, Czech Republic, bartik@karlov.mff.cuni.cz,
[2] Ambient Air Quality Department, Czech Hydrometeorological Institute, Prague, Czech Republic
[3] Institute of Computer Science, Czech Academy of Sciences, Prague, Czech Republic

Keywords: Organic aerosol modelling, CAMx, Central Europe

INTRODUCTION

For decades, chemical transport modelling of organic aerosols has been problematic, with models often underestimating their concentrations (e.g. Giani et al., 2019; Jiang et al., 2021; and articles therein). Among the frequently mentioned and studied possible causes of these shortcomings in the models are missing emissions of semi-volatile and intermediate-volatile organic compounds (SVOCs and IVOCs), which can be very effective precursors of secondary organic aerosols. In practice, therefore, these emissions are often built into models using parameterizations, which scale them typically based on experimental data using emissions included in emission databases. An overview of different parameterizations of IVOC/SVOC source-specific emissions from recent literature and a proposal for new such parameterizations can be found in Giani et al. (2019). In addition, Jiang et al. (2021) showed that adjusting the parameters used in air quality models obtained from chamber experiments to correct for semi-volatile vapour losses from biomass burning on the chamber walls contributes to improving model prediction of organic aerosols in Europe during wintertime.

Because the papers mentioned above assess the impacts of different parameterizations on different domains and at different times, as part of this work, we decided to study the impacts of using some of these parameterizations on organic aerosol concentrations in the region of our interest (i.e. in Central Europe) during wintertime and summertime in the relatively current time period (namely in the period 2018–2019). To evaluate the potential contribution of these parameterizations to the refinement of model outputs, we performed a basic validation of model concentrations obtained in a sensitivity study with station measurements.

EXPERIMENTAL SETUP

As part of the sensitivity study, we performed a total of 5 model experiments using the Comprehensive Air Quality Model with Extensions (CAMx) (Environ, 2020) on a European model domain centred over Prague, the Czech Republic (50.075° N, 14.44° E, Lambert Conic Conformal projection used) for the period between 2018–2019. The model domain was represented in horizontal layers by 172 x 152 grid boxes with a horizontal resolution of 9 km; in the vertical direction, it consisted of 20 layers from the Earth's surface up to approximately 12 km, with the height of the lowermost layer about

Tab. 1: IVOC/SVOC source-specific emission parameterizations used in the experiments. For each of the parameterizations, the superscript indicates a reference to the used source: [a] Giani et al. (2019), [b] Jathar et al. (2014), [c] Ciarelli et al. (2017), [d] Jiang et al. (2021), [e] Robinson et al. (2007). Gianni's approach refers to the SVOC determination procedure described in the article of Giani et al. (2019).

Chem. Species	Experiment	Gasoline vehicles (GV)	Diesel vehicles (DV)	Biomass burning (BB)	Other sources (OS)
IVOC	SOAP_withIVOA	$0.0397 * VOC_{GV}$ [a]	$1.2748 * VOC_{DV}$ [a]	$4.5 * POA_{BB}$ [c]	$1.5 * POA_{OS}$ [e]
	VBS_base	$0.0397 * VOC_{GV}$ [a]	$1.2748 * VOC_{DV}$ [a]	$4.5 * POA_{BB}$ [c]	$1.5 * POA_{OS}$ [e]
	VBS_Jiang_orig	$0.25 * NMVOG_{GV}$ [b]	$0.2 * NMVOG_{DV}$ [b]	$12 * POA_{BB}$ [d]	$1.5 * POA_{OS}$ [e]
	VBS_Jiang_modif	$0.0397 * VOC_{GV}$ [a]	$1.2748 * VOC_{DV}$ [a]	$12 * POA_{BB}$ [d]	$1.5 * POA_{OS}$ [e]
SVOC	VBS_base	Giani's approach	Giani's approach	$3 * POA_{BB}$ [d]	$3 * POA_{OS}$ [d]
	VBS_Jiang_orig	$3 * POA_{GV}$ [d]	$3 * POA_{DV}$ [d]	$3 * POA_{BB}$ [d]	$3 * POA_{OS}$ [d]
	VBS_Jiang_modif	Giani's approach	Giani's approach	$3 * POA_{BB}$ [d]	$3 * POA_{OS}$ [d]

48–50 m. Driving meteorological fields (the same for all experiments) were derived using the WRFCAMx preprocessor from the weather forecast simulation performed using the WRF (Weather Research and Forecasting) Model Version 4.0.3., which detailed description can be found in Ďoubalová et al. (2020). All needed emission inputs (before adding IVOC and/or SVOC emissions) were prepared in the same manner as Huszar et al. (2020) did.

Since CAMx allows the calculation of organic aerosol-gas partitioning and oxidation chemistry using two options, namely using a semi-volatile equilibrium scheme called SOAP or a hybrid 1.5-dimensional volatility basis set (1.5-D VBS) approach, detailed descriptions of which are given in Environ (2020), we used both approaches in the sensitivity study. Here, it is worth mentioning that one of the main differences between the two approaches lies in the fact that in the SOAP scheme, the POA is considered non-volatile, while in the VBS approach, a part of the POA is considered semi-volatile. From this, it is immediately evident that while IVOC parameterisations (IVOCs represent transitional substances between SVOCs and VOCs on the basis of volatility) are connected with both mechanisms, SVOC parameterisations are exclusively considered when using the VBS concept.

In the first model experiment, which further serves as a reference within the sensitivity study, we implemented the SOAP scheme and emissions that did not include contributions of IVOCs (and, for understandable reasons, neither of SVOCs). Next, we carried out one more experiment using the SOAP scheme (labelled as SOAP_withIVOA) and three experiments using the VBS approach (labelled as VBS_base, VBS_Jiang_orig and

VBS_Jiang_modif) in which we already used emissions with the inclusion of IVOCs and SVOCs. We calculated them based on the parameterizations shown in Table 1, considering their sources. Furthermore, while the first three experiments (i.e. the SOAP_noIVOA, SOAP_withIVOA, and VBS_base experiments) were performed using the default setting of SOAP or VBS scheme in CAMx version 7.10, the last two experiments (i.e. the VBS_Jiang_orig, VBS_Jiang_modif experiments) were performed using the VBS approach in a modified version of the CAMx version 6.50 with optimized parameterizations (SOA yields, emissions of IVOCs from biomass burning, and enthalpy of vaporization) created by Jiang et al. (2021). Experiments also differ in the use of gas phase mechanisms: in the SOAP_noIVOA, SOAP_withIVOA, and VBS_base experiments, the fifth revision of the Carbon Bond Version 6 (CB6r5) mechanism was used (references to all furher mentioned mechanisms can be found in Environ (2020)); in the VBS_Jiang_orig, VBS_Jiang_modif experiments, the original Carbon Bond Version 6 (CB6) mechanism was used. Finally, in all experiments, the partitioning of inorganic aerosol constituents between the gas and aerosol phases was calculated using the ISORROPIA mechanism.

RESULTS AND CONCLUSIONS

To get an idea of the spatial distribution of organic aerosol (OA) in the reference experiment, we have shown the average winter and summer concentrations of primary OA (POA) and secondary OA (SOA) from it in Figure 1. It can be seen that the pollution of POA is usually significantly higher during the year in the winter period, with the Po Valley, the Silesia region and the central region of Bohemia being among the particularly polluted areas. On the other hand, it can be seen that SOA usually reaches higher values in the summer, especially in the northwestern region of the Balkan Peninsula.

To quantify spatial and temporal impacts of different parameterizations in the experiments, we calculated relative impacts on POA and SOA, which we defined as the ratios of the seasonal concentrations of POA and SOA from the experiments to their equivalents from the SOAP_noIVOA experiment. These impacts are shown in Figure 2. For the case of introducing IVOCs emission when using the SOAP scheme, it can be seen that there are relatively insignificant changes in POA in winter and summer. At the same

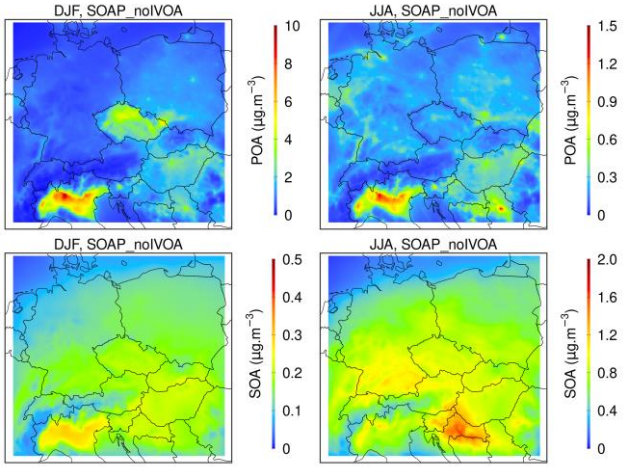

Fig. 1: Average winter (DJF, left) and summer (JJA, right) concentrations of primary organic aerosols (POA, top) and secondary organic aerosols (SOA, bottom) from SOAP_noIVOA experiment.

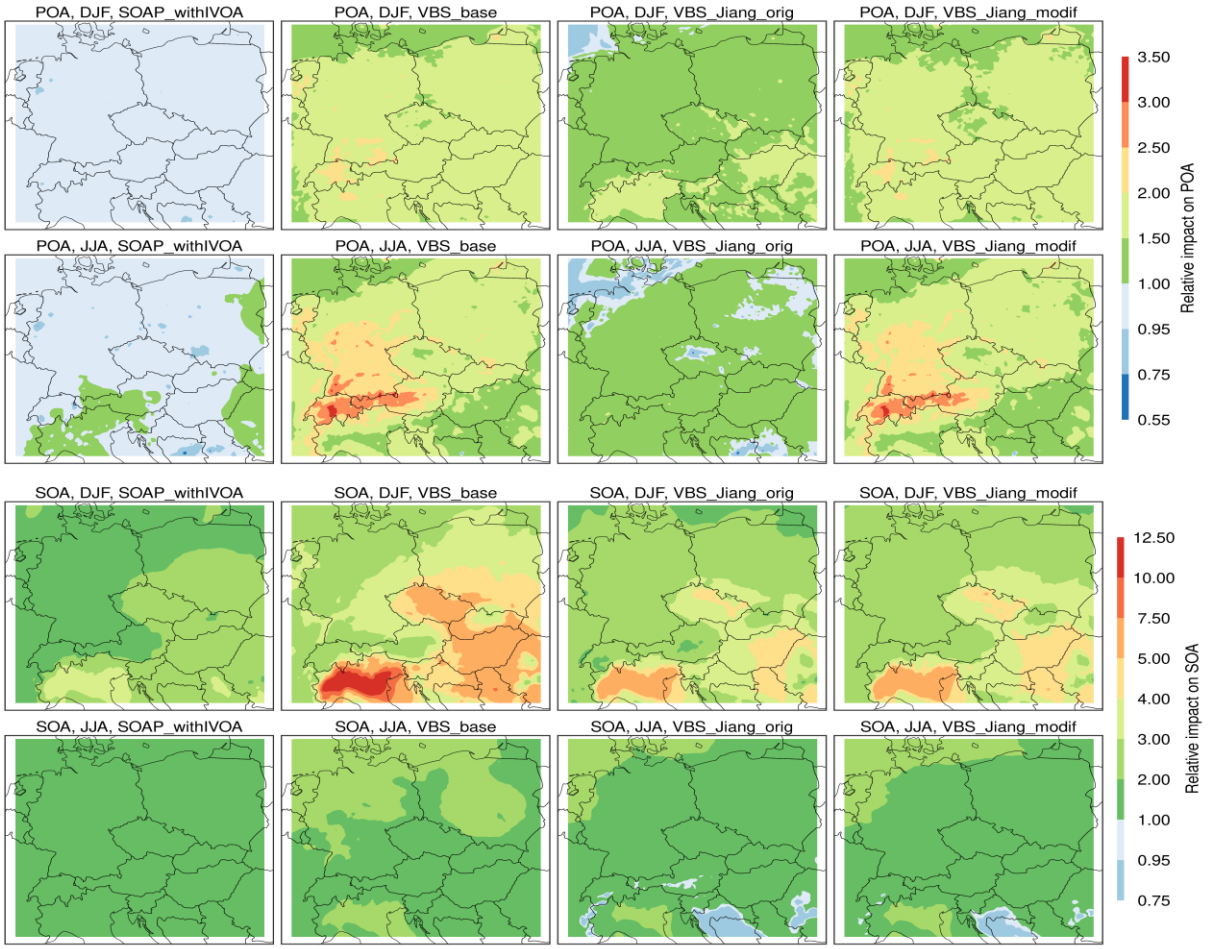

Fig. 2: Relative impact on average winter (DJF, 1st and 3rd row) and summer (JJA, 2nd and 4th row) concentrations of primary organic aerosols (POA, 1st and 2nd row) and secondary organic aerosols (SOA, 3rd and 4th row) from SOAP_withIVOA, VBS_base, VBS_Jiang_orig and VBS_Jiang_modif experiments (1st–4st column respectively).

time, in this case, the relative impacts on SOA are the lowest of all investigated cases, with values in the range of 1-4 (1-2) in winter (summer). On the other hand, it can be seen that the introduction of SVOCs into the VBS formalism and their subsequent parameterisations are usually manifested by an increase in the POA concentration. In both seasons, it can be seen that regardless of the model version used, parameterisations derived from traffic emissions using the approach proposed by Giani et al. (2019) lead to higher POA concentrations. The most pronounced relative impacts are evident for SOA in the winter season in the experiments with the VBS approach, with the highest ones being achieved in the VBS_base experiment, with values exceeding 10 in the Po Valley area.

Finally, to assess the potential benefit of using these parameterisations to refine model outputs, we provide a very simplified evaluation of the model surface daily concentrations of organic carbon (OC), $PM_{2.5}$, ammonium, nitrate and sulfate from the experiments against their surface measurements using bias and root mean square error (RMSE) as statistical indicators. For this purpose, we used available data for these pollutants from background stations included in the Co-operative Programme for Monitoring and Evaluation of the Long-range Transmission of Air Pollutants in Europe database (EMEP) and those included in the European Environment Agency's AirBase European air quality dataset. The values of the calculated indicators are listed in Table 2.

Both the bias and RMSE values for OC indicate an improvement in its prediction in both seasons, with the VBS_base experiment producing the best results. On the other hand, it can be seen from the biases for all other pollutants that adding IVOC and SVOC emissions leads to a decrease in their concentrations, which is subsequently reflected in the improvement of the bias for pollutants overestimated by the model (i.e. ammonium and nitrates in winter) and, conversely, in the worsening of the bias for pollutants underestimated by the model. A possible explanation for the negative correlation between OA concentrations and concentrations of secondary inorganic aerosols (ammonia, nitrates and sulfates) could be a decreased availability of OH radicals (as a result of an increase in SOA precursors) for oxidation of precursor gases such as NO_2 and SO_2 that is analogous to the one used by Aksoyoglu et al. (2017).

Tab. 2: Comparison of modelled and observed daily concentrations of organic carbon (OC), $PM_{2.5}$, ammonium (NH_4^+), nitrate (NO_3^-) and sulfate (SO_4^{2-}). Biases and root mean square errors (RMSEs) are given in $\mu g.m^{-3}$. The green (red) colour of the numbers indicates an improvement (deterioration) of statistical indicators compared to their values from the SOAP_noIVOA experiment. The best values of the indicators in the framework of individual comparisons are marked in bold.

Chem. species	Statistics	SOAP_noIVOA / SOAP_withIVOA / VBS_base / VBS_Jiang_orig / VBS_Jiang_modif	
		Winter (DJF)	Summer (JJA)
OC	bias	-3.86 / -3.78 / **-3.08** / -3.39 / -3.19	-2.49 / -2.45 / **-2.13** / -2.39 / -2.25
	RMSE	6.53 / 6.45 / **5.69** / 5.96 / 5.79	2.77 / 2.73 / **2.43** / 2.68 / 2.54
$PM_{2.5}$	bias	**-1.91** / -3.30 / -2.13 / -2.73 / -2.42	**-5.59** / -6.56 / -5.75 / -6.30 / -6.07
	RMSE	10.99 / 11.31 / **10.50** / 10.75 / 10.63	**7.04** / 7.89 / 7.18 / 7.68 / 7.47
NH_4^+	bias	0.83 / 0.55 / 0.55 / **0.53** / **0.53**	**-0.10** / -0.30 / -0.30 / -0.31 / -0.30
	RMSE	1.61 / 1.32 / 1.32 / **1.31** / **1.31**	**0.41** / 0.47 / 0.47 / 0.47 / 0.47
NO_3^-	bias	2.11 / 1.67 / 1.69 / **1.62** / 1.63	**-0.20** / -0.32 / -0.31 / -0.33 / -0.33
	RMSE	3.54 / 3.00 / 3.01 / **2.96** / 2.97	0.74 / **0.72** / **0.72** / 0.73 / 0.73
SO_4^{2-}	bias	**-0.84** / -1.36 / -1.36 / -1.37 / -1.37	**-1.35** / -1.81 / -1.81 / -1.81 / -1.81
	RMSE	**2.37** / 2.47 / 2.47 / 2.47 / 2.47	**1.80** / 2.18 / 2.18 / 2.18 / 2.18

ACKNOWLEDGEMENT

This work has been funded by the Technology Agency of the Czech Republic (TAČR) project ARAMIS (Air quality Research, Assessment and Monitoring Integrated System) No.SS02030031. We further thank the Netherlands Organisation for Applied Scientific Research (TNO) for providing tne Monitoring Atmospheric Composition and Climate (MACC)-III emissions dataset, the Czech Hydrometeorological Institute for providing the Register of Emissions and Air Pollution Sources (REZZO) dataset, ATEM (Studio of ecological models) for providing their traffic emissions dataset, the European Environment Agency (EEA) for providing the AirBase European air quality data and the Co-operative Programme for Monitoring and Evaluation of the Long-range Transmission of Air Pollutants in Europe (EMEP) for providing their air quality data.

REFERENCES

Aksoyoglu, S., Ciarelli, G., El-Haddad, I., Baltensperger, U., and Prévôt, A. S. H.: Secondary inorganic aerosols in Europe: sources and the significant influence of biogenic VOC emissions, especially on ammonium nitrate, *Atmos. Chem. Phys.*, 17, 7757–7773, (2017).

Ciarelli, G., Aksoyoglu, S., El Haddad, I., Bruns, E. A., Crippa, M., Poulain, L., Äijälä, M., Carbone, S., Freney, E., O'Dowd, C., Baltensperger, U., and Prévôt, A. S. H., Modelling winter organic aerosol at the European scale with CAMx: evaluation and source apportionment with a VBS parameterization based on novel wood burning smog chamber experiments, *Atmos. Chem. Phys.*, 17, 7653–7669, (2017).

Ďoubalová, J., Huszár, P., Eben, K., Benešová, N., Belda, M., Vlček, O., Karlický, J., Geletič, J., and Halenka, T., High Resolution Air Quality Forecasting over Prague within the URBI PRAGENSI Project: Model Performance during the Winter Period and the Effect of Urban Parameterization on PM, *Atmosphere*, 11, 625, (2020).

Environ, CAMx User's Guide, Comprehensive Air Quality model with Extentions, version 7.10, available at: http://www.camx.com, Novato, California, (2020).

Giani, P., Balzarini, A., Pirovano, G., Gilardoni, S., Paglione, M., Colombi, C., Gianelle, V. L. , Belis, C. A., Poluzzi, V., Lonati, G., Influence of semi- and intermediate-volatile organic compounds (S/IVOC) parameterizations, volatility distributions and aging schemes on organic aerosol modelling in winter conditions, *Atmospheric Environment*, 213, 11–24, (2019).

Huszar, P., Karlický, J., Ďoubalová, J., Šindelářová, K., Nováková, T., Belda, M., Halenka, T., Žák, M., and Pišoft, P., Urban canopy meteorological forcing and its impact on ozone and $PM_{2.5}$: role of vertical turbulent transport, *Atmos. Chem. Phys.*, 20, 1977–2016, (2020).

Jathar, S. H., Gordon, T. D., Hennigan, C. J., Pye, H. O. T., Pouliot, G., Adams, P. J., Donahue, N. M., and Robinson, A. L., Unspeciated organic emissions from combustion sources and their influence on the secondary organic aerosol budget in the United States, *P. Natl. Acad. Sci. USA*, 111, 10473–10478, (2014).

Jiang, J., El Haddad, I., Aksoyoglu, S., Stefenelli, G., Bertrand, A., Marchand, N., Canonaco, F., Petit, J.-E., Favez, O., Gilardoni, S., Baltensperger, U. and Prévôt, A. S. H., Influence of biomass burning vapor wall loss correction on modeling organic aerosols in Europe by CAMx v6.50, *Geosci. Model Dev.*, 14, 1681–1697, (2021).

Robinson, A. L., Donahue, N. M., Shrivastava, M. K., Weitkamp, E. A., Sage, A. M., Grieshop, A. P., Lane, T. E., Pierce, J. R., and Pandis, S. N.: Rethinking organic aerosols: semivolatile emissions and photochemical aging, *Science*, 315, 1259–1262, (2007).

EXPERIMENTAL MEASURING OF HOMOGENEOUS NUCLEATION RATE OF WATER IN THE PRESENCE OF VARIOUS GASES IN PULSE EXPANSION CHAMBER

Tetiana LUKIANOVA[1], Mykola LUKIANOV[1], Jan HRUBÝ[1]

[1] Institute of Thermomechanics AS CR, v.v.i., Prague, Czech Republic,
lukianova@it.cas.cz

Keywords: Homogeneous nucleation, Nucleation rate, Formation of new particles

INTRODUCTION

To understand the condensation process, we need to know the thermodynamic parameters of nucleation and growth of water droplets. This process can be studied by adiabatic expansion of ga s mixtures of carbon dioxide/water and argon/water. In this case, the temperature of the mixture decreases and the supersaturation increases. This creates the conditions under which homogeneous nucleation is possible.

The influence of carrier gases on homogeneous nucleation has been studied several times. The first publication was by Viisanen et al. (1993) and the last publication was by Campagna et al. (2021).

EXPERIMENTAL SETUP

We performed experiments using the expansion pulse chamber developed by Wagner and Strey in 19846. The study was conducted with the carrier gases CO_2 and argon in a range of nucleation temperatures of 220-260 K and nucleation pressures of 35-75 kPa at various concentrations of water vapor. Fig. 1 shows nucleation rate J (number of droplets formed per unit of time and unit of volume) as function of supersaturation S (ratio of vapor pressure to the saturation pressure of water at given temperature) and temperature for the two carrier gases.

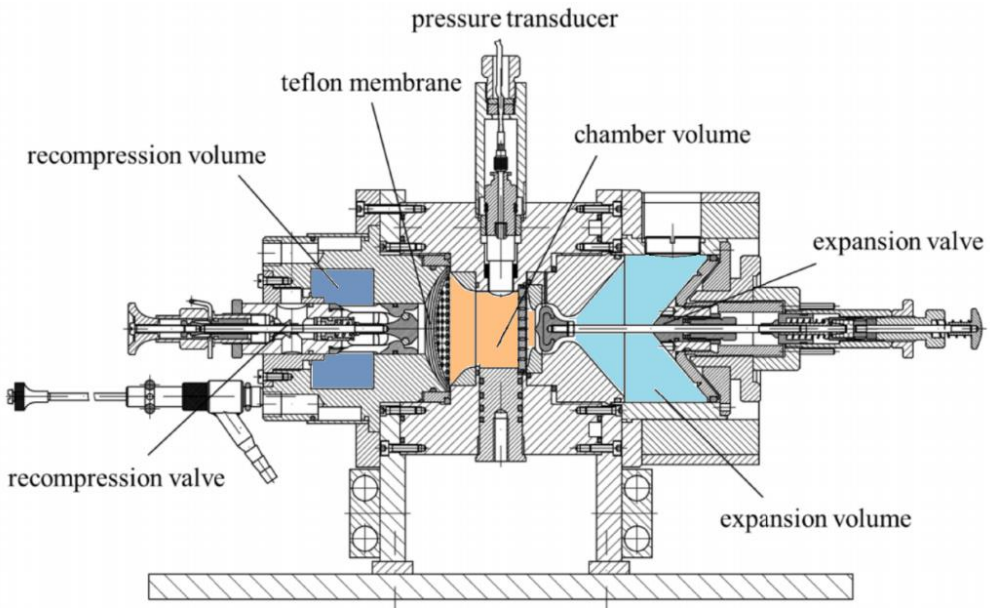

Fig. 1: Cross section of nucleation pulse chamber.

RESULTS AND CONCLUSIONS

In this abstract, we present experimental results on the homogeneous nucleation of water with the carrier gases CO_2 and argon. In addition, the real gas correction was applied to the temperature and supersaturation calculations. As it can be seen from Fig. 1 there is significant difference in the nucleation rate behavior of mixtures with argon and CO_2 carrier gases. CO_2 appears to enhance the nucleation rate. The isotherms showed in Fig. 2 have smaller slope for CO_2 carrier gas. By application of the nucleation theorem this allows to conclude that the presence of CO_2 decreases the number of water molecules forming the critical cluster.

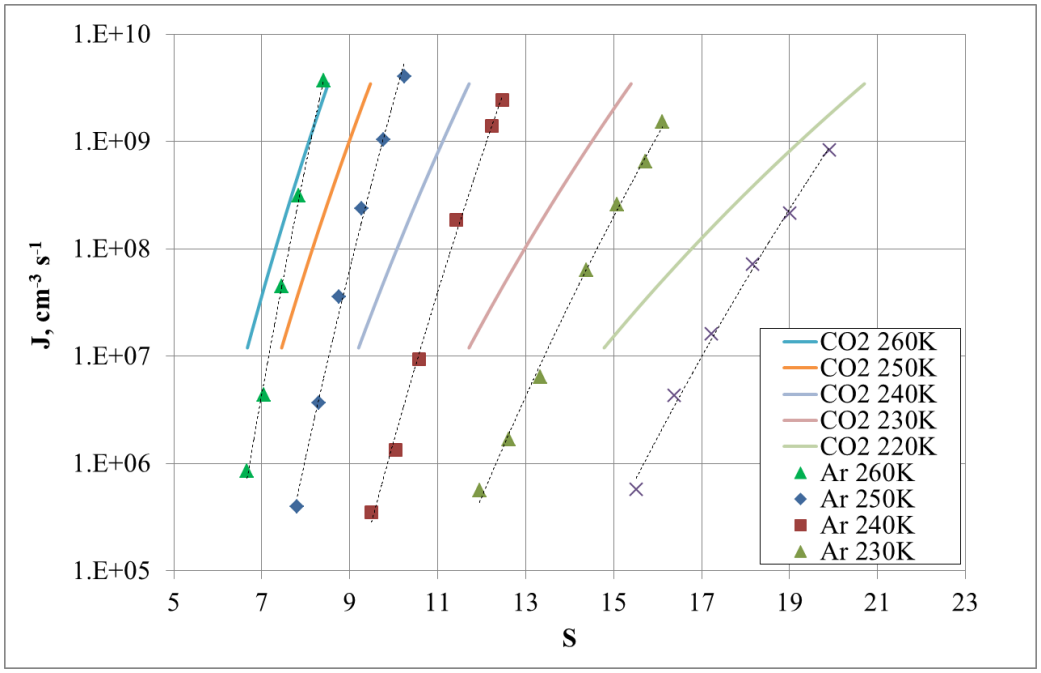

Fig. 2: Comparison of water nucleation rates with carrier gas CO2 and argon at different isotherms of nucleation.

Supersaturation and nucleation temperature are corrected with real gas thermodynamic.

ACKNOWLEDGEMENT

A support from the Ministry of Education, Youth and Sports of the Czech Republic under OP RDE Grant No. CZ.02.1.01/0.0/0.0/16_019/0000753 “Research center for low carbon energy technologies” and institutional support RVO:61388998 are gratefully acknowledged.

REFERENCES

Campagna, M.M., Hrubý, J., van Dongen, M.E.H., Smeulders, D.M.J., Homogeneous water nucleation in carbon dioxide–nitrogen mixtures: Experimental study on pressure and carrier gas effects. *J. Chem. Phys.* 154, 154301, (2021).

Viisanen, Y., Strey, R., Reiss, H., Homogeneous nucleation rates for water. *J. Chem. Phys.* 99, 4680–4692, (1993).